4

Black hole binaries

Jeffrey E. McClintock
Harvard–Smithsonian Center for Astrophysics

Ronald A. Remillard
Center for Space Research, MIT

4.1 Introduction

4.1.1 Scope of this review

We focus on 18 black holes with measured masses that are located in X-ray binary systems. These black holes are the most visible representatives of an estimated ∼300 million stellar-mass black holes that are believed to exist in the Galaxy (van den Heuvel 1992; Brown & Bethe 1994; Timmes *et al*. 1996; Agol *et al*. 2002). Thus the mass of this particular form of dark matter, assuming $\sim 10\,M_\odot$ per black hole, is ∼4% of the total baryonic mass (i.e., stars plus gas) of the Galaxy (Bahcall 1986; Bronfman *et al*. 1988). Collectively this vast population of black holes outweighs the galactic-center black hole, SgrA*, by a factor of ∼1000. These stellar-mass black holes are important to astronomy in numerous ways. For example, they are one endpoint of stellar evolution for massive stars, and the collapse of their progenitor stars enriches the Universe with heavy elements (Woosley *et al*. 2002). Also, the measured mass distribution for even the small sample of 18 black holes featured here is used to constrain models of black hole formation and binary evolution (Brown *et al*. 2000a; Fryer & Kalogera 2001; Nelemans & van den Heuvel 2001). Lastly, some black hole binaries appear to be linked to the hypernovae believed to power gamma-ray bursts (Israelian *et al*. 1999; Brown *et al*. 2000b; Orosz *et al*. 2001).

This review concentrates on the X-ray timing and spectral properties of these 18 black holes, plus a number of black hole candidates, with an eye to their importance to physics as potential sites for tests of general relativity (GR) in the strongest possible gravitational fields. There are several current areas of research that probe phenomena in these systems that are believed to occur very near the event horizon. These X-ray phenomena include quasi-periodic oscillations (QPOs) at high frequency (40–450 Hz) observed from seven systems, relativistically broadened iron lines from the inner accretion disk, and thermal disk emission from near the innermost stable circular orbit allowed by GR. We also comment on evidence for the existence of the event horizon, which is based on a comparison of black-hole and neutron-star binaries and on models for advective accretion flows.

The black hole binaries featured here are mass-exchange binaries that contain an accreting black hole primary and a non-degenerate secondary star. They comprise about 10% of all bright X-ray binaries. For background on X-ray binaries, see Chapter 1, and references therein. For comprehensive reviews on black hole binaries, see Tanaka & Lewin (1995; hereafter TL95) and Tanaka & Shibazaki (1996; hereafter TS96). In this review, we emphasize the results of the past decade. Throughout we make extensive use of the extraordinary database amassed since January 1996 by NASA's Rossi X-ray Timing Explorer (Swank 1998). Due

Compact Stellar X-Ray Sources, eds. Walter Lewin and Michiel van der Klis.
Published by Cambridge University Press.

to space constraints several important topics are omitted such as X-ray reflection studies (Done & Nayakshin 2001), the estimated number of black-hole X-ray novae in the Galaxy (which is ∼1000; van den Heuvel 1992; TS96; Romani 1998), and the present and projected rates of discovery of black hole binaries.

The main elements of the review are organized as follows. In the remainder of this section we catalog a total of 40 black hole binaries and candidate black hole binaries and discuss several introductory subjects, notably the physics of accretion onto black holes. In Section 4.2 we present X-ray light curves for 20 systems. In Section 4.3 we provide modified definitions of the canonical states of black hole binaries. Both low- and high-frequency quasi-periodic oscillations are discussed in Section 4.4. A recurring theme of the review is the importance of these black holes as potential sites for tests of general relativity.

4.1.2 The 18 black hole binaries

The first black hole binary (BHB), Cygnus X-1, was established by Webster and Murdin (1972) and Bolton (1972); the second, LMC X-3, was identified by Cowley *et al*. (1983). Both of these systems are persistently bright in X-rays; furthermore, they are classified as high-mass X-ray binaries (HMXBs) because their secondaries are massive O/B stars (White *et al*. 1995). The third BHB to be established, A0620–00, is markedly different (McClintock & Remillard 1986). A0620–00 was discovered as an X-ray nova in 1975 when it suddenly brightened to an intensity of 50 Crab[1] to become the brightest non-solar X-ray source ever observed (Elvis *et al.* 1975). Then, over the course of a year, the source decayed back into quiescence to become a feeble (1 μCrab) source (McClintock *et al*. 1995). Similarly, the optical counterpart faded from outburst maximum by $\Delta V \approx 7.1$ mag to $V \approx 18.3$ in quiescence, thereby revealing the optical spectrum of a K-dwarf secondary.

During the past 20 years, black holes (BHs) have been established in 15 additional X-ray binaries. Remarkably, nearly all these systems are X-ray novae like A0620-00. Thus, in all there are now 18 confirmed BHBs. They are listed in Table 4.1 in order of right ascension. The coordinate name of each source is followed in the second column by its variable star name (or other name, such as Cyg X-1), which is useful for web-based literature searches. For X-ray novae, the third column gives the year of discovery and the number of outbursts that have been observed. As indicated in the table, among the confirmed BHBs, there are six recurrent X-ray novae and three persistent sources, Cyg X-1, LMC X-3 and LMC X-1. As indicated in the fourth column, these latter three sources are high-mass X-ray binaries and are the only truly persistent sources among the BHBs.

Two of the X-ray novae are peculiar: GRS 1915+105 has remained bright for more than a decade since its eruption in August 1992; GX339–4 (1659–487), which was discovered by Markert *et al*. in 1973, undergoes frequent outbursts followed by very faint states, but it has never been observed to reach the *quiescent* state (Hynes *et al*. 2003). Columns 5 and 6 give the peak X-ray flux and a distance estimate for each source. The orbital period is given in the seventh column (a colon denotes an uncertain value) and the spectral type in the eighth. The first one or two references listed for each binary contain information on the orbital period and the spectral type. The remaining references support the distance estimates.

[1] 1 Crab $= 2.6 \times 10^{-9}$ erg cm^{-2} s^{-1} keV^{-1} (averaged over 2–11 keV) $= 1.06$ mJy at 5.2 keV for a Crab-like spectrum with photon index $\Gamma = 2.1$.

Table 4.1. *Confirmed black hole binaries: primary properties*

Source	Alternative name[a]	Year[b]	Type[c]	FX,max (μJy[d])	D (kpc)	P_{orb} (hr)	Spec.	References
0422+32	V518 Per	1992/1	L,T	3000	2.6 ± 0.7	5.1	M2V	1,2
0538–641	LMC X-3	–	H,P	60	50 ± 2.3	40.9	B3V	3,4
0540–697	LMC X-1	–	H,P	30	50 ± 2.3	101.5	O7III	3,5,6
0620–003	V616 Mon	1975/2	L,T	50000	1.2 ± 0.1	7.8	K4V	7,8,9,10
1009–45	MM Vel	1993/1	L,T	800	5.0 ± 1.3	6.8	K7/M0V	11,12
1118+480	KV UMa	2000/1	L,T	40	1.8 ± 0.5	4.1	K5/M0V	13,14
1124–684[e]	GU Mus	1991/1	L,T	3000	5 ± 1.3	10.4	K3/K5V	15,15a,16
1543–475	IL Lupi	1971/4	L,T	15000	7.5 ± 0.5	26.8	A2V	17,18
1550–564	V381 Nor	1998/5	L,T	7000	5.3 ± 2.3	37.0	G8/K8IV	19
1655–40	V1033 Sco	1994/2	L,T	3900	3.2 ± 0.2	62.9	F3/F5IV	20,21,22
1659–487[f]	V821 Ara	1972/[f]	L,T	1100	4	42.1:	–	23,24
1705–250	V2107 Oph	1977/1	L,T	3600	8 ± 2	12.5	K3/7V	7,25,26
1819.3–2525	V4641 Sgr	1999/1	L,T	13000	7.4–12.3	67.6	B9III	27
1859+226	V406 Vul	1999/1	L,T	1500	11	9.2:	–	28,29
1915+105	V1487 Aql	1992/1	L,T	3700	11–12	804.0	K/MIII	30,31,32,33
1956+350	Cyg X-1	–	H,P	2300	2.0 ± 0.1	134.4	O9.7Iab	34,35
2000+251	QZ Vul	1988/1	L,T	11000	2.7 ± 0.7	8.3	K3/K7V	35a,7,36,37
2023+338	V404 Cyg	1989/3	L,T	20000	2.2–3.7	155.3	K0III	38,39,40

[a] Name recognized by the SIMBAD Database and the Astrophysics Data System (ADS).
[b] Year of discovery/number of outbursts observed (Chen *et al*. 1997; this work).
[c] 'H' – HMXB, 'L' – LMXB, 'T' – transient, 'P' – persistent; Liu *et al*. 2000, 2001; this work.
[d] 1 μJy $= 10^{-29}$ erg cm^{-2} s^{-1} Hz^{-1} $= 2.42 \times 10^{-12}$erg cm^{-2} s^{-1} keV^{-1}.
[e] Commonly known as Nova Muscae 1991.
[f] Commonly known as GX339–4; number of outbursts ~ 10 (Kong *et al*. 2002). References: [1]Esin *et al*. 1997; [2]Filippenko *et al*. 1995a; [3]Freedman *et al*. 2001; [4]Cowley *et al*. 1983; [5]Hutchings *et al*. 1987; [6]Cowley *et al*. 1995; [7]Barret *et al* . 1996b; [8]Gelino *et al*. 2001b; [9]Marsh *et al*. 1994; [10]McClintock & Remillard 2000; [11]Barret *et al*. 2000; [12]Filippenko *et al*. 1999; [13]McClintock *et al*. 2001a; [14]Wagner *et al*. 2001; [15]Orosz *et al*. 1996; [15a]Gelino *et al*. 2001a; [16]Shahbaz *et al*. 1997; [17]Orosz *et al*. 2002b; [18]Orosz *et al*. 1998; [19]Orosz *et al*. 2002a; [20]Hjellming & Rupen 1995; [21]Orosz & Bailyn 1997; [22]Shahbaz *et al*. 1999; [23]Cowley *et al*. 1987; [24]Hynes *et al*. 2003; [25]Remillard *et al*. 1996; [26]Filippenko *et al*. 1997; [27]Orosz *et al*. 2001; [28]Zurita *et al*. 2002; [29]Filippenko & Chornock 2001; [30]Mirabel & Rodriguez 1994; [31]Fender *et al*. 1999b; [32]Greiner *et al*. 2001a; [33]Greiner *et al*. 2001b; [34]Mirabel & Rodrigues 2003; [35]Gies & Bolton 1982; [35a]Harlaftis *et al*. 1996; [36]Filippenko *et al*. 1995b; [37]Casares *et al*. 1995; [38]Shahbaz *et al*. 1994; [39]Casares & Charles 1994; [40]Casares *et al*. 1993.

The data in Table 4.1 reveal considerable diversity among the BHBs. For example, these 18 binaries range in size from tiny XTE J1118+480 with $P_{orb} = 0.17$ days and a separation between the BH and its companion of $a \approx 2.8$ R$_\odot$ to GRS 1915+105 with $P_{orb} = 33.5$ days and $a \approx 95$ R$_\odot$. Only 6 of these 18 systems were established as BHBs a decade ago (van Paradijs & McClintock 1995). As indicated in Table 4.1, all of the 15 X-ray novae are low-mass X-ray binaries (LMXBs), which typically contain a secondary with a mass of roughly 1 M$_\odot$ or less (White *et al*. 1995). The BHBs 4U1543–47 and SAX J1819.3–2525 have relatively massive secondaries: 2.7 ± 1.0 M$_\odot$ and 2.9 ± 0.2 M$_\odot$, respectively (Orosz *et al*.

2002b). We classify them as LMXBs because their secondary masses are comparable to the mass of the secondary of Her X-1 (2.3 ± 0.3 $M_\odot$; Reynolds *et al*. 1997), which is a well-known LMXB (Liu *et al*. 2001). Furthermore, a 2–3 $M_\odot$ secondary is much less massive than the O/B secondaries ($\gtrsim$10 $M_\odot$) found in HMXB systems.

BHBs manifest themselves in five rather distinct spectral/temporal states defined in the 1–10 keV band (e.g., van der Klis 1994; TL95; TS96). The three most familiar are (1) the *high/soft* (HS) state, a high-intensity state dominated by thermal emission from an accretion disk; (2) the *low/hard* (LH) state, a low-intensity state dominated by power-law emission and rapid variability; and (3) the *quiescent* state, an extraordinarily faint state also dominated by power-law emission. The remaining two states, (4) the *very high* (VH) state and (5) the *intermediate* state, are more complex; recently they have come to the fore, as they have now been observed in an appreciable number of sources. These five BH states and the transitions between them are the focus of Section 4.3, where they are redefined and illustrated in detail.

Additional data specific to the BH primaries are contained in Table 4.2. Of special importance is the mass function, $f(M) \equiv P_{\rm orb}K_2^3/2\pi G = M_1 \sin^3 i/(1+q)^2$. The observables on the left side of the equation are the orbital period, $P_{\rm orb}$, and the half-amplitude of the velocity curve of the secondary, K_2. On the right, the quantity of most interest is the BH mass, M_1; the other parameters are the orbital inclination angle, i, and the mass ratio, $q \equiv M_2/M_1$, where M_2 is the mass of the secondary. Thus a secure value of the mass function can be determined for a quiescent X-ray nova or an HMXB by simply measuring the radial velocity curve of the secondary star. The mass function values are given in the second column of Table 4.2 An inspection of the equation for $f(M)$ shows that the value of the mass function is the absolute minimum mass of the compact primary. Thus, for 12 of the 18 BHBs, the very secure value of $f(M)$ alone is sufficient to show that the mass of the compact X-ray source is at least 3 $M_\odot$ (Table 4.2), which is widely agreed to exceed the maximum stable mass of a neutron star (NS) in GR (Rhoades & Ruffini 1974; Kalogera & Baym 1996). For the remaining half-dozen systems, some additional data are required to make the case for a BH. The evidence for BHs in these 18 systems is generally very strong (see Chapter 5). Thus, assuming that GR is valid in the strong-field limit, we choose to refer to these compact primaries as BHs, rather than as BH candidates. We note, however, our reservations about three of the systems listed in Table 4.2: (1) The mass function of LMC X–1 (0540–697) is quite uncertain; (2) the orbital period of XTE J1859+226 is not firmly established (Filippenko & Chornock 2001; Zurita *et al*. 2002); and (3) the dynamical data for GX 339–4 (1659–487) were determined in outburst by a novel technique, and neither the orbital period nor the velocity amplitude are securely determined (Hynes *et al*. 2003).

The mass of a BH can be derived from the measurement of its mass function in combination with estimates for M_2 and $\sin i$. The ratio of the mass of the BH to the mass of the secondary star is usually deduced by measuring the rotational velocity of the latter. The binary inclination angle can be constrained in several ways; commonly, one models the photometric variations associated with the gravitationally distorted secondary star that is seen to rotate once per binary orbit in the plane of the sky (e.g., Greene *et al*. 2001). Mass estimates for the known BHBs are given in the third column of Table 4.2. In an astrophysical environment, a BH is completely specified in general relativity by two numbers, its mass and its specific angular

Table 4.2. *Confirmed black hole binaries: X-ray and optical data*

Source	$f(M)^a$ ($M_\odot$)	M_1^a ($M_\odot$)	f(HFQPO) (Hz)	f(LFQPO) (Hz)	Radio[b]	$E^c_{\max}$ (MeV)	References
0422+32	1.19±0.02	3.2–13.2	–	0.035–32	P	0.8, 1–2:	1,2,3,4,5
0538–641	2.3±0.3	5.9–9.2	–	0.46	–	0.05	6,7
0540–697	0.14±0.05	4.0–10.0:	–	0.075	–	0.02	8,7
0620–003	2.72±0.06	3.3–12.9	–	–	P,J?	0.03:	9,10,11,11a
1009–45	3.17±0.12	6.3–8.0	–	0.04–0.3	–[d]	0.40, 1:	12,4,13
1118+480	6.1±0.3	6.5–7.2	–	0.07–0.15	P	0.15	14,15,16,17
1124–684	3.01±0.15	6.5–8.2	–	3.0–8.4	P	0.50	18,19,20,21
1543–475	0.25±0.01	7.4–11.4[e]	–	7	–[f]	0.20	22,4
1550–564	6.86±0.71	8.4–10.8	92,184,276	0.1–10	P,J	0.20	23,24,25,26,27
1655–40	2.73±0.09	6.0–6.6	300,450	0.1–28	P,J	0.80	28,29,30,31,54
1659–487	> 2.0[g]	–	–	0.09–7.4	P	0.45, 1:	32,33,4,13
1705–250	4.86±0.13	5.6–8.3	–	–	–[d]	0.1	34,35
1819.3–2525	3.13±0.13	6.8–7.4	–	–	P,J	0.02	36,37
1859+226	7.4±1.1	7.6–12:	190	0.5–10	P,J?	0.2	38,39,40,41
1915+105	9.5±3.0	10.0–18.0:	41,67,113,168	0.001–10	P,J	0.5, 1:	42,43,44,4,13
1956+350	0.244±0.005	6.9–13.2	–	0.035–12	P,J	2–5	45,46,47,48,49
2000+251	5.01±0.12	7.1–7.8	–	2.4–2.6	P	0.3	18,50,51
2023+338	6.08±0.06	10.1–13.4	–	–	P	0.4	52,53

[a] Orosz *et al*. 2002b, except for 1659–487; colon denotes uncertain value.
[b] Radio properties: 'P' – persistent over 10 or more days and/or inverted spectrum; 'J' – relativistic jet detected.
[c] Maximum energy reported; colon denotes uncertain value.
[d] No observations made.
[e] Orosz, private communication.
[f] Very faint (e.g., see IAUC 7925).
[g] For preferred period, $P = 1.76$ days, $f(M) = 5.8 \pm 0.5\ M_\odot$; Hynes *et al*. 2003.

References: [1]van der Hooft *et al*. 1999; [2]Vikhlinin *et al*. 1992; [3]Shrader *et al*. 1994; [4]Grove *et al*. 1998; [5]van Dijk *et al*. 1995; [6]Boyd *et al*. 2000; [7]Nowak *et al*. 2001; [8]Ebisawa *et al*. 1989; [9]Owen *et al*. 1976; [10]Kuulkers *et al*. 1999; [11]Coe *et al*. 1976; [11a] Marsh *et al*. 1994; [12]van der Hooft *et al*. 1996; [13]Ling *et al*. 2000; [14]Wood *et al*. 2000; [15]Revnivtsev *et al*. 2000b; [16]Fender *et al*. 2001; [17]McClintock *et al*. 2001a; [18]Rutledge *et al*. 1999; [19]Belloni *et al*. 1997; [20]Ball *et al*. 1995; [21]Sunyaev *et al*. 1992; [22]This work; [23]Remillard *et al*. 2002b; [24]Corbel *et al*. 2001; [25]Wu *et al*. 2002; [26]Corbel *et al*. 2003; [27]Sobczak *et al*. 2000b; [28]Remillard *et al*. 1999; [29]Strohmayer 2001a; [30]Hjellming & Rupen 1995; [31]Hannikainen *et al*. 2000; [32]Revnivtsev *et al*. 2001; [33]Corbel *et al*. 2000; [34]Wilson & Rothschild 1983; [35]Cooke *et al*. 1984; [36]Hjellming *et al*. 2000; [37]Wijnands & van der Klis 2000; [38]Cui *et al*. 2000a; [39]Markwardt 2001; [40]Brocksopp *et al*. 2002; [41]Dal Fiume *et al*. 1999; [42]Morgan *et al*. 1997; [43]Strohmayer 2001b; [44]Mirabel & Rodriguez 1994; [45]Vikhlinin *et al*. 1994; [46]Cui *et al*. 1997b; [47]Stirling *et al*. 2001; [48]Ling *et al*. 1987; [49]McConnell *et al*. 2002; [50]Hjellming *et al*. 1988; [51]Sunyaev *et al*. 1988; [52]Han & Hjellming 1992; [53]Sunyaev *et al*. 1991b; [54]Tomsick *et al*. 1999.

momentum or spin, $a = J/cM_1$, where J is the BH angular momentum and c is the speed of light (e.g., Kato *et al*. 1998). The spin value is conveniently expressed in terms of a dimensionless spin parameter, $a_* = a/r_g$, where the gravitational radius is $r_g \equiv GM/c^2$. The value of a_* lies between 0 for a Schwarzschild hole and 1 for a maximally rotating Kerr hole. The radius of the BH event horizon depends on both M_1 and a_*; this topic is discussed further in Section 4.1.5.

High-frequency QPOs (HFQPOs) in the range 40–450 Hz are observed for the four systems with data given in the fourth column. Low-frequency QPOs (LFQPOs) are also observed from these systems and ten others, as indicated in column 5. Most of the systems were at one time or another detected as radio sources and at least five have exhibited resolved radio jets (column 6; see Mirabel & Rodriguez 1999). An X-ray jet (two-sided) has been observed from XTE J1550–564 (Corbel *et al*. 2002). As shown in column 7, power-law emission extending to $\sim$1 MeV has been observed for six sources. The references listed in the last column support the X-ray QPO, radio, and $E_{\max}$ data given in columns 4–7.

The dynamical evidence for massive ($M > 3\ M_{\odot}$) collapsed stellar remnants is indisputable. However, this evidence alone can never establish the existence of BHs. At present, the argument for BHs depends on the assumption that GR is the correct theory of strong gravity. To make an airtight case that a compact object is a BH with an event horizon, we must make clean quantitative measurements of relativistic effects that occur near the collapsed object. That is, we must measure phenomena that are predicted by GR to be unique to BHs. A possible route to this summit is to measure and interpret the effects of strong-field gravity that are believed to be imprinted on both HFQPOs (Section 4.4.3) and X-ray emission lines (Section 4.2.3). Another approach, which is discussed in Section 4.3.4, is based on sensing the qualitative differences between an event horizon and the material surface of a NS.

4.1.3 Black hole candidates

Certain characteristic X-ray properties of the 18 established BHs are often used to identify a candidate BH when the radial velocities of the secondary cannot be measured (e.g., because the secondary is too faint). These frequently observed characteristics of the established BHBs, which are discussed in detail by TL95, include an ultrasoft X-ray spectrum (1–10 keV), a power-law spectral tail that extends beyond 20 keV, characteristic state transitions (Section 4.1.2; Section 4.3), and rapid temporal variability. However, none of these putative BH signatures has proved to be entirely reliable; each of them has been forged by one or more systems known to contain a NS primary (TL95). This is not surprising since the X-ray spectral/temporal properties originate in an accretion flow that is expected to be fairly similar whether the primary is a BH or a weakly magnetized NS. Another characteristic of all BHBs is a complete absence of either periodic pulsations or Type I X-ray bursts, which are the very common signatures of NS systems.

Nevertheless, despite the limitations of these spectral/temporal identifiers, they have served as useful guides and have allowed the identification of a number of probable BH primaries, which we refer to as BH candidates or BHCs. In order to economize on acronyms, we also use BHC to refer to the binary system that hosts the BH candidate. A list of 22 BHCs is given in Table 4.3 These systems are less well known than the BHBs listed in Table 4.1. Therefore, to aid in their identification we have included in most cases the prefix to the coordinate source name that identifies the discovery mission (e.g., EXO = EXOSAT). For the four sources with variable star names, the prefix is omitted. In columns 2–4, we give the best available coordinates and their uncertainties (if they exceed 10″). These coordinates are also an excellent resource for interrogating ADS and SIMBAD.

In column 5 we list the characteristics that indicate the BHC classification, e.g., an observation of one or more of the canonical states of a BHB. A source classified as "ultrasoft" in the older literature (e.g., White & Marshall 1984) is assumed here to have been observed in the HS state. Three BHCs with resolved radio jets are also noted in column 5. Variability

Table 4.3. *Candidate black hole binaries*[a]

Source	RA(2000)	DEC(2000)	r_X[b]	BH trait[c]	Grade[d]	References
1354–645 (BW Cir)	13 58 09.74	−64 44 05.2		LH,HS	A	1,2,3,4
1524–617 (KY TrA)	15 28 16.7	−61 52 58		LH,HS	A	5,6,7
4U 1630–47	16 34 01.61	−47 23 34.8		LH,HS	A	8,9,10,11
XTE J1650–500	16 50 01.0	−49 57 45		LH,HS,VH	A	12,13,14,15,16
SAX J1711.6–3808	17 11 37.1	−38 07 06		LH,HS	B	17,18
GRS 1716–249[e]	17 19 36.93	−25 01 03.4		LH	B	19,20,21
XTE J1720–318	17 19 59.06	−31 44 59.7		LH:,HS	C	22,23,24
KS 1730–312	17 33 37.6	−31 13 12	30″	LH,HS	C	25,26
GRS 1737–31	17 40 09	−31 02.4	30″	LH	B	27,28,29
GRS 1739–278	17 42 40.03	−27 44 52.7		LH,HS,VH	A	30,31,32,33,34
1E 1740.7–2942	17 43 54.88	−29 44 42.5		LH,HS,J	A	35,36,37,38,39
A 1742–289	17 45 37.3	−29 01 05		HS:	C	40,41,42,43
H 1743–322	17 46 15.61	−32 14 00.6		HS,VH	A	44,45,46,80,81,82
XTE J1748–288	17 48 05.06	−28 28 25.8		LH,HS,VH,J	A	47,48,49,50,51
SLX 1746–331	17 49 50.6	−33 11 55	35″	HS:	C	52,53,54
XTE J1755–324	17 55 28.6	−32 28 39	1′	LH,HS	B	55,56,57,58
1755–338 (V4134 Sgr)	17 58 40.0	−33 48 27		HS	B	59,42,60,61,62
GRS 1758–258	18 01 12.67	−25 44 26.7		LH,HS,J	A	63,38,64,65,66
EXO 1846–031	18 49 16.9	−03 03 53	11″[f]	HS	C	67
XTE J1908+094	19 08 53.08	+09 23 04.9		LH,HS	B	68,69,70,71
1957+115 (V1408 Aql)	19 59 24.0	+11 42 30		HS	C	72,42,73,74,75
XTE J2012+381	20 12 37.70	+38 11 01.2		LH,HS	B	76,77,78,79

[a] For additional references and information, see TL95 and Liu *et al*. 2001.
[b] Positional uncertainty given if $r_X > 10''$.
[c] LH – low/hard state, HS – high/soft state, VH – very high state, J – radio jet.
[d] Qualitative grade indicating the likelihood that the candidate is in fact a BH.
[e] GRS 1716–249 = GRO J1719–24 = X-ray Nova Oph 1993.
[f] Alternative position also possible; see Parmar *et al*. 1993. References: [1]Kitamoto *et al*. 1990; [2]Brocksopp *et al*. 2001; [3]Revnivtsev *et al*. 2000a; [4]Fender 2001; [5]Murdin *et al*. 1977; [6]Kaluzienski *et al*. 1975; [7]Barret *et al*. 1992; [8]Hjellming *et al*. 1999; [9]Tomsick & Kaaret 2000; [10]Dieters *et al*. 2000; [11]Augusteijn *et al*. 2001; [12]Groot *et al*. 2001; [13]Kalemci *et al*. 2002; [14]Homan *et al*. 2003a; [15]Miller *et al*. 2002b; [16]Sanchez–Fernandez *et al*. 2002; [17]in 't Zand *et al*. 2002a; [18]Wijnands & Miller 2002; [19]Mirabel *et al*. 1993; [20]van der Hooft *et al*. 1996; [21]Revnivtsev *et al*. 1998b; [22]Rupen *et al*. 2003; [23]Remillard *et al*. 2003a; [24]Markwardt & Swank 2003; [25]Borozdin *et al*. 1995; [26]Vargas *et al*. 1996; [27]Ueda *et al*. 1997; [28]Cui *et al*. 1997a; [29]Trudolyubov *et al*. 1999; [30]Marti *et al*. 1997; [31]Vargas *et al*. 1997; [32]Borozdin *et al*. 1998; [33]Wijnands *et al*. 2001; [34]Greiner *et al*. 1996; [35]Cui *et al*. 2001; [36]Churazov *et al*. 1993; [37]Smith *et al*. 1997; [38]Smith *et al*. 2002; [39]Marti *et al*. 2000; [40]Davies *et al*. 1976; [41]Wilson *et al*. 1977; [42]Branduardi *et al*. 1976; [43]Kennea & Skinner 1996; [44]Gursky *et al*. 1978; [45]Cooke *et al*. 1984; [46]White & Marshall 1984; [47]Hjellming *et al*. 1998b; [48]Revnivtsev *et al*. 2000c; [49]Kotani *et al*. 2000; [50]Miller *et al*. 2001; [51]Rupen *et al*.1998; [52]Skinner *et al*. 1990; [53]White & van Paradijs 1996; [54]Motch *et al*. 1998; [55]Remillard *et al*. 1997; [56]Ogley *et al*. 1997; [57]Revnivtsev *et al*. 1998a; [58]Goldoni *et al*. 1999; [59]Bradt & McClintock 1983; [60]White *et al*. 1988; [61]Pan *et al*. 1995; [62]Seon *et al*. 1995; [63]Rodriguez *et al*. 1992; [64]Sunyaev *et al*. 1991a; [65]Smith *et al*. 2001; [66]Rothstein *et al*. 2002; [67]Parmar *et al*. 1993; [68]Rupen *et al*. 2002; [69]in't Zand *et al*. 2002b; [70]Woods *et al*. 2002; [71]Chaty *et al*. 2002; [72]Margon *et al*. 1978; [73]Wijnands *et al*. 2002; [74]Yaqoob *et al*. 1993; [75]Nowak & Wilms 1999; [76]Hjellimg *et al*. 1998a; [77]Campana *et al*. 2002; [78]Vasiliev *et al*. 2000; [79]Hynes *et al*. 1999; [80]Revnivtsev *et al*. 2003; [81]Steeghs *et al*. 2003; [82]Homan *et al*. 2003b.

characteristics (Section 4.4) and broad Fe Kα emission lines (Section 4.2.3) can also be important BH indicators, but these are not explicitly noted in Table 4.3. Selected references are cited in the last column. The coordinate data can be found in the first reference. The following few references support the BH characteristics given in column 5. For several sources, a few additional references provide limited information on optical/IR/radio counterparts, etc.

We have assigned a grade to each BHC that is based both on how thoroughly the candidate has been observed and on the characteristics it displayed. In fact, this grade is qualitative and subjective and meant only as a guide. Our sense of the grade is as follows: We would be surprised if even one of the nine A-grade BHCs contains a NS, but not surprised if one of the six C-grade BHCs contains a NS. In compiling Table 4.3, we have been selective. For example, we did not include SAX J1805.5–2031 (Lowes *et al*. 2002) and XTE J1856+053 (Barret *et al*. 1996a) primarily because we judged that the available information was too scanty. Thus the total number of BH or BHC cases considered here is 40. For narrative discussions about many of the systems in Tables 4.1 and 4.3, see TL95. For additional data and as a supplement to the list of references given in Table 4.3, see Liu *et al*. (2001).

4.1.4 X-ray novae

If we include the X-ray novae observed during the past decade, then about 300 bright binary X-ray sources are known (van Paradijs 1995; Liu *et al*. 2000, 2001). More than half of them are LMXBs, and roughly half of each type (i.e., LMXB and HMXB) are classified as transient sources. The HMXB transients are neutron-star/Be-star binaries, which are not relevant to this review. The well-studied LMXB transients, on the other hand, include all of the X-ray novae that are listed in Tables 4.1–4.3. The principal hallmarks of an X-ray nova include both the discovery of the source during a violent outburst and a very large ratio of maximum to minimum X-ray intensity. The behavior of A0620–00, described in Section 4.1.2 provides a classic example of an X-ray nova. Indeed, it is the extreme faintness of the quiescent accretion disk in these systems that allows one to view the companion star, leading to secure dynamical measurements of the BH mass (Sections 4.1.2, and 4.3.4; Chapter 5).

Recurrent eruptions have been observed for several of the X-ray novae listed in Table 4.1: e.g., A0620–00 in 1917 and 1975; H1743–322 in 1977 and 2003; GS 2023+338 in 1938, 1956 and 1987; 4U 1543–47 in 1971, 1983, 1992 and 2002; and 4U 1630–472 and GX 339–4 at ∼1–2 year intervals. (Outbursts prior to 1970 are inferred from studies of optical plates *ex post facto*.) Most X-ray novae, however, have been observed to erupt only once. Nevertheless, all X-ray novae are thought to be recurrent, with cycle times for some possibly as long as several centuries or more. TS96 suggest an average cycle time of 10–50 years. The infrequent outbursts are due to a sudden surge in the mass accretion rate onto the BH. The generally accepted mechanism driving the outburst cycle is that described by the disk instability model, which was developed initially for dwarf novae (Smak 1971; Osaki 1974; Cannizzo 1993; Lasota *et al*. 2001) and extended to X-ray novae (e.g., Dubus *et al*. 2001).

4.1.5 Accretion onto black holes

The desire to understand observations of BHBs compels us to model the hydrodynamics and radiation processes of gas orbiting in the gravitational potential of a compact object (see Chapter 13 for a detailed review). The best-known such model is the thin accretion

disk (Pringle & Rees 1972; Novikov & Thorne 1973; Shakura & Sunyaev 1973; Lynden-Bell & Pringle 1974). For nearly all of the systems included in Tables 4.1–4.3, the companion star fills its Roche equipotential lobe and a narrow stream of gas escapes the star through the inner Lagrangian (L_1) point. This gas has high specific angular momentum and cannot accrete directly onto the BH. It feeds into a thin disk of matter around the BH known as an accretion disk. Once entrained in the disk, the gas moves in Keplerian orbits with angular velocity $(GM/R^3)^{1/2}$. However, viscous dissipation slowly taps energy from the bulk orbital motion, and viscosity transports angular momentum outward. As a result, the gas gets hotter as it sinks deeper into the gravitational potential well of the BH. Near the BH the disk terminates because there are no stable particle orbits possible in the extreme gravitational field. The existence of an innermost stable circular orbit (ISCO) and other properties of BHs are discussed in many texts (e.g., Shapiro & Teukolsky 1983; Kato *et al*. 1998). A defining property of a BH is its event horizon, the immaterial surface that bounds the interior region of spacetime that cannot communicate with the external universe. The radius of the event horizon of a Schwarzschild BH ($a_* = 0$) is $R_S \equiv 2R_g \equiv 2(GM/c^2) = 30\,\mathrm{km}(M/10\,\mathrm{M}_\odot)$, the ISCO lies at $R_{ISCO} = 6R_g$, and the corresponding maximum orbital frequency is $\nu_{ISCO} = 220\,\mathrm{Hz}(M/10\,\mathrm{M}_\odot)^{-1}$ (see Section 4.1.2 for the definition of a_*). For an extreme Kerr BH ($a_* = 1$), the radii of both the event horizon and the minimum stable (prograde) orbit are identical, $R_K = R_{ISCO} = R_g$, and the maximum orbital frequency is $\nu_{ISCO} = 1615\,\mathrm{Hz}(M/10\,\mathrm{M}_\odot)^{-1}$. For the Kerr BH, it is well known that the rotational energy can be tapped electromagnetically (Blandford & Znajek 1977). The gas flows driven by this process are both anisotropic and self-collimating (Blandford 2002, and references therein), and they may be the source of the relativistic jets seen from several BHBs and BHCs (Tables 4.2–4.3).

Even for XTE J1118+480, the smallest system in Table 4.1, the outer radius of the accretion disk is expected to be roughly one solar radius, $\sim 10^5 R_g$, vastly larger than the BH event horizon. Thus a gas element of mass m that is destined to enter the BH via the thin disk starts far out with negligible binding energy. When it reaches the ISCO it will have radiated $0.057mc^2$ for a Schwarzschild BH or a theoretical maximum of $0.42mc^2$ for an extreme Kerr BH. Moreover, 90% of this colossal energy is radiated within about $20R_g$ of the center. At all disk radii, the energy liberated by viscous dissipation is radiated locally and promptly and results in a gas temperature that increases radially inward reaching a maximum of $T \sim 10^7$ K near the BH. This picture is the basis of the standard thin accretion disk model (Shakura & Sunyaev 1973). A non-relativistic approximation to this thin disk spectrum has been formulated conveniently as a multi-temperature blackbody (Mitsuda *et al*. 1984; Makishima *et al*. 1986). The total disk luminosity in a steady state is $L_{disk} = GM\dot{M}/2R_{in}$, where $\dot{M}$ is the mass accretion rate and R_{in} is the radius of the inner edge of the disk. This model, often referred to as the multicolor disk (MCD) model, is used to describe the thermal component that is dominant in the HS state and is also present in the VH state (Sections 4.2.2, 4.3.5 and 4.3.7). The MCD model has been available within XSPEC ("diskbb"; Arnaud & Dorman 2002) for many years and has been widely used. Despite the successes of the MCD model, it is important to note a significant limitation, namely, the neglect of a torque-free boundary condition at the ISCO (Gierlinski *et al*. 1999). In the MCD model, the temperature profile is simply $T(R) \propto R^{-3/4}$, which rises to a maximum at the ISCO, whereas a proper inner boundary condition produces null dissipation at the ISCO with the temperature peaking at $R > R_{ISCO}$ (Pringle 1981; Gierlinski *et al*. 1999). The current MCD model requires attention and improvement.

Efforts have also been made to include relativistic corrections to the MCD model (e.g., Ebisawa *et al*. 1991; Zhang *et al*. 1997a; Gierlinski *et al*. 2001). However, quantitative analyses (e.g., a spectroscopic measurement of the inner disk radius when the source distance and inclination angle are known) will require more sophisticated models. Accretion disk models are being developed to incorporate MHD effects in the context of GR (e.g., McKinney & Gammie 2002), with additional considerations for radiation pressure and radiative transfer (Turner *et al*. 2002; Shimura & Takahara 1995). Early results show that magnetic fields may couple matter in the "plunging region" to matter at radii greater than the ISCO, and thereby extract energy from very near the horizon (Agol & Krolik 2000). In the case of a rapidly rotating Kerr hole, the spin/electromagnetic effects mentioned above may not only drive relativistic jets, but also may modify grossly the spectrum of the inner accretion disk (Wilms *et al*. 2001b; Miller *et al*. 2002b).

At lower mass accretion rates corresponding to several percent of the Eddington luminosity, a BHB usually enters the LH (i.e., *low/hard*) state and at very low accretion rates it reaches the *quiescent* state, which may be just an extreme example of the LH state. In both of these states, the spectrum of a BHB is dominated by a hard, non-thermal power-law component (photon index $\sim$1.7; Sections 4.3.4 and 4.3.6), which cannot be accounted for by a thermal accretion disk model; it is most plausibly explained as due to Comptonization of soft photons by a hot optically thin plasma. Early models for the spectrum of the quiescent state postulated that the disk does not extend all the way down to the ISCO (Narayan 1996; Narayan *et al*. 1996). The disk is truncated at some larger radius ($\sim$100 R_S; Esin *et al*. 2001), and the interior volume is filled with a hot ($T_e \sim 100$ keV) advection-dominated accretion flow or ADAF (Narayan & Yi 1994, 1995; Narayan *et al*. 1996; Quataert & Narayan 1999). In an ADAF, most of the energy released via viscous dissipation remains in the accreting gas rather than being radiated away (as in a thin disk). The bulk of the energy is advected with the flow. Only a small fraction of the energy is radiated by the optically thin gas before the gas reaches the center. Consequently, the radiative efficiency of an ADAF (which depends on the uncertain fraction of the viscous energy that is channeled to the electrons) is expected to be only $\sim$0.1–1%, whereas the radiative efficiency discussed above for disk accretion is definitely $\geq 5.7\%$. There is wide agreement that these radiatively inefficient flows have been observed in quiescent BHBs (Section 4.3.4) and from galactic nuclei (Baganoff *et al*. 2001; Loewenstein *et al*. 2001). However, the theoretical picture has become complex with variant models involving winds (ADIOS; Blandford & Begelman 1999) and convection (CDAFs; Igumenshchev & Abramowicz 1999; Stone *et al*. 1999; Narayan *et al*. 2000; Quataert & Gruzinov 2000).

One attempt has been made to unify four of the five states of a BHB using both the MCD and ADAF models (Esin *et al*. 1997). This approach is illustrated in Fig. 4.1, which shows how the geometry of the accretion flow changes as the mass accretion rate $\dot{m}$ varies ($\dot{m}$ is the mass accretion rate expressed in Eddington units). The scenario indicates how a BH system progresses through five distinct states of increasing $\dot{m}$ from the quiescent state to the VH state. In the three states at lower $\dot{m}$, the flow consists of two zones (disk and ADAF), as described above. For the two states of highest $\dot{m}$, the disk extends down to the ISCO. In all five states, the disk is bathed in a corona that is a seamless continuation of the ADAF. Apart from the VH state, the model treats consistently the dynamics of the accreting gas, the thermal balance of the ions and electrons in the ADAF and corona, and the radiation processes. The model

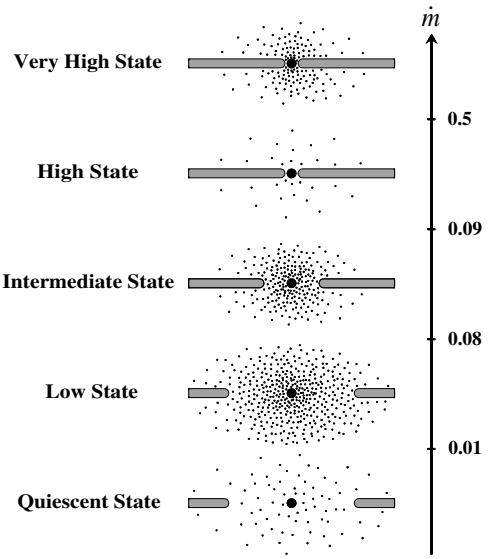

Fig. 4.1. Schematic sketch of the accretion flow in different spectral states as a function of the total Eddington-scaled mass accretion rate $\dot{m}$. The ADAF is represented by dots and the thin disk by the horizontal bars. The very high state is illustrated, but it is not included in the unification scheme (Esin *et al*. 1997).

has had significant successes in describing the spectral evolution of several BHBs (Esin *et al*. 1997, 1998; for further discussion of the ADAF model, see Section 4.3.4.)

However, the multi-state model of Esin *et al*. (1997) has important limitations. For example, it does not unify the most luminous state, the *very high* state, which is characterized by an unbroken power-law spectrum extending out to a few hundred keV or more (Section 4.3.7). Also, this simple ordering of the states by $\dot{m}$ or luminosity is naive (Section 4.3). Moreover, the model does not account for the dynamic behavior of the corona, including strong flares and powerful low-frequency quasi-periodic oscillations (Section 4.4), nor does it account for the radio emission observed from most BHBs (Table 4.2). Finally, the "evaporation" process by which the cold gas in a thin disk feeds into a hot ADAF is at best qualitatively understood, and there is no quantitative model relating the disk truncation radius to the accretion rate $\dot{m}$ (Narayan 2002, and references therein).

There are alternative models of the X-ray states, and many of them invoke a dynamic accretion disk corona that is fed by MHD instabilities in the disk. For example, in the model of Merloni and Fabian (2001a, 2001b) the hot corona that generates the power-law component is intimately connected with the thin accretion disk. Magnetic energy generated (presumably) by the sheared Keplerian disk creates magnetic flares that rise out of the disk because of the Parker instability. Within the framework of this model, Di Matteo *et al*. (1999) present a magnetic flare model for the two common states of GX339–4. In the HS state, the flares occur near the disk and heat it. The disk reradiates the observed soft thermal component, whereas the faint hard component is produced by Comptonization of the soft flux. In the LH state, the flares occur far above the disk and the density of soft seed photons is greatly reduced. Thus, the system is photon-starved, and the resultant Comptonized spectrum is hard.

Merloni and Fabian (2002) also consider coronae as sources of powerful jets/outflows. They find that such outflows can render a source radiatively inefficient even if advection of energy into the BH is unimportant.

It is generally agreed that the temperatures in the corona are in the range 100–300 keV, with optical depths of 0.1–1 (e.g., Merloni & Fabian 2001b). There is little agreement, however, on the geometry and physical properties of the corona. Thus, a wide range of coronal models have been proposed (e.g., Haardt & Maraschi 1991; Dove *et al*. 1997a, 1997b; Kawaguchi *et al*. 2000; Rozanska & Czerny 2000; Meyer *et al*. 2000; Liu *et al*. 2002; Nowak *et al*. 2002). Liu *et al*. conclude that the primary difficulty in modeling the corona is the magnetic field that produces time variations and spatial inhomogeneities; in addition, one must consider complicated radiation/energy interactions between the disk and the corona. Because of the complexity of the problem, some students of the corona choose to apply their models to large quantities of X-ray (and radio) data, an approach that has proved fruitful (Wardzinski *et al*. 2002; Zdziarski *et al*. 2002, 2003).

Timing studies have been used to isolate the fast X-ray variability in BHBs as primarily emanating from the corona rather than from the accretion disk (Churazov *et al*. 2001). Timing studies have also created requirements to explain X-ray QPOs, such as the strong low-frequency QPOs that are prevalent in the VH state. Many coronal models do not deal with fast variability or QPOs explicitly, although there are exceptions, such as the "accretion–ejection instability" model (Tagger & Pellat 1999). In this model, magnetic spiral waves heat and accelerate material at those locations where the spiral waves and the disk are in corotation. During BHB outbursts, it has become exceedingly clear that spectral and timing characteristics at both X-ray and radio frequencies may change dramatically and abruptly. Therefore, no single model can account for all of the complex behavior, and our goal in this review is to summarize what is known about each X-ray state and to then discuss physical models in the context of a given state.

In addition to the models discussed above, we mention briefly the jet model (e.g., Falcke & Biermann 1995). This model is motivated by the observations of resolved radio and X-ray jets (Tables 4.2–4.3), by observations of radio/X-ray correlations (e.g., Hannikainen *et al*. 2001; Corbel *et al*. 2000), and by successes in modeling the broadband spectra of some systems as synchrotron radiation.

4.1.6 Some consequences of an event horizon

The properties of BHs and BH accretion flows are discussed in many texts (e.g., Shapiro & Teukolsky 1983; Abramowicz 1998; Kato *et al*. 1998). As mentioned above, a defining feature of a BH is its event horizon. Since BHs lack a material surface, some effects observed for NSs (e.g., Type I bursts) are absent for a BH. Similarly, a BH cannot sustain a magnetic field anchored within it, and hence cannot generate periodic X-ray pulsations, which are observed for many NSs.

Both Type I bursts and periodic pulsations are considered firm signatures of a NS (TL95). It is interesting to ask what fraction of cataloged, bright sources show either pulsations or Type I bursts. We examined this question using the catalog of van Paradijs (1995), selecting only the brighter sources ($F_X > 30$ μJy) that have been optically identified. We excluded the confirmed and candidate BH systems listed in Tables 4.1–4.3. For the 21 HMXB systems that met our selection criteria, we found that 18 out of 21 (86%) pulse. For 21 LMXB systems, we found that 12 burst and 2 pulse (67% burst or pulse). Thus a very high fraction of these

sources manifest behavior that identifies them as NSs. It is also interesting to consider which systems have failed to produce detectable bursts or pulsations because they are either an unusual NS source or they contain a BH. The three non-pulsing HMXB sources are 1700–37, 1947+30 and Cyg X-3; the six corresponding LMXB sources are LMC X-2, 1543–62, Sco X-1, GX349+2, GX9+9 and 1822–00.

4.1.7 The Rossi X-ray Timing Explorer (RXTE): 1996.0–present

RXTE has been in continuous operation since its launch on 1995 December 30. Its prime objective is to investigate the fundamental properties of BHs, NSs and white dwarfs by making high time resolution observations of extremely hot material located near BH event horizons or stellar surfaces. It is the largest X-ray detector array ever flown, and it provides energy coverage from 2 to 200 keV. It features high throughput (up to $\sim$150 000 counts s^{-1}) and $\sim$ 1 μs time resolution. RXTE's year-round, wide-sky coverage and its fast response time have made it an important vehicle for the study of transient phenomena and for the support of multiwavelength science.

The observatory comprises two large-area instruments (PCA and HEXTE) that act in concert, viewing the sky through a common 1° field of view. The third instrument is an All-Sky Monitor (ASM) that surveys about 80% of the sky each orbit. For descriptions of the instruments, see Levine *et al*. (1996), Swank (1998), Rothschild *et al*. (1998), and Bradt *et al*. (2001). The Proportional Counter Array (PCA), which has a total net area of 6250 cm^2, is the chief instrument. The High Energy X-ray Timing Experiment (HEXTE) covers the energy range 20–200 keV and has provided important spectral information beyond the reach of the PCA. However, the modest count rates of the HEXTE (e.g., 290 counts s^{-1} for the Crab) limit its use for timing studies. Indeed, it is the PCA (12,800 counts s^{-1} for the Crab with 5 PCUs) that has achieved groundbreaking results in high-energy astrophysics.

The ASM comprises three wide-field proportional counters that are mounted on a rotating boom. On a daily basis, it surveys about 90% of the sky to a sensitivity of about 10 mCrab for sources with known positions. New sources can be located down to 20 mCrab on a weekly basis with a typical position accuracy of $\sim 5'$. The ASM has proved indispensable in alerting PCA/HEXTE observers to targets of opportunity, and the ASM public archive containing the continuous lightcurves of $\sim$400 X-ray sources (both galactic and extragalactic) has been invaluable in studying the multiyear behavior of X-ray sources and in supplementing X-ray and multiwavelength (e.g., Chandra and HST) studies of individual sources. The data are also important to observers of AGN and gamma-ray bursts.

4.2 X-ray lightcurves, spectra and luminosity data

4.2.1 ASM lightcurves of BH binaries and BH candidates

To illustrate the diversity of behavior among BHBs and BHCs, we show in Figs. 4.2–4.5 the 1.5–12 keV ASM lightcurves and the (5–12 keV)/(3–5 keV) hardness ratio (HR2) for 20 of the systems listed in Tables 4.1–4.3 that were active during the past seven years. These lightcurves should be compared to the heterogeneous collection of $\sim$20 X-ray lightcurves collected by Chen *et al*. (1997). In making such comparisons, note that we use a linear intensity scale, whereas Chen *et al*. and most authors use a log scale. The lightcurves in Figs. 4.2–4.5 are ordered by RA, although we discuss them roughly in order of increasing

complexity. An intensity of 1 Crab corresponds to 75.5 ASM c s^{-1}. A hardness ratio (HR2) of 0.5 (1.5) generally corresponds to the HS state (LH state). All good data are included, although the time interval for binning the counts has been tailored to the source intensity. The hardness ratio is not plotted in the absence of a detectable 5–12 keV flux. References are cited sparingly in the narrative descriptions of the lightcurves given below; see Tables 4.1–4.3 for further references. In the following, the term "classic" lightcurve refers to an outburst profile that exhibits a fast rise and an exponential decay, like those observed for several pre-RXTE BH X-ray novae, including A0620–00, GS/GRS 1124–68, GS 2000+25 and GRO J0422+32 (TL95; Chen *et al*. 1997). Such classic lightcurves often show a secondary maximum (roughly a doubling of intensity) that occurs during the decline phase about 40–100 days after the onset of the outburst (TL95; Chen *et al*. 1997).

4.2.1.1 Black hole binaries

Figure 4.2 shows the lightcurves of all six of the X-ray novae with short outburst cycles that were detected by the ASM (Tables 4.1–4.2). *4U 1543–47*: An exceptionally clean example of a classic lightcurve with an e-folding decay time of ≈14 days. It lacks a secondary maximum, presumably because the outburst is so brief. For details and references on three prior outbursts of this source, see Chen *et al*. (1997). *XTE J1859+226*: A second example of a classic lightcurve that does show a secondary maximum (at about 75 days after discovery). Note the intense variability near the primary maximum. *XTE J1118+480*: One of five X-ray novae that remained in a hard state throughout the outburst and failed to reach the HS state. Note the prominent precursor peak.

Also shown in Fig. 4.2 are the complex and similar lightcurves of two X-ray novae with long orbital periods, GRO J1655–40 and XTE J1550–564. *GRO J1655–40*: This source has undergone two outbursts since its discovery in 1994 July. Shown here is the full lightcurve of the second, 16-month outburst. The double-peaked profile is quite unlike the classic profile of 4U 1543–47. During the first maximum in 1996, the source exhibited strong flaring and intense non-thermal emission (VH state). In 1997 the source spectrum was soft and thermal except for a hard episode at the very end of the outburst (Sobczak *et al*. 1999). Note the several absorption dips in the lightcurve of this high inclination system (Kuulkers *et al*. 1998). *XTE J1550–564*: The complex profile includes two dominant peaks during 1998–9, followed several hundred days later by a smaller peak in 2000. Not shown here are three very small outbursts (LH states) that have occurred subsequently. Some unusual characteristics include the slow 10-day rise following the source's discovery on 1998 September 6, followed by the dominant X-ray flare (6.8 Crab; September 19–20), and the abrupt ∼10-day decay timescale following each outburst. The source was predominantly in the VH or *intermediate* states during the first peak (1998), softening to the HS state during the second peak (1999). The spectral evolution through all of the X-ray states occurred much more rapidly during the small peak in 2000. *SAX J1819.3–2525 = V4641 Sgr*: As this extraordinary lightcurve shows, the source became active at a low level in the spring of 1999 (dashed line shows intensity × 50). Five months later it underwent a brief, violent flare during which the 1.5–12 keV intensity increased very rapidly (within 7 hours) from 1.6 to 12.2 Crab. Within two hours thereafter, the intensity declined to less than 0.05 Crab (Wijnands & van der Klis 2000, and references therein).

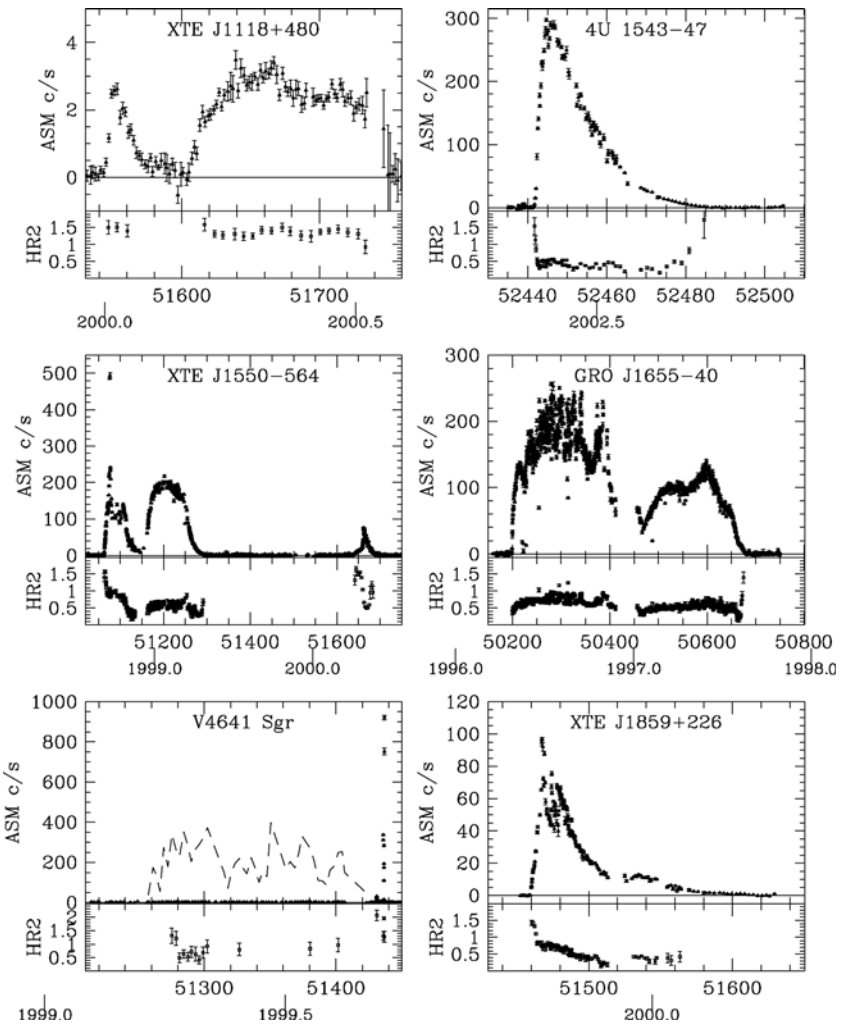

Fig. 4.2. Transient ASM lightcurves of six black hole binaries. For V4641 Sgr, the dashed line shows intensity ×50 in order to highlight the low-level activity that preceded the violent and short-lived flare.

Figure 4.3 shows the lightcurves of the two persistent BHBs (LMC X-3 and Cyg X-1) and two other BHBs that have been active throughout the RXTE era. *LMC X–3*: The lightcurve shows the large-amplitude cyclic modulation in the flux reported by Cowley *et al*. (1991); however, their ∼198 day cycle time is shorter than is indicated by these data. As the hardness ratio plot shows, the source remains in the HS state most of the time. However, at the local intensity minima, where there are gaps in the HR2 plot due to statistical limitations, the PCA observations show transitions to the LH state (Wilms *et al*. 2001a). *GX 339–4*: As shown, the source underwent major eruptions into a soft spectral state (HR ≈ 0.5) in 1998 and 2002. In the time between these two outbursts, the source was very faint (<2 mCrab) compared to its customary hard-state intensity of ∼30 mCrab, which it enjoyed prior to its 1998 outburst.

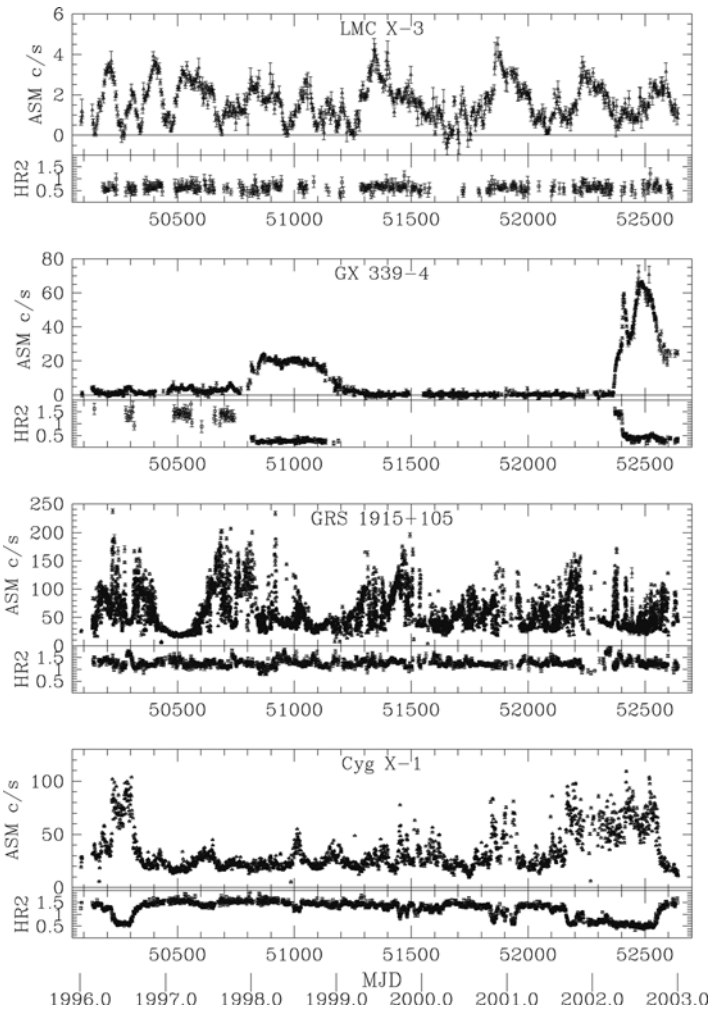

Fig. 4.3. Seven-year ASM light curves of four black hole binaries.

Remarkably, this transient BHB has never been observed in a fully *quiescent* state (Hynes *et al*. 2003). *GRS 1915+105*: This source exhibits extraordinary variations in both the X-ray and radio bands. Astonishing and yet repetitive patterns are sometimes seen in the X-ray lightcurves (Muno *et al*. 1999; Belloni *et al*. 2000; Klein-Wolt *et al*. 2002). For a 1992 X-ray lightcurve showing the birth of this source, see Chen *et al*. (1997). *Cyg X–1*: Transitions between the LH and HS states were first observed in this archetypal BH source (Section 4.3.1). However, as this record shows, there are both gradual and rapid variations in the hardness ratio that suggest both rapid state transitions and intermediate conditions between the HS and hard states (see Section 4.3.9).

4.2.1.2 Black hole candidates

Figure 4.4 displays the lightcurves of six BHCs with short outburst cycles. *XTE J748–288*: This short duration outburst that begins and ends in a hard spectral state is similar

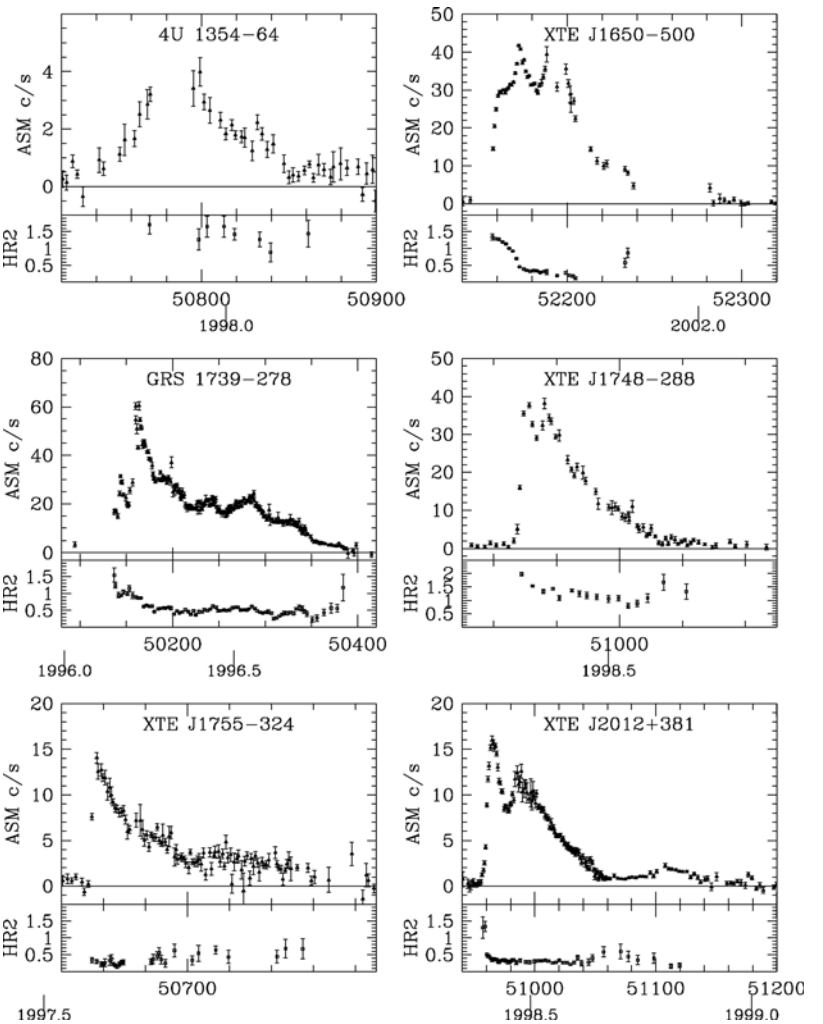

Fig. 4.4. Transient ASM light curves of six black hole candidates.

to the classic lightcurve of 4U 1543–47 (Fig. 4.2). The 1/e decay time is ≈16 days. This source is heavily absorbed, and the values of the hardness ratio are consequently increased. *GRS 1739–278*: A somewhat longer duration outburst with a nearly classic profile that includes a precursor peak, ∼40% variability near maximum, and undulations in intensity during the decay. Again, the outburst begins and ends with a hard spectrum. *XTE J1755–324*: This brief outburst, which follows an abrupt rise, provides yet another example of a classic lightcurve. This outburst is locked in the HS state. *XTE J2012+381*: This unusual lightcurve combines a classic rise to maximum followed directly by a precipitous drop in intensity. Also unusual are a large secondary maximum occurring just 30 days after discovery plus an additional late maximum at ∼140 days. *XTE J1650–500*: A complex lightcurve. At the onset of the outburst there is a very rapid rise followed by a slow rise. This unusual behavior is accompanied by a remarkable, slow (∼15 day) transition from a hard spectral state to a soft

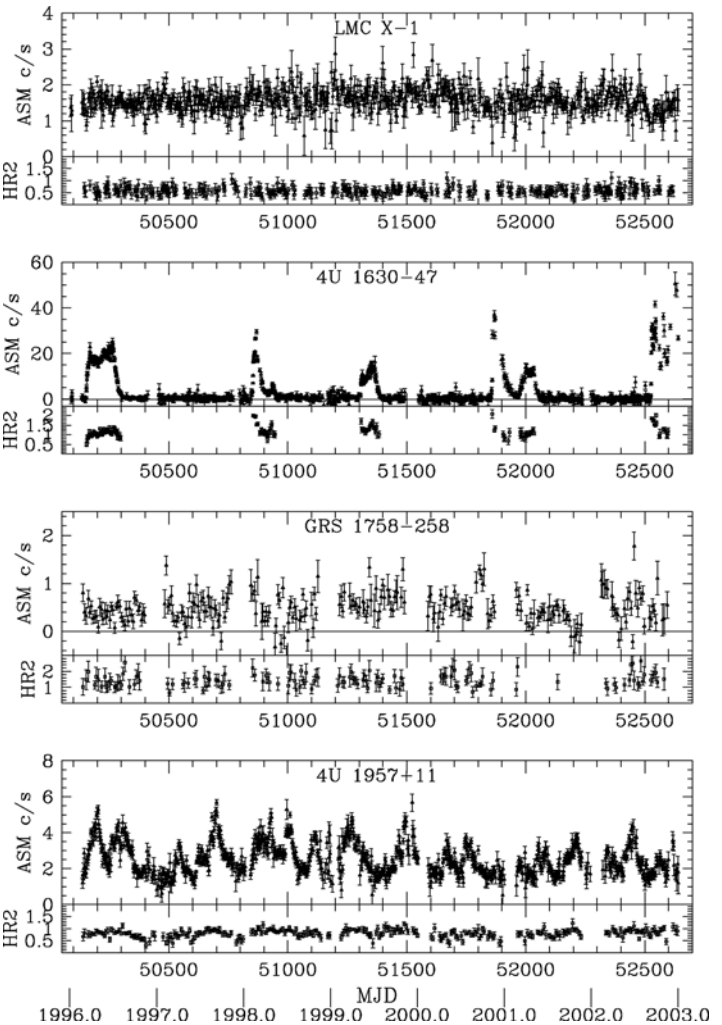

Fig. 4.5. Seven-year ASM light curves of three black hole candidates and the black hole binary LMC X-1.

one. *4U 1354–64*: A slow rise followed by a rather rapid decline. During this outburst, the source remained in the LH state (Brocksopp *et al*. 2001), whereas the HS state was reached during a brighter outburst in 1987 (Kitamoto *et al*. 1990). This source may be identical to Cen X-2, which reached a peak intensity of 13 Crab in 1967 (Brocksopp *et al*. 2001).

In Fig. 4.5 we show the lightcurves of the BHB LMC X-1 and the lightcurves of three BHCs. *LMC X-1*: The source is continually in a soft spectral state and maintains a relatively steady intensity. *4U 1630–47*: The ∼600 day recurrence time has been known for 25 years (Jones *et al*. 1976). Here we see five, nearly equally spaced outbursts. Note the very different profiles and fluences of the outbursts. Note also that the 1996 outburst starts with a soft spectrum. *GRS1758–258*: This hard galactic center source was discovered by GRANAT/SIGMA in 1991. Its spectrum extends to at least 300 keV (Sunyaev *et al*. 1991a). During 2001 it

underwent a transition to an unusual soft state of very low intensity (Smith *et al*. 2001; Miller *et al*. 2002d); the low flux level during that event is evident in the ASM record shown here. *4U 1957+11*: The source has long been considered a BHC based on its "ultrasoft" spectrum (White & Marshall 1984), although Yaqoob *et al*. (1993) have argued that the primary is a NS. The source displays a consistent flaring behavior and a soft spectrum over the 7 year interval.

It is often said that during its initial rise the spectrum of a BH X-ray nova transitions from a hard spectral state to a soft one. For several sources, the data in Figs. 4.2–4.5 support this view: 4U 1543–47, XTE J1550–564, XTE J1859+226, XTE J1650–500, GRS 1739–278, and XTE J2012+381. However, there are two clear counter-examples, sources whose spectra *hardened* during the initial rise: GRO J1655–40 (Fig. 4.2) and 4U 1630–47 (Fig. 4.5; first of five outbursts).

4.2.2 Synoptic studies of selected black hole binaries

It is important to follow the several-month spectral evolution of individual sources and to construct unified spectral models that can be used to represent the energy spectra of all BHBs. The necessary elements of such models can be deduced from a simple appraisal of the observational data: e.g., Cyg X-1 and other BHBs in the LH state show that the model must contain a non-thermal component, which can be well represented by a power-law function (TL95). On the other hand, the soft spectrum observed for most BH X-ray novae in the HS state is most widely modeled as a multi-temperature blackbody, which approximates the emission from an optically thick (relativistic) accretion disk. Many studies of spectral evolution therefore choose a composite model comprising disk blackbody and power-law components. Although this simple model has significant limitations, nevertheless it has proven to be widely applicable and quite effective in monitoring the spectra of BHBs, as we now discuss briefly by pointing to two examples.

Important studies of Ginga spectra using this model were made by Ebisawa *et al*. (1991, 1993, 1994). The authors added one refinement to the model, namely, a broad absorption feature above 7 keV. This feature is associated with the reflection of X-rays by an optically thick accretion disk (Ebisawa *et al*. 1994). With this model a successful and quantitative comparison was made of the spectra of Cyg X-1, LMC X-3, GS 2000+25, LMC X-1, GX339–4 and GS/GRS 1124–68 (Nova Mus 1991). This latter source, which exhibited a classic lightcurve, was observed 51 times in 1991 over a span of 235 days using the Ginga Large Area Counter (LAC). We direct the reader's attention to Figure 15 in Ebisawa *et al*. (1994), which shows the evolution over a full outburst cycle of the spectral parameters and fluxes for GS/GRS 1124–68. In their figure, it is evident that an important transition occurs 130 days into the outburst. For example, the photon spectral index suddenly decreases from 2.2–2.6 to a value near 1.6, the hard flux increases substantially and the soft disk flux decreases. This characteristic behavior, which has been observed for a number of BH X-ray novae, marks the transition from the HS state to the LH state.

We now compare the results obtained for GS/GRS 1124–68 to the results of an analogous study of the irregular BH X-ray nova XTE J1550–564, which was observed extensively by RXTE during its 1997–8 outburst (Sobczak *et al*. 2000b). A total of 209 pointed observations spanning the entire 255-day outburst were made using the PCA and HEXTE detectors. The 1998–9 lightcurve of the source is complex and includes a slow (10 day) rise to maximum, an intense (6.8 Crab) flare that occurred early in the outburst, and a "double-peaked" profile that

roughly separates the outburst into two halves of comparable intensity (Fig. 4.2). Sobczak *et al*. adopted very nearly the same spectral model and methodology as Ebisawa *et al*. (1994). We direct the reader's attention to Figure 4 and the accompanying text in Sobczak *et al*. (2000b), which describes a complex course of evolution relative to that of GS/GRS 1124–68. Very briefly, Sobczak *et al*. show that during the first half of the outburst QPOs are ubiquitous and the spectrum is dominated by the power-law component, which are conditions that mark the very high/intermediate state. In contrast, during the second half of the outburst QPOs are scarce and the spectrum is dominated by emission from the accretion disk, which corresponds to the HS state. During this state, the inner disk radius (Section 4.1.5) remained nearly constant for 4 months (Sobczak *et al*. 2000b). Very similar behavior has been observed for GS/GRS 1124–68 (Ebisawa *et al*. 1994) and for several other sources (TL95). The constancy of the disk inner radius is remarkable, given the accompanying, large variations in luminosity that are usually observed (TL95).

In overview, in both GS/GRS 1124–68 and XTE J1550–564 there are observations where thermal emission from the disk dominates the spectrum; such instances would surely be interpreted as the HS state. At other times, the disk spectrum is substantially modified and a *power-law component may dominate at either high or low luminosity, with a spectral shape that may appear either soft or hard.* In the case of Cyg X-1, the non-thermal LH state may be stable for many months or years. However, its soft-state spectrum was revealed to be a steep power law rather than a thermal spectrum (see Section 4.3.1), adding further ambiguity to any physical interpretation of the HS state. These results highlight the need to restructure our definitions of X-ray states, while avoiding the confusing terminology that has developed during the past 30 years. Accordingly, in Section 4.3 we address this issue and describe definitions of the X-ray states based on quantified properties of the X-ray energy spectra and power density spectra.

4.2.3 Relativistic iron emission lines

Strong evidence for accretion disks in active galactic nuclei has come from X-ray observations of broad iron Kα lines. In particular, in some Seyfert galaxies the very asymmetric profile of the Fe Kα line (e.g., its extended red wing) suggests strongly that the emission arises in the innermost region of a relativistic accretion disk (for reviews see Fabian *et al*. 2000; Reynolds & Nowak 2003). The good energy resolution of ASCA provided the first clear evidence for such a line profile (Tanaka *et al*. 1995). In some cases, the line profile indicates the presence of an accretion disk extending down to the ISCO (Weaver *et al*. 2001). The broad Fe Kα fluorescence line is thought to be generated through the irradiation of the cold (weakly ionized) disk by a source of hard X-rays (likely an optically thin, Comptonizing corona). Relativistic beaming and gravitational redshifts in the inner disk region can serve to create an asymmetric line profile.

In fact, the first broad Fe Kα line observed for either a BHB or an AGN was reported in the spectrum of Cyg X-1 based on EXOSAT data (Barr *et al*. 1985). It was this result that inspired Fabian *et al*. (1989) to investigate the production of such a line in the near vicinity of a Schwarzschild BH, a result that was later generalized by Laor (1991) to include the Kerr metric. Other early studies of relativistically smeared Fe Kα lines from BHBs were conducted by Done *et al*. (1992) and others. Their work was one part of a broader examination of the accretion geometry that is produced as hard X-rays from an overlying corona illuminate an

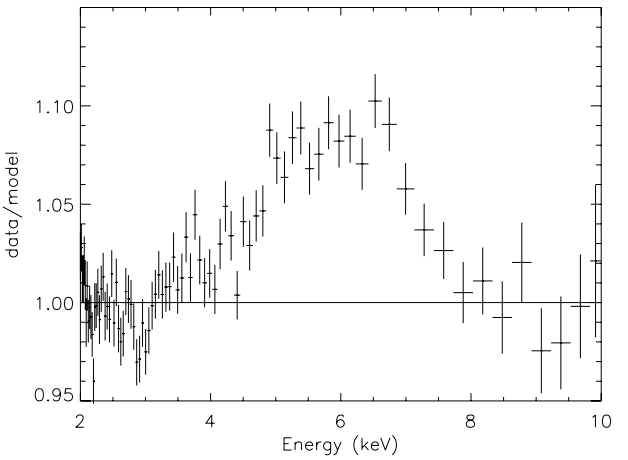

Fig. 4.6. Data/model ratio for XTE J1650–500. The model consists of multicolor disk blackbody and power-law components (Miller *et al*. 2002b). Note the non-Gaussian shape and low-energy extent of the line profile.

optically thick accretion disk. An Fe Kα line and a reflected continuum are always generated in this case (George & Fabian 1991; Matt *et al*. 1991). One example is a Ginga study of the reflected spectrum of V404 Cyg (Zycki *et al*. 1999a, 1999b). A limitation of this study is the use of proportional counter detectors (e.g., the Ginga LAC and RXTE PCA, which have an energy resolution of only FWHM $\approx$ 1.2 keV at Fe Kα). Such Fe Kα studies suffer both because the energy resolution is marginal and because the response matrices of the detectors are uncertain at the 1–2% level, while the Fe line profile in BHBs is typically only 1–5% above the X-ray continuum. Consequently, the results from these instruments must be considered with caution. Some Fe Kα sources that have been studied with RXTE include: GRO J1655–40 (Balucinska–Church & Church 2000); XTE J1748–288 (Miller *et al*. 2001); and GX 339–4 (Feng *et al*. 2001; Nowak *et al*. 2002).

More telling studies of the Fe Kα line have been achieved using the MECS and HP-GSPC detectors aboard BeppoSAX, which have a resolution of $\approx$0.6 keV at Fe Kα. Broad line profiles ($\sim$4–9 keV) have been observed for SAX J1711.6–3808 (in't Zand *et al*. 2002a) and XTE J1908+094 (in't Zand *et al*. 2002b); however, these profiles are rather symmetric and may be more a product of Compton scattering than relativistic broadening. BeppoSAX studies have also revealed other systems with broad, asymmetric Fe K profiles that resemble the predictions of relativistic smearing: GRS 1915+105 (Martocchia *et al*. 2002) and V4641 Sgr (Miller *et al*. 2002a). Interestingly, for both of these systems the inner disk radius deduced from the line profile is consistent with the radius of the ISCO for a Schwarzschild BH, suggesting that rapid spin is not required.

Spectral studies at higher resolution have been made recently with XMM-Newton and Chandra. Using the XMM EPIC-MOS1 detector, Miller *et al*. (2002b) find for XTE J1650–500 a broad, skewed Fe Kα emission line (Fig. 4.6) which suggests the presence of an extreme Kerr BH and indicates a steep radial falloff of disk emissivity with radius. An observation of Cyg X-1 with the HETGS grating and ACIS-S detector aboard Chandra revealed a broad

line centered at ≈5.82 keV with a FWHM of ≈1.9 keV (Miller *et al*. 2002c). Also present was a smeared Fe edge at ≈7.3 keV. The authors conclude that the line is predominantely shaped by Doppler/gravitational effects and to a lesser degree by Compton scattering due to reflection.

4.2.4 Super-Eddington luminosities

Recently there has been considerable interest in ultraluminous X-ray sources (ULXs) in external galaxies with 0.5–10 keV luminosities in the range $10^{39}-10^{40.5}$ erg s^{-1} (Makishima *et al*. 2000; Fabbiano *et al*. 2001; Humphrey *et al*. 2003; Miller *et al*. 2003b; Chapter 12). The luminosities of ULXs greatly exceed the Eddington limit of a 1.4 $M_\odot$ NS: $L_{\rm Edd} = 1.3 \times 10^{38}(M_1/M_\odot)$ erg s^{-1}. The most luminous systems also exceed by a factor of ∼20 the Eddington luminosity of a typical 10 $M_\odot$ BH. This fact has led to the suggestion that the most luminous ULXs are a new class of accreting BHs with masses ∼100 $M_\odot$ (Makishima *et al*. 2000; Fabbiano *et al*. 2001). Alternatively, it has been suggested that the ULXs are powered by conventional stellar-mass BHs that radiate anisotropically (King *et al*. 2001; Chapter 13). We examine this question by comparing as directly as possible the luminosities of the ULXs to the luminosities of the 18 BHBs listed in Tables 4.1–4.2. We also mention briefly apparent differences between ULXs and BHBs in their spectra and duty cycles.

In terms of the maximum flux density of a BHB, $F_{\rm X,max}$ (Table 4.1), the 2–11 keV luminosity is: $L_{\rm X}/L_{\rm Edd} \approx 2.6 \times 10^{35} \times F_{\rm X,max}(\mu{\rm Jy}) \times (D/10\ {\rm kpc})^2$ (Bradt & McClintock 1983). For a Crab-like spectrum (Section 4.1.2), the flux in the 0.5–10 keV (ULX) band is a factor of 1.9 greater (although this is somewhat of an overestimate compared to the use of a thermal spectrum). Including this factor and using the distances and peak fluxes in Table 4.1, we find that the three most luminous BHBs are V4641 Sgr (6.2×10^{39} erg s^{-1}), 4U 1543–47 (4.2×10^{39} erg s^{-1}) and GRS 1915+105 (2.4×10^{39} erg s^{-1}). Thus, at peak luminosity these three BHBs appear to be in the same league as many of the ULXs observed in external galaxies. Moreover, using the mass measurements from Table 4.2, it appears that all three BHBs were super-Eddington at maximum (0.5–10 keV): $L_{\rm X}/L_{\rm Edd} = 7.0$, 3.5 and 1.4 for V4641 Sgr, 4U 1543–47 and GRS 1915+105, respectively.

This comparison of BHBs and ULXs is somewhat problematic: First, the distances of the BHBs are uncertain, and we have no direct measurements of their fluxes in the 0.5–2 keV band. Nevertheless, the results quoted above suggest that the peak luminosities of a few BHBs approach the peak luminosities observed for ULXs to within a factor of ≈5 (e.g., Miller *et al*. 2003b). Second, the luminosity shortfall of BHBs may be ascribable to the small sample of 18 BHBs compared to the much larger sample of comparable systems that have likely been detected in surveys of external galaxies. Finally, some ULXs exhibit spectral properties unlike those of BHBs. In particular, the cool disk spectra and the longevity at high luminosity of the most luminous ULXs may distinguish them from BHBs in the Milky Way (Miller *et al*. 2003a, 2003b). The differences among ULX spectra also suggest that the sample may be heterogeneous.

We conclude by noting that super-Eddington luminosities have plainly been observed for a few NS systems. The most clear-cut case is A0535–668, the "LMC transient." This pulsating NS binary with a firm distance of $D = 50$ kpc (Freedman *et al*. 2001) achieved a peak luminosity of $L_{\rm X} \approx 1.2 \times 10^{39}$ erg s^{-1} , assuming isotropic emission (Bradt & McClintock

1983, and references therein). This is 6.9 times the Eddington luminosity of a canonical 1.4 $M_\odot$ NS or 3.8 times the Eddington luminosity of a hypothetical 2.5 $M_\odot$ NS.

4.3 Emission states of black hole binaries

As discussed in Sections 4.1 and 4.2, BHBs exhibit thermal and non-thermal components of X-ray emission, both of which can vary widely in intensity. It has long been recognized that BHBs undergo transitions between quasi-stable states in which one or the other of these components may dominate the X-ray luminosity. In the past, the study of BH emission states was based almost exclusively on X-ray spectral and timing studies. More recently, however, the results of X-ray studies have been supplemented with critical contributions by radio, optical and gamma-ray observers to give us a more physical and fruitful framework for regarding the emission states. In the following sections, we review the characteristic behavior that defines each of the principal X-ray states of BHBs. We then describe the current picture of each state in terms of physical structures and the nature of the accretion flow. Finally, we discuss the prospects of using these states to deduce the properties of BHs.

4.3.1 Historical notes on X-ray states

In the spring of 1971, Tananbaum *et al*. (1972) observed a remarkable X-ray state change in Cyg X-1 during which the average soft flux (2–6 keV) decreased by a factor of 4 and the average hard flux increased by a factor of 2. Simultaneously, the radio counterpart of Cyg X-1 brightened. It was later found that luminous X-ray novae such as A0620–00 exhibited similar spectral transitions, suggesting that common emission mechanisms were at work in both persistent and transient BHCs (Coe *et al*. 1976). These early results suggested that such global spectral changes might signify important changes in accretion physics.

As the many lightcurves in Section 4.2 illustrate, the soft X-ray state is generally seen at higher luminosity, motivating frequent references to the *high/soft* (HS) state. In this state, the spectrum may also display a "hard tail" that contributes a small percentage of the total flux. As shown by the synoptic studies discussed in Section 4.2.2, the soft state is best explained as $\sim$1 keV thermal emission from a multi-temperature accretion disk (see Section 4.1.5), as foreseen in the standard theory for accretion in BHBs (Shakura & Sunyaev 1973). However, it has been found that the soft state of Cyg X-1 is not consistent with a thermal interpretation (Zhang *et al*. 1997b), and this has caused considerable confusion as to the proper way to understand Cyg X-1 and/or describe the HS state. In seeking a physical basis for describing X-ray states, it turns out that Cyg X-1 is not a good choice as a prototype, and further remarks about the states in Cyg X-1 are given in a separate section below (Section 4.3.9).

In the hard state the 2–10 keV intensity is comparatively low, prompting the name *low/hard* (LH) state. The spectrum is non-thermal and conforms to a power law with a typical photon index $\Gamma \sim 1.7$ (2–20 keV). In this state, the disk is either not detected at 2–10 keV (e.g., Belloni *et al*. 1999), or it appears much cooler and larger than it does in the soft state (Wilms *et al*. 1999; McClintock *et al*. 2001b).

An additional X-ray state of BHBs was identified in the Ginga era (Miyamoto *et al*. 1993). It is characterized by the appearance of QPOs in the presence of both disk and power-law components, each of which contributes substantial luminosity (e.g., $> 0.1 L_{\rm Edd}$; van der Klis 1995). In this state, which is referred to as the *very high* (VH) state, the power-law component is observed to be steep ($\Gamma \sim 2.5$). Initially, there were only two BHBs (GX339–4 and Nova

Mus 1991) that displayed this behavior, but many additional examples have been seen in the RXTE era.

It was first thought that the two non-thermal states (i.e., LH and VH states) could be distinguished through differences in their photon spectral indices, luminosities, and power density spectra. However, as shown below, the latter two differences have become blurred; nevertheless, the spectral index continues to be a valid discriminator. The importance of distinguishing between the LH and VH states was emphasized in a ∼40–500 keV study of seven BHBs with the OSSE instrument aboard the Compton Gamma-Ray Observatory (Grove *et al*. 1998). The gamma-ray spectra of these sources separate naturally into two distinct groups which correspond to the LH state and the VH state, respectively. (1) For the first group it was shown that the X-ray LH state corresponds with a "breaking gamma-ray state" in which the spectrum below ∼100 keV is harder than that of the VH state, but then suffers an exponential cutoff near 100 keV. (2) The second group exhibits a power-law gamma-ray spectrum with photon index $2.5 < \Gamma < 3.0$ over the entire range of statistically significant measurements. This gamma-ray photon index is consistent with the X-ray photon index of the VH state. Furthermore, contemporaneous X-ray observations (e.g., with ASCA) confirmed that a luminous thermal component coexists with the power-law component, which is one characteristic of the VH state noted above.

4.3.2 X-ray states as different physical accretion systems

Several recent developments in the study of BHBs have taken us beyond a largely phenomenological description of X-ray states to one based on physical elements (e.g., accretion disk, ADAF, jet, and corona). Although this work is still incomplete, the fundamental distinctions between the states are becoming clearer. For example, a key development in this regard is the recognition of a persistent radio jet associated with the LH state that switches off when the source returns to the HS state (Section 4.3.6; Chapter 9). Another example, revealed by gamma-ray observations, is the very different coronal structure that is responsible for the clear-cut distinction between the LH state and the VH state (Section 4.3.1). Arguably, each X-ray state can be regarded as a different accretion system that can be used in unique ways to study accretion physics and the properties of accreting BHs.

In the sections below, we review each of the four canonical X-ray states of BHBs, including the long-lived *quiescent* state. We illustrate the uniform X-ray properties of each of the three active states by showing X-ray spectra and power spectra for several BHBs and BHCs observed by RXTE. We also examine a possible fifth X-ray state, the *intermediate* state, as part of our discussion of the VH state. While presenting this overview, we suggest an alternative set of state names that are motivated by the kinds of emergent physical pictures mentioned above. Although the new state names depend critically on multi-wavelength results (i.e., radio to gamma-ray), we nevertheless attempt to define them on the basis of X-ray data. Furthermore, based on extensive observations of many sources with RXTE (e.g., see Section 4.2.2), *we abandon luminosity as a criterion for defining the states of BHBs* (with the exception of the quiescent state). We do not deny that there are correlations between states and luminosity in many sources, in particular the tendency of the HS to occur at higher luminosity compared with the hard state. However, as shown below, there are clear exceptions to these trends and each X-ray state has now been observed to span a range of two or more decades in X-ray luminosity.

4.3.3 Notes on X-ray spectral analyses

Many spectral models have been developed to describe one or more of the spectral states of BHBs. Most models for the non-thermal continuum components invoke inverse Compton or synchrotron emission, but these mechanisms can be applied with many different assumptions and geometric details. Some models closely constrain the relationship between spectral components (e.g., thermal emission providing seed photons for Comptonization), while others allow the spectral components to vary independently. In presenting this review, we have adopted the following pragmatic and generic strategy. As discussed in Section 4.2.2, the spectra of BHBs are well described by a model consisting of a multi-temperature accretion disk component and a power-law component (which may require an exponential cutoff at high energy). This model provides a robust, first-order description of BHB spectra that covers all of the emission states, and we adopt it to help define the states and to compare the luminosities of the thermal and non-thermal components. We also include additional features in the model, such as Fe line emission and a disk reflection component, when the normalization parameter for such a feature is significant at the level of 5σ. In the following discussions of each X-ray state, we comment on some physical interpretations and controversies related to the problem of determining the origin of the power-law component.

4.3.4 Quiescent state

A BHB spends most of its life in a quiescent state that can be summarized as *an extraordinarily faint state* ($L_X = 10^{30.5}$–$10^{33.5}$erg s^{-1}), *with a spectrum that is distinctly non-thermal and hard* ($\Gamma = 1.5 - 2.1$). The first short-period X-ray nova to be detected in quiescence was A0620–00 ($P_{orb} = 7.8$ hr); its X-ray luminosity was several times 10^{30} erg s^{-1}, which is only $\sim 10^{-8}$ of its outburst luminosity (McClintock *et al*. 1995; Narayan *et al*. 1996). The long-period systems, however, are significantly more luminous in quiescence because their mass transfer rates are driven by the nuclear evolution of their secondaries rather than by gravitational radiation (Menou *et al*. 1999). For example, the X-ray luminosity of V404 Cyg ($P_{orb} = 155.3$ hr) is typically $L_X \sim 10^{33}$ erg s^{-1} (Kong *et al*. 2002), but can vary by an order of magnitude in one day (Wagner *et al*. 1994).

It is now possible to make sensitive measurements in the quiescent state using Chandra and XMM-Newton. The minimum quiescent-state luminosities (0.5–10 keV) of five BHs and stringent upper limits on two others have been reported by Garcia *et al*. (2001) and Narayan *et al*. (2002). Three additional BHBs were observed in quiescence more recently (Sutaria *et al*. 2002; Hameury *et al*. 2003; McClintock *et al*. 2003a). Considering only the five short-period systems ($P_{orb} \lesssim 1$ day; see Narayan *et al*. 2002) that have been detected, one finds that four of them (XTE J1118+480, GRO J0422+32, GS 2000+25, and A0620–00) have Eddington-scaled luminosities that are $\approx 10^{-8.5}$. GS 1124–68 is more luminous by about an order of magnitude. As Garcia *et al*. (2001) and Narayan *et al*. (2002) show, the Eddington-scaled luminosities of several ostensibly similar X-ray novae that contain NS primaries are about 100 times higher, a conclusion that is quite robust. In the context of the advection-dominated accretion flow model, these authors argue that the relative faintness of the BH X-ray novae provides strong evidence that they possess event horizons. For a thorough discussion of their model and several alternative models, see Narayan *et al*. (2002). Apart from any specific model, it appears quite reasonable to suppose that the established faintness of quiescent BHs is somehow connected with the existence of the event horizon.

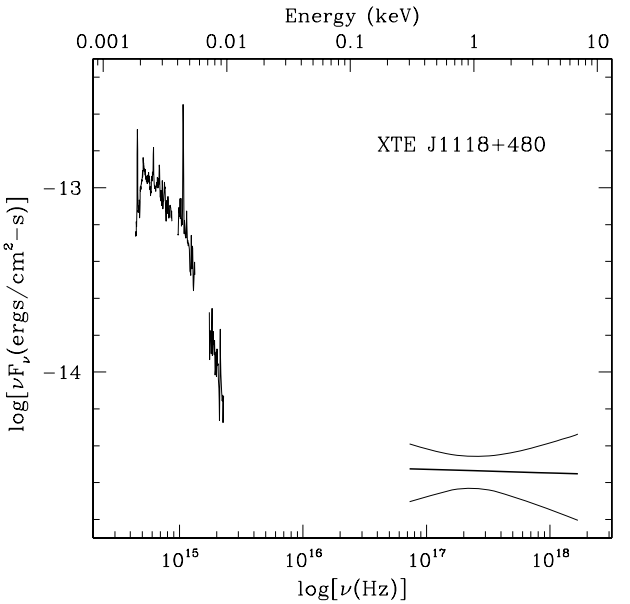

Fig. 4.7. Spectrum of XTE J1118+480 in the quiescent state based on simultaneous, multiwavelength observations. The optical spectrum of the mid-K dwarf secondary has been subtracted. Note the Planckian shape of the optical/UV continuum, which is punctuated by a dominant Mg II 2800 Å line and a strong Hα line on the far left. The best-fit X-ray model is indicated by the heavy, horizontal line; the 90% error box is defined by the flanking curved lines.

The quiescent spectra of BHBs are well fitted by a single power-law plus interstellar absorption. The best-determined photon spectral indices are consistent with the value $\Gamma \approx 2$. Specifically, for A0620–00 and XTE J1118+480, respectively, one has $\Gamma = 2.07(+0.28, -0.19)$ (Kong *et al*. 2002) and $\Gamma = 2.02 \pm 0.16$ (McClintock *et al*. 2003), where the column density is determined from the optical extinction. Only V404 Cyg allows a useful determination of both the column density and the photon index: $N_{\rm H} = (6.98 \pm 0.76) \times 10^{21}$ cm^{-2} and $\Gamma = 1.81 \pm 0.14$ (Kong *et al*. 2002).

A multiwavelength spectrum of XTE J1118+480 in quiescence is shown in Fig. 4.7 (McClintock *et al*. 2003). This shortest-period BHB ($P_{\rm orb} = 4.1$ hr) is located at b= 62°, where the transmission of the ISM is very high (e.g., 70% at 0.3 keV). A very similar multiwavelength spectrum was observed earlier for A0620–00 (McClintock & Remillard 2000), which implies that the spectrum shown in Fig. 4.7 represents the canonical spectrum of a BHB radiating at $10^{-8.5} L_{\rm Edd}$. The spectrum comprises two apparently disjoint components: a hard X-ray spectrum with a photon index $\Gamma = 2.02 \pm 0.16$, and an optical/UV continuum that resembles a 13 000 K disk blackbody spectrum punctuated by several strong emission lines.

The ADAF/disk model (see Section 4.1.5) accounts well for the following properties of BHBs in the quiescent state: (1) The hard power-law spectra (Narayan *et al*. 1996, 1997; Hameury *et al*. 1997; Quataert & Narayan 1999; McClintock *et al*. 2003); (2) the faintness of BHs relative to NSs (Narayan *et al*. 1997, 2002; Garcia *et al*. 2001; (3) the several-day delay in the optical/UV lightcurve when X-ray novae go into outburst (Hameury *et al*. 1997); and

(4) the broadband spectrum shown in Fig. 4.7 (McClintock *et al*. 2003). Especially significant is the prediction, confirmed by observations, that the accretion disk is truncated at a large inner radius in both the quiescent and LH states (Narayan 1996; Esin *et al*. 1997; McClintock et al. 2001b, 2003a).

4.3.5 Thermal-dominant (TD) state or high/soft (HS) state

As discussed in Section 4.1.5, considerations of basic principles of physics predict that accreting BHs should radiate thermal emission from the inner accretion disk (Shakura & Sunyaev 1973). It was therefore readily accepted that the soft X-ray state of BHBs represents thermal emission. Confirmations of this picture are largely based on the successful ability to describe the soft X-ray component using the simple multi-temperature accretion disk model (MCD model; Section 4.1.5). In Figs. 4.8 and 4.9 we show the energy spectra and power spectra, respectively, of 10 BHBs in the "thermal-dominant" (TD) or high/soft (HS) X-ray state as observed by RXTE. The thermal component of the model, where it can be distinguished from the data, is shown as a solid line, and the power-law component is shown as a dashed line. Typically, below about 10 keV the thermal component is dominant. With a few exceptions, the temperature of this component is in the range 0.7–1.5 keV (Table 4.4). The power-law component is steep ($\Gamma = 2.1-4.8$) and faint. In GRS 1915+105 the power-law falls off even more steeply with an e-folding cutoff energy of 3.5 keV; similar behavior has been reported for GRO J1655–40 (Sobczak *et al*. 1999).

In Fig. 4.8 we feature data for BHBs obtained during pointed observations with RXTE, while data for BHCs are shown in Fig. 4.9. The spectra of four of the sources in the figures (4U 1543–47, GX 339–4, XTE J1755–324, and XTE J2012+381) correspond to the maximum 2–20 keV luminosities observed during RXTE pointings (i.e., considering all possible states). The power density spectra (PDS) in Figs. 4.8 and 4.9 show that the variability in the TD state is either weak or the power scales roughly as ν^{-1}, which is a characteristic of many physical processes including turbulence (Mandelbrot 1999). The total rms power (r) integrated over 0.1–10 Hz in the PDS (2–30 keV) is in the range $0.01 \lesssim r \lesssim 0.06$, which is significantly below that of the LH state. QPOs in the range 0.1–30 Hz are generally not seen in individual TD observations, but large groups of PDS in the TD state have yielded weak QPOs in two cases. A 0.3% (rms) QPO at 27 Hz was seen in a sum of 27 observations ("1997 soft state") of GRO J1655–40 (Remillard *et al*. 1999), and a similar (0.3%) QPO at 17 Hz was seen in 69 observations of XTE J1550–564 in the soft state during 1998–9 (MJD 51160–51237; Homan *et al*. 2001).

In the following section, we show that a transition to the LH state is followed by the appearance of a hard and dominant power-law spectrum, while the accretion disk, if visible, shows a substantial decrease in temperature. On the other hand, a transition to the VH state (Section 4.3.7) is marked by a steeper power-law spectrum accompanied by either a normal ($\sim$1 keV) disk or one that appears hot with a small inner radius. This latter transition is also accompanied by the presence of QPOs that appear when the disk contribution to the total, unabsorbed flux at 2–20 keV falls below the level of 0.75 (Sobczak *et al*. 2000a). *We thus define the TD state as the set of conditions for which the disk-flux fraction is above 75% (2–20 keV), the PDS (2–30 keV) shows no QPOs or very weak features ($rms \ll 1\%$), and the power continuum is also weak:* $r \lesssim 0.06$ *integrated over 0.1–10 Hz.*

As further support for a thermal interpretation of the soft X-ray component, many studies have found evidence for disk luminosity variations in which the inner disk radius (which

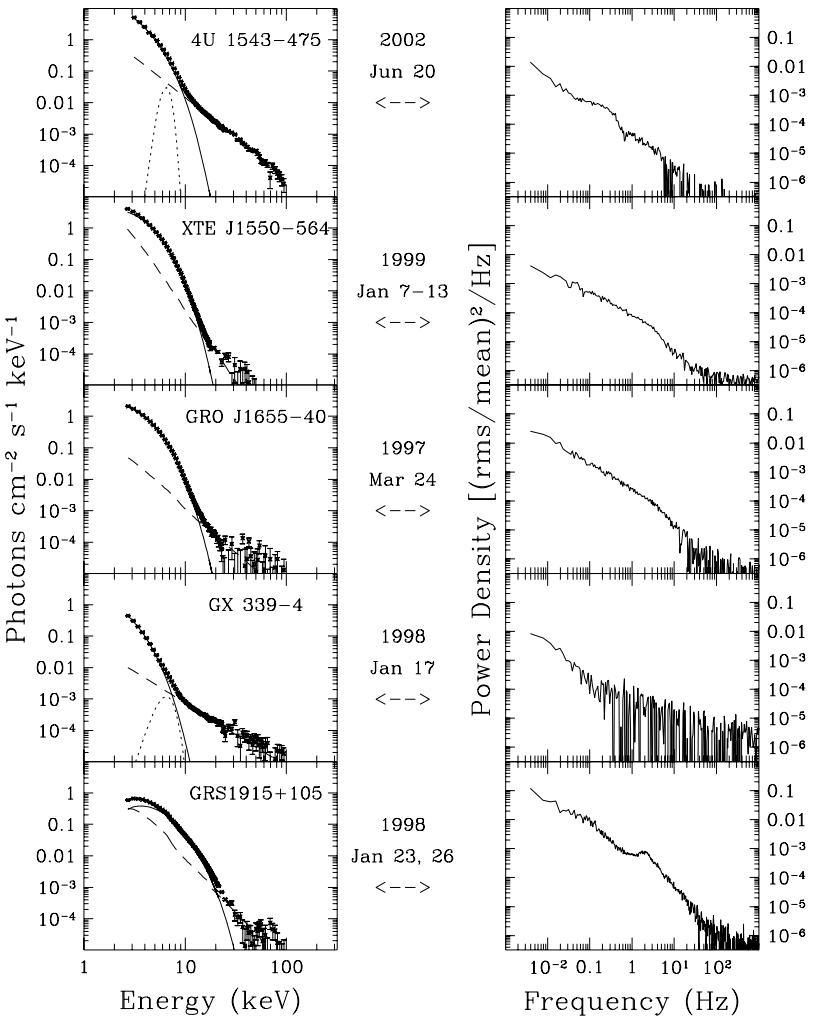

Fig. 4.8. Sample X-ray spectra of BHBs in the X-ray state for which the dominant component is thermal emission from the accretion disk. The energy spectra (*left*) are decomposed into a thermal component, which dominates below ∼10 keV (solid line), and a faint power-law component (dashed line); GRS 1915+105 is modeled with a cutoff power-law (see text). For two of the BHBs, an Fe line component is included in the model (dotted line). The corresponding power spectra (2–30 keV) are shown in the panels on the right.

scales as the square root of the MCD normalization parameter) appears constant while the luminosity variations depend only on changes in temperature (Section 4.2.2). This effect is reported in a study of LMC X-3 (Kubota *et al*. 2001) and is illustrated in Fig. 4.10. The measured disk flux and apparent temperature successfully track the relation $L \propto T^4$ (solid line) expected for a constant inner disk radius. The figure also shows gross deviations from this relation associated with the VH state of GRO J1655–40, a topic that is addressed below in Section 4.3.7.

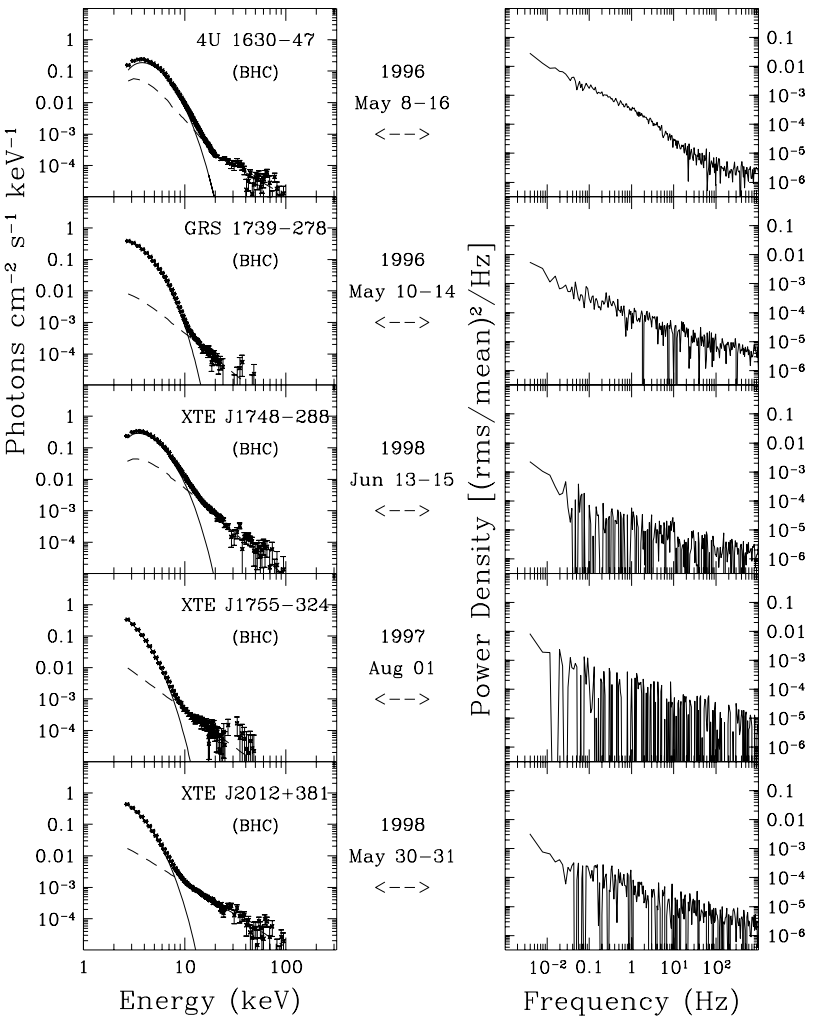

Fig. 4.9. Sample X-ray spectra of BHCs in the TD X-ray state. In the panels on the left, the energy spectra are shown deconvolved into a thermal component due to the accretion disk (solid line) and a power-law component (dashed line). The corresponding power spectra (2–30 keV) are shown in the right half of the figure.

Because of the successes of the simple MCD model, the inner disk radius has been used to provide a type of spectroscopic parallax. In principle, the inner disk radius can be deduced for those sources for which the distance and disk inclination are well constrained from the disk normalization parameter, $(R_{\rm in}/{\rm D})^2 \cos\theta$, where $R_{\rm in}$ is the inner disk radius in kilometers, D is the distance to the source in units of 10 kpc, and θ is the inclination angle of the system (e.g., Arnaud & Dorman 2002). However, the MCD model is Newtonian, and the effects of GR and radiative transfer need to be considered. GR predicts a transition from azimuthal to radial accretion flow near $R_{\rm ISCO}$, which depends only on mass and spin and ranges from 1 to 6 $R_{\rm g}$ for a prograde disk (Section 4.1.5). Therefore, for a system with a known distance and inclination, in principle it may be possible to estimate the spin parameter via an

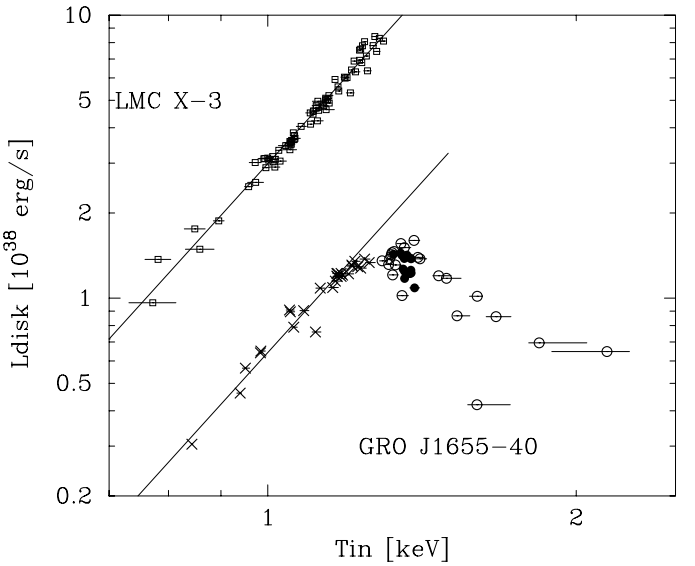

Fig. 4.10. The accretion disk luminosity vs. temperature at the inner accretion disk (Kubota *et al*. 2001). For GRO J1655–40, the symbol type denotes the time periods: early outburst (filled circles), first phase (open circles), and second phase (crosses). The solid lines represent the $L_{\rm disk} \propto T_{\rm in}^4$ relation.

X-ray measurement of the inner radius and an optical determination of the mass. In lieu of a fully relativistic MHD model for the accretion disk, one could attempt to correct the MCD model parameters to account for the effects of radiative transfer through the disk atmosphere (Shimura & Takahara 1995) and for modifications on the structure and emissivity of the inner disk due to GR (Zhang *et al*. 1997a). However, the accuracy of these corrections has been challenged (Merloni *et al*. 2000; Gierlinski *et al*. 1999), and at present the chief value of the MCD model is in monitoring the temperature and the fractional flux contribution from the accretion disk.

4.3.6 Hard X-ray state associated with a steady radio jet

The conventional name for this state is the *low/hard* (LH) state; however, henceforth we refer to it simply as the *hard* state for the reasons given in Section 4.3.2. As noted earlier (Section 4.3.1), Cyg X-1 and many transient sources have been observed to undergo transitions to a hard, non-thermal X-ray spectral state. This usually occurs at luminosities below that of the TD state, and the spectrum can be modeled (e.g., in the range 1–20 keV) as a power-law function with a photon index ∼1.7. In some sources, such as Cyg X-1 and GS 1354–64, this hard state is accompanied by a broad enhancement at 20–100 keV, which is interpreted as reflection of the power-law component from the surface of the inner accretion disk (Di Salvo *et al*. 2001). This component is discussed further at the end of this section.

In recent years there have been rapid advances in associating the X-ray hard state with the presence of a compact and quasi-steady radio jet (for a thorough review, see Chapter 9). This relationship, which constitutes one of the foundations of the "disk:jet" connection, is based on at least three arguments. First, VLBI radio images have shown a spatially resolved

radio jet during episodes of quasi-steady radio and hard X-ray emission from GRS 1915+105 (Dhawan *et al*. 2000) and Cyg X-1 (Stirling *et al*. 2001). In both instances the radio spectrum was flat or inverted. In the case of GRS 1915+105, the radio jet in the hard state appears smooth at many different spatial scales, in contrast to the rapidly separating knots seen for ballistic, superluminal jets from the same source. Second, more generally (i.e., when VLBI images are not available), X-ray sources that remain in the hard state for prolonged periods (weeks to years) are highly likely to show correlated X-ray and radio intensities and a flat radio spectrum (Fender *et al*. 1999a; Fender 2001; Corbel *et al*. 2000, 2003; Klein-Wolt *et al*. 2002; Marti *et al*. 2002). In one of these examples, GX 339–4, the jet interpretation is further supported by the detection of 2% linear radio polarization with a nearly constant position angle (Corbel *et al*. 2000). Finally, it is now routine to witness the quenching of the persistent radio emission whenever an X-ray source exits the hard state and returns to the TD state (Fender *et al*. 1999b; Brocksopp *et al*. 1999; Corbel *et al*. 2000).

In Fig. 4.11, the five BHBs shown in the hard state are the same sources shown earlier in the TD state (Fig. 4.8). In the following cases, the X-ray data have been selected to coincide with specific radio observations: Flat-spectrum radio emission was reported for both XTE J1550–564 on 2000 June 1 during the decay of its second outburst (Corbel *et al*. 2001) and for GX 339–4 on 1999 March 3 (Corbel *et al*. 2000). In addition, both the radio and X-ray emission of GRS 1915+105 are fairly steady on 1997 October 22, which coincides with one of the days on which the core radio image shows the extended structure of a nuclear jet (Dhawan *et al*. 2000).

A second sample of BHBs and BHCs in the hard state is shown in Fig. 4.12. The hard state for XTE J1748–288 occurred during decay from the HS state (Revnivtsev *et al*. 2000c). On the other hand, the data shown for XTE J1118+480 and GS 1354–64 correspond with outburst maxima; these outbursts never reached the HS state (Revnivtsev *et al*. 2000a; Frontera *et al*. 2001b). Associated radio emission for these two sources was reported with jet interpretations by Fender *et al*. (2001) and Brocksopp *et al*. (2001), respectively. Finally, GRS 1758–258 and Cyg X-1 spend most of their time in the hard state, and their energy spectra are shown in the bottom two panels of Fig. 4.12. These RXTE observations happened to coincide with radio observations that confirm a flat radio spectrum. In the case of GRS 1758–258, core radio emission (as distinct from the extended radio lobes observed for this source) was reported on 1998 August 3 and 5 by Marti *et al*. (2002), and a clear detection of Cyg X-1 during 1997 December 12–17 is evident in the public archive of the Greenbank Interferometer available on the NRAO website.

The physical condition of the accretion disk in the hard state is a subject of great significance in the effort to build a detailed physical model for both the jet and the X-ray source. Observations with ASCA, which provided sensitivity in the range 0.5 to 9 keV, showed that the hard states of both GX 339–4 (Wilms *et al*. 1999) and Cyg X-1 (Takahashi *et al*. 2001) exhibit power-law spectra with an additional soft X-ray excess that can be modeled as a large and cool ($\sim$0.1–0.2 keV) accretion disk. The spectral decompositions illustrated in Fig. 4.11 provide some evidence for a soft disk component in both GRO J1655–40 and GRS 1915+105, although RXTE is much less sensitive than ASCA to thermal spectra with temperatures well below 1 keV. By far the best direct measurements of the temperature and inner radius of an accretion disk in the hard state have been made for XTE J1118+480, which has an extraordinarily small interstellar attenuation (e.g., only 30% at 0.3 keV). Based on simultaneous HST, EUVE and Chandra observations made in outburst, it was determined that

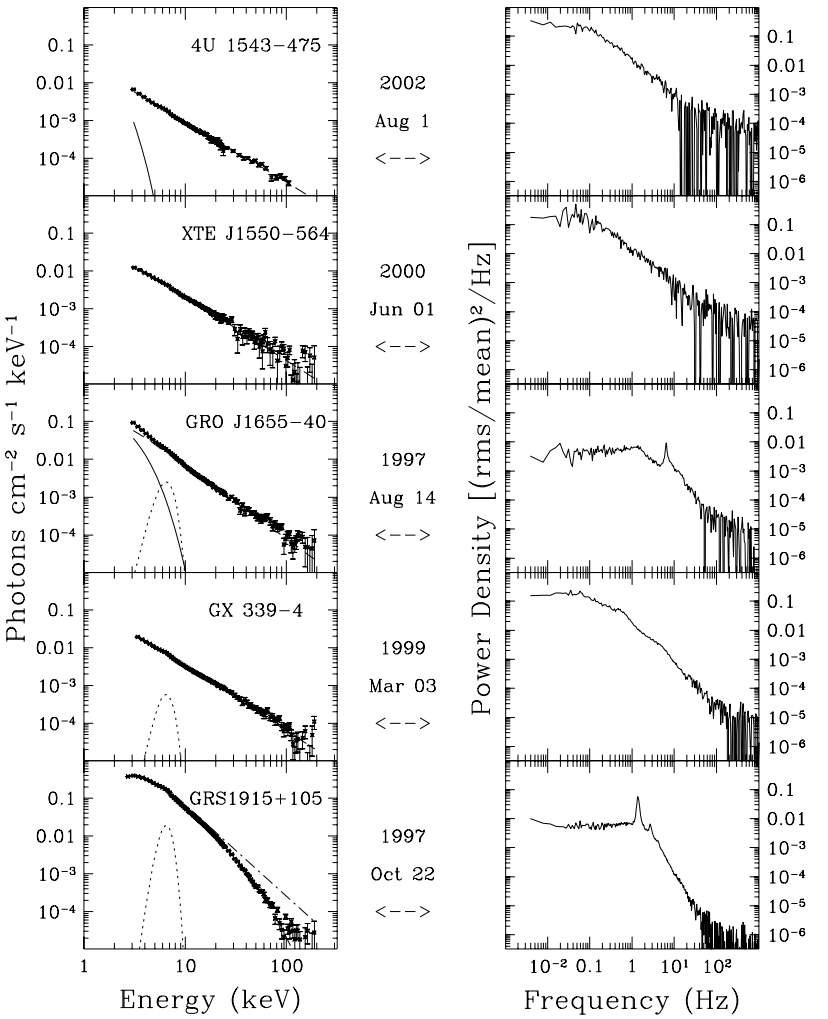

Fig. 4.11. Sample spectra of BHBs in the hard state. The selected X-ray sources are the same BHBs shown in Fig. 4.8. The individual spectral components include the power-law (dashed line) and, if detected, the accretion disk (dotted line) and a reflection component (long dashes). The energy spectra are characterized by a relatively flat power-law component that dominates the spectrum above 1 keV. A second characteristic of the hard state is the elevated continuum power in the PDS, here shown for the range 2–30 keV. This state is associated with the presence of a steady type of radio jet (see text). Radio emission was detected during three of the five observations shown here, but there was no radio coverage for GRO J1655–40 and 4U 1543–47.

the inner disk radius and temperature for the MCD model were $\gtrsim$100 R_g and $\approx$0.024 keV, respectively (McClintock *et al*. 2001b). Somewhat higher temperatures ($\approx$0.035–0.052 keV) have been inferred from observations using BeppoSAX (Frontera *et al*. 2003).

While it seems clear that the blackbody radiation appears truncated at a large radius ($\sim 100 R_g$) in the hard state, the physical state of the hot material within this large radius is still a matter of debate. Is the disk density truncated at this radius, as envisioned in the ADAF

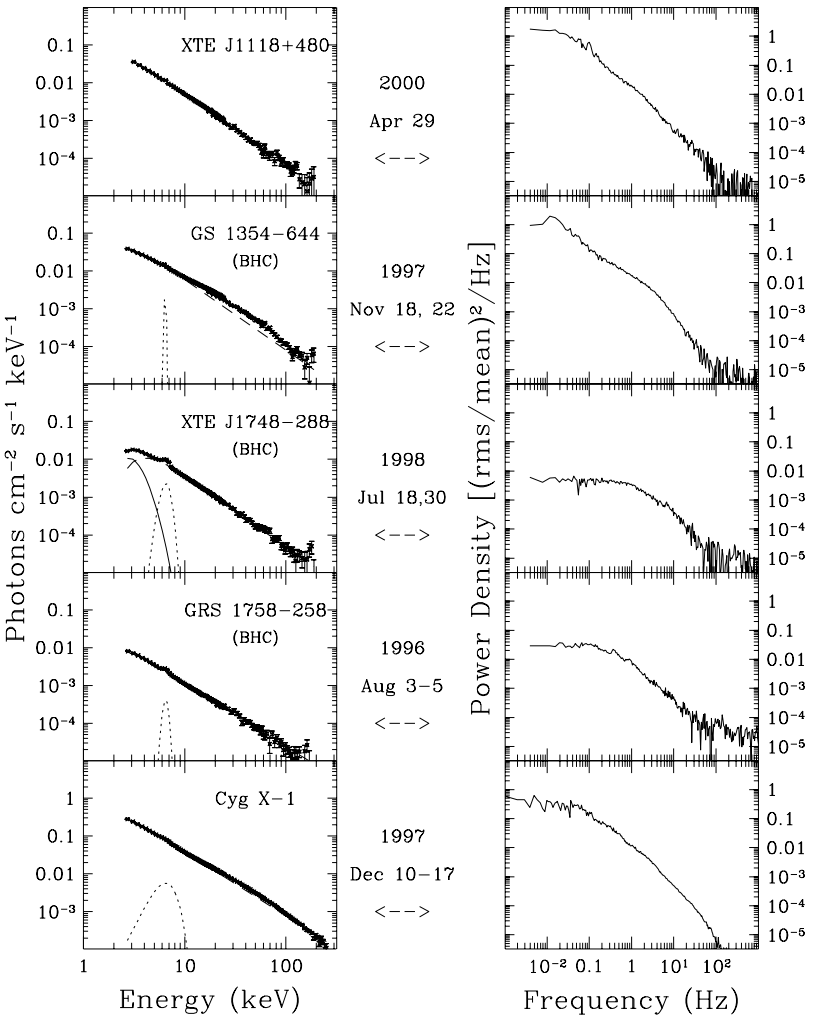

Fig. 4.12. A second sample of BHBs or BHCs seen in the hard state. The observations of XTE J1748–288 occurred during outburst decay, while XTE J1118+480 and GS 1354–64 are seen in the hard state at the peaks of their respective outbursts. GRS 1758–258 and Cyg X-1 spend most of their time in the hard state. There is radio coverage that confirms the presence of a flat radio spectrum for all the sources except XTE J1118+480. The line types denoting the spectral components follow the convention of Fig. 4.11

.

model, or is a substantial amount of matter present in a relativistic flow that is entrained in a jet (e.g., Markoff *et al*. 2001)? Or is the inner disk basically intact and either depleted of energy or veiled in some type of Compton corona? For the latter possibility, the properties of the corona would be strongly constrained by the absence of any normal (∼1 keV) thermal component in the hard state of XTE J1118+480 (Esin *et al*. 2001; Frontera *et al*. 2003).

Guidance in sorting out these options may eventually come from other types of investigations, such as the study of correlated optical/X-ray variability (Malzac *et al*. 2003). Also

promising are spectral analyses that focus on broad Fe emission features (Section 4.2.3) or the X-ray reflection component (Done & Nayakshin 2001). These spectral features depend on substantial density in the inner disk, while the Fe line additionally reveals the pattern of Keplerian flow modified by effects due to GR. Systematic studies of these features during different BHB states and transitions could help to determine the physical changes in the inner disk associated with the hard state. The reflection component is most apparent when the disk is observed nearly face-on. One such system is Cyg X-1, and a reflection analysis has been reported by Done and Zycki (1999). They find that the disk is physically truncated, but the transition radius (tens of $R_{\rm g}$) is not as far from the event horizon as suggested by the value of $R_{\rm in}$ inferred from the disk spectrum in the hard state (Takahashi *et al*. 2001).

The origin of the X-ray power law is another aspect of the controversy concerning the appropriate physical model for the hard state. As noted above, we regard the power-law fit as a general signature of non-thermal radiation; however, the observed spectrum can be produced by several different radiation mechanisms. This is well illustrated in the case of XTE J1118+480, where the X-ray spectrum has been fitted by an ADAF model (Esin *et al*. 2001), a synchrotron model (Markoff *et al*. 2001) and a thermal-Comptonization model (Frontera *et al*. 2001b).

Despite the large uncertainties that remain for physical models, it would appear that the association of the hard state with a steady radio jet is an important step forward. And it does remain possible to identify the hard state solely from X-ray spectral and temporal properties, as had been done in the past (TL95). Using Figs. 4.11 and 4.12 and Table 4.4, *we conclude that the hard state is well characterized by three conditions: the spectrum is dominated (>80% at 2–20 keV) by a power-law spectrum, the spectral index is in the range* $1.5 < \Gamma < 2.1$, *and the integrated power continuum (0.1–10 Hz) is strong and typically in the range* $0.1 < r < 0.3$.

4.3.7 Steep power-law (SPL) state or very high (VH) state

There are times when BHBs become exceedingly bright ($L_{\rm X} > 0.2 L_{\rm Edd}$), and the X-ray spectrum again displays substantial non-thermal radiation, which may constitute 40–90% of the total flux. In such cases the photon index is typically $\Gamma \geq 2.4$, which is steeper than the index ($\Gamma \sim 1.7$) seen in the hard state. The strength of this steep power-law component also coincides generally with the onset of X-ray quasi-periodic oscillations (QPOs) in the range 0.1–30 Hz. This suite of characteristics was initially seen in only two instances: during a bright outburst of GX 339–4 (Miyamoto & Kitamoto 1991) and near the time of maximum flux in X-ray Nova Muscae 1991 (= GS/GRS 1124–68; Miyamoto *et al*. 1993). At the time, this very high (VH) state was interpreted as a signature of the highest rate of mass accretion in a BHB system (van der Klis 1995).

As mentioned previously (Section 4.3.1), the high-energy spectra of several BHCs observed with OSSE on CGRO (40–500 keV) reinforced the distinction between the X-ray hard and VH states, showing that the hard-state spectra exhibit a steep cutoff near 100 keV (Grove *et al*. 1998). On the other hand, the VH-state spectra showed no evidence for a high-energy cutoff, while the photon index in the X-ray and gamma-ray bands is the same ($\Gamma \sim 2.5$–3.0). The unbroken power-law spectra observed by OSSE for five sources suggested that these BHBs had been observed in the VH state, although most of the observations were not accompanied by X-ray observations that could assess the presence of QPOs.

Table 4.4. *Spectral fit parameters*

X-ray name	N_H (10^{22})	T_{DBB} (keV)	± (keV)	N_{DBB}	±	Γ_{PL}	±	N_{PL}	±	Fe FWHM	N_{Fe}	±	χ^2_ν	Additional details
TD state: Figs. 4.8 & 4.9														
4U 1543−475	0.3	1.01	0.02	7419	165	2.57	0.02	5.42	0.21	0.61	.0479	.0031	3.62	feature at 4.4 keV
XTE J1550−564	2.0	1.12	0.03	3289	74	4.76	0.04	152	17	–	–	–	0.98	smedge at 9.2 keV
GRO J1655−40	0.9	1.16	0.03	1559	21	2.85	0.23	1.01	0.65	–	–	–	2.00	smedge at 8.0 keV
GX 339−4	0.2	0.71	0.03	2520	62	2.02	0.04	0.08	0.01	1.05	.0032	.0003	1.45	
GRS 1915+105	6.0	2.19	0.04	62	5	3.46	0.02	33.4	1.61	–	–	–	3.13	smedge at 6.7 keV
4U 1630−47	11.0	1.33	0.03	315	7	3.75	0.03	17.4	1.40	–	–	–	1.06	break at 20.8 keV to $\Gamma = 1.9$
GRS 1739−278	3.0	0.95	0.04	972	23	2.65	0.15	0.210	0.008	1.11	.0068	.0008	1.42	
XTE J1748−288	10.4	1.79	0.02	42.4	2.1	2.60	0.02	14.6	0.4	–	–	–	1.18	
XTE J1755−324	0.2	0.75	0.08	1486	133	2.40	0.15	0.11	0.04	–	–	–	1.78	
XTE J2012+381	0.8	0.85	0.05	1176	56	2.06	0.04	0.16	0.015	–	–	–	1.32	
Hard state: Figs. 4.11 & 4.12														
4U 1543−475	0.3	0.38	0.07	645	1338	1.67	0.02	0.041	0.001	–	–		1.57	
XTE J1550−564	2.0	–	–	–	–	1.70	0.10	0.108	0.021	–	–	–	1.13	
GRO J1655−40	0.9	0.77	0.02	228	37	1.93	0.02	0.571	0.021	1.00	.0065	.0006	1.83	
GX 339−4	0.2	–	–	–	–	1.75	0.02	0.168	0.028	0.90	.0013	.0003	0.98	plus reflection
GRS1915+105	6.0	–	–	–	–	2.11	0.02	0.231	0.043	0.91	.0458	.0003	2.39	plus reflection
XTE J1118+480	0.01	–	–	–	–	1.72	0.04	0.267	0.024	–	–	–	1.23	
GS 1354−644	0.7	–	–	–	–	1.48	0.09	0.470	0.032	0.1	.0008	.0002	1.15	plus reflection
XTE J1748−288	10.4	0.48	0.05	5302	479	1.88	0.09	0.293	0.065	0.66	.0045	.0003	1.65	
GRS 1758−258	1.0	–	–	–	–	1.67	0.07	0.053	0.010	0.36	.0004	.0001	1.84	
Cyg X-1	0.5	–	–	–	–	1.68	0.07	0.446	0.025	1.44	.0206	.0018	3.40	plus reflection
SPL state: Figs. 4.13 & 4.14														
4U 1543−47	0.3	0.93	0.07	3137	138	2.47	0.02	6.85	0.21	0.82	.0347	.0034	1.90	
XTE J1550−564	2.0	3.31	0.20	7.76	0.70	2.82	0.05	200	1.5	1.30	.2136	.0314	2.16	smedge at 8.5 keV
GRO J1655−40	0.9	2.22	0.20	9.89	1.6	2.65	0.05	75.3	1.1	1.32	.2321	.0157	4.45	
GX 339−4	0.2	0.89	0.08	1917	109	2.42	0.02	2.34	0.08	0.97	.0178	.0017	1.39	
GRS 1915+105	6.0	1.19	0.07	115	31	2.62	0.08	28.5	0.6	0.90	.0396	.0065	4.13	
4U 1630−47	11.0	1.73	0.02	46.0	2.4	2.65	0.02	17.0	0.4	–	–	–	1.10	
GRS 1739−278	3.0	1.01	0.06	1116	38	2.61	0.03	2.95	0.19	1.53	.0341	.0021	0.94	
XTE J1748−288	10.4	1.36	0.02	210	11	2.92	0.02	26.2	1.2	–	–	–	0.96	
XTE J1859+226	0.5	1.03	0.02	1164	91	2.55	0.08	14.5	0.31	1.33	.0426	.0060	1.36	
Cyg X-1	0.5	0.49	0.03	55708	2962	2.68	0.03	7.65	0.37	0.73	.0270	.0016	1.78	breaks to $\Gamma = 1.83$ above 12 keV
Unusual spectra: Fig. 4.15														
XTE J1550−564	2.0	0.74	0.02	6932	562	2.24	0.02	23.0	0.87	1.03	.121	.008	1.34	p.l. cutoff energy 51.7 keV
GRS 1915+105	6.0	0.88	0.03	775	156	1.91	0.02	4.51	0.18	1.28	.053	.004	1.45	p.l. cutoff energy 50.0 keV
SAX J1819.3−2525	0.3	1.63	0.06	38	6	0.59	0.03	0.25	0.02	0.47	.038	.003	1.46	p.l. cutoff energy 39.3 keV

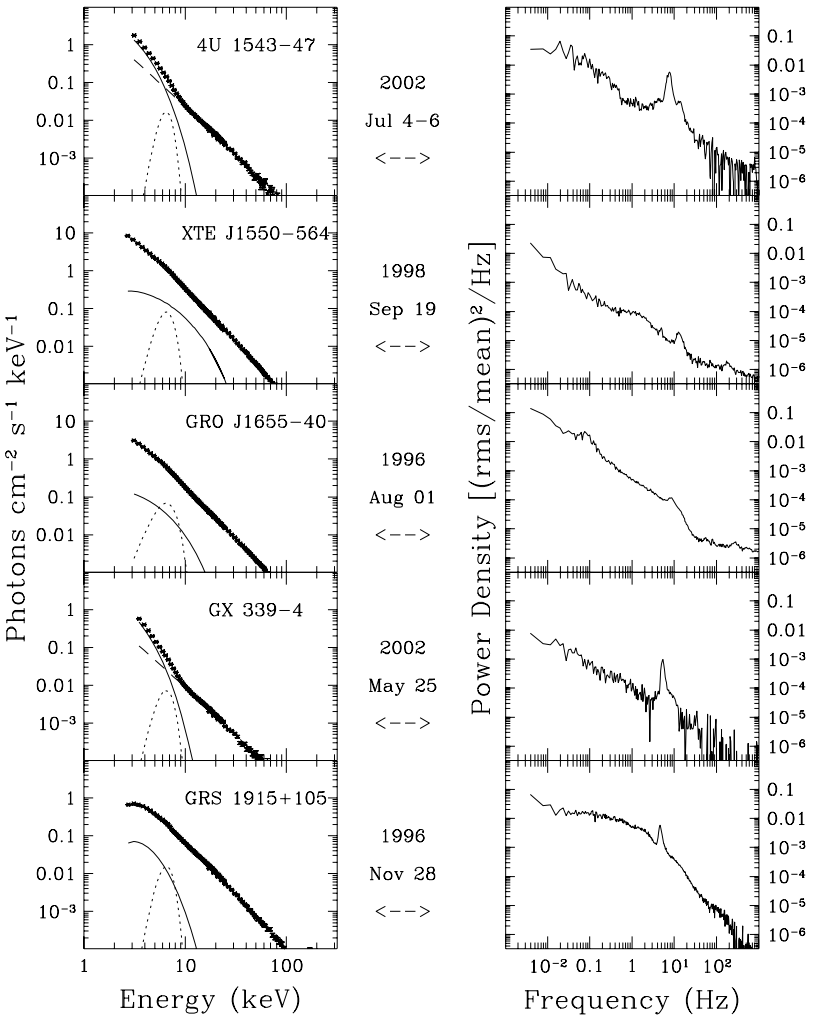

Fig. 4.13. X-ray spectra of BHBs in the SPL state, which is characterized by a strong and steep power-law component in the energy spectrum, along with the presence of X-ray QPOs. The dashed and dotted lines follow the convention of earlier figures.

The monitoring programs of RXTE have shown that the VH state is both more common and more complicated than originally envisioned. Some sources display both X-ray QPOs and a steep power-law component at luminosity levels that are well *below* the maxima seen even in their TD (HS) state (Remillard *et al*. 2002b; Section 4.5). This topic is considered further in Section 4.3.8 below. In response to these developments, we hereafter refer to this state as the "steep power–law" state, or the SPL state, rather than the VH state. We adopt this new name because the steep power-law is a fundamental property of this state, whereas a very high luminosity is not. We view the presence of QPOs as a confirming property of the SPL state.

In Fig. 4.13 we show examples of the SPL state for the same five BHBs considered in Figs. 4.8 and 4.11. The photon index of the steep power-law component covers the range

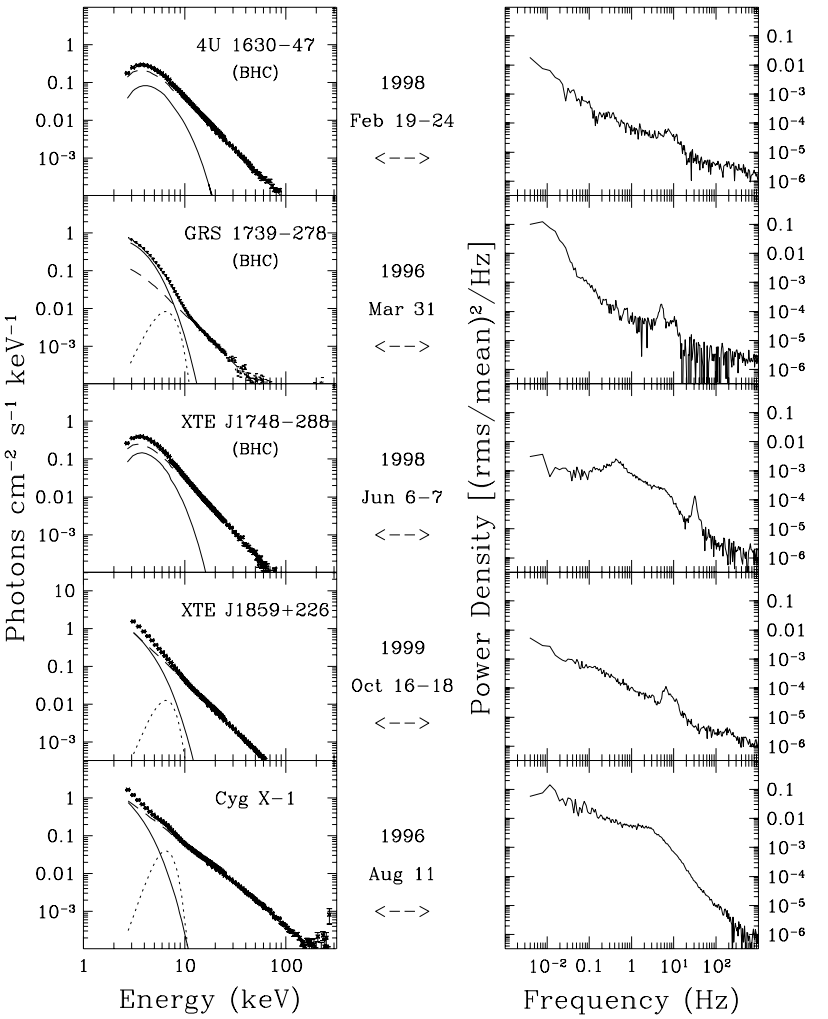

Fig. 4.14. Additional examples of sources in the SPL state. The observations were selected near the times of global or local maxima in the X-ray flux. Cyg X-1 is exceptional for its relatively low luminosity and for the absence of QPOs (see Section 4.3.9). The dashed and dotted lines follow the convention of earlier figures.

$2.4 < \Gamma < 3.0$ as shown in Table 4.4, and QPOs are present with central frequencies over the range 5–13 Hz. The spectra of XTE J1550–564 and GRO J1655–40 (Fig. 4.13) correspond to the highest luminosities observed for these sources during pointed observations with RXTE (Sobczak *et al*. 2000b, 1999). Moreover, both observations revealed the presence of high-frequency QPOs, 186 Hz and 300 Hz, respectively (Remillard *et al*. 2002b). The relationship between the SPL state and HFQPOs will be discussed further in Section 4.4.3.

In Fig. 4.14 we show spectra of the SPL state for three BHCs and two additional BHBs. For three of the sources we have selected observations near the time of maximum flux, as seen in RXTE pointed observations. For the two remaining sources we consider local maxima: the 1996 soft-state episode of Cyg X-1 and the second outburst of 4U 1630–47. X-ray QPOs are

seen in the top four panels (5–8 Hz in three cases and 31 Hz in the case of XTE J1748–288). The power spectrum of Cyg X-1 contains broad continuum features but no X-ray QPOs, although the energy spectrum indicates that the source is in an SPL-like state.

We can encompass all of these SPL examples with the following criteria (see also Sobczak *et al*. 2000a). *The SPL state is defined first by the presence of a power-law component in the X-ray spectrum with photon index* $\Gamma > 2.4$. *Second, either there are X-ray QPOs present (0.1–30 Hz) while the power-law contributes more than 20% of the total (unabsorbed) flux at 2–20 keV, or the power-law contributes more than 50% of the total flux without detections of QPOs. Third, we adopt an upper limit for the integrated rms power (0.1–10 Hz) in the PDS (2–30 keV),* $r \lesssim 0.15$. This latter criterion avoids one type of intermediate condition in which a strong, band-limited PDS and a high-energy spectral break suggest evolution away from the SPL state, even while the photon index remains steep (i.e., $\Gamma > 2.4$). Intermediate state conditions are further discussed in Section 4.3.8.

Transitions between the TD and hard states frequently pass through intervals of the SPL state, and this has led some authors to suggest that the SPL (or VH) state is itself an "intermediate state" that lies between the TD and hard states (Rutledge *et al*. 1999; Homan *et al*. 2001). However, this appears to be a radical suggestion that gives inadequate weight to other SPL observations associated with (1) the episodes of highest absolute luminosity in many BHBs, (2) a distinct gamma-ray spectrum, and (3) occurrences of QPOs at both high and low frequency. We therefore conclude that the SPL state is a bona fide state of BHBs, and we note that nothing in our state definitions constrains the order in which state transitions should occur.

The radio properties of the SPL state are an important and complicated topic that calls for the heightened attention of observers. Here we highlight several salient results. The brightest days of GRO J1655–40 during its 1996–7 outburst occurred in the SPL state (1996 August) when the source appeared radio quiet (e.g., Tomsick *et al*. 1999). Similarly, Cyg X-1 becomes radio quiet whenever the spectrum switches from the hard state to the SPL state. On the other hand, the SPL state is also associated with the explosive formation of radio jets. For example, the giant X-ray flare in XTE J1550–564 (shown in Figs. 4.2 and 4.13) has been linked to a relativistic mass ejection seen as a superluminal separation of bipolar radio jets (Hannikainen *et al*. 2001). However, there is a distinct possibility that the X-ray flare in the SPL state may have occurred after the moment of ejection, at a time when the radio properties of the core (i.e., the inner disk) are unknown. This conjecture is supported by radio observations of the same source during the 2000 outburst when a radio flare was observed to decay below detectable levels while the source remained in the SPL (VH) state (Corbel *et al*. 2001). We conclude that the best available evidence suggests that the SPL state is essentially radio quiet, while the instability that causes impulsive jets is somehow associated with the SPL state.

The physical origin of the SPL spectrum remains one of the outstanding problems in high-energy astrophysics. The SPL spectrum extends to $\sim$1 MeV in several sources: e.g., Cyg X-1, GRO J1655–40 and GRO J0422+32 (Table 4.2). The spectrum may extend to even higher energies, but present investigations are limited by photon statistics. At stake is our understanding of accretion physics at the extraordinary times of peak BHB luminosity. Equally important is our need to interpret the high-frequency QPOs associated with the SPL state.

Most models for the SPL state invoke inverse Compton scattering as the operant radiation mechanism (e.g., Zdziarski 2000). The MeV photons suggest that the scattering occurs in

a non-thermal corona, which may be a simple slab operating on seed photons from the underlying disk (Gierlinski *et al*. 1999; Zdziarski *et al*. 2001). Efforts to define the origin of the Comptonizing electrons has led to more complicated geometric models with feedback mechanisms, such as flare regions that erupt from magnetic instabilities in the accretion disk (Poutanen & Fabian 1999). One early model, which was applied to AGN, invokes a strongly magnetized disk and predicts power-law spectra extending to tens of MeV (Field & Rogers 1993). An analysis of extensive RXTE observations of GRO J1655–40 and XTE J1550–564 has shown that as the power-law component becomes stronger and steeper, the disk luminosity and radius appear to decrease while maintaining a high temperature (see Fig. 4.10). These results can be interpreted as an observational confirmation of strong Comptonization of disk photons in the SPL state (Kubota *et al*. 2001; Kubota & Makishima 2003).

There are a number of alternative models for the SPL state. For example, bulk motion Comptonization has been proposed in the context of a converging sub-Keplerian flow within 50 R_g of the BH (e.g., Titarchuk & Shrader 2002). Turolla *et al*. (2002) have suggested pair production as a means of extending the photon spectrum beyond the ∼350 keV limit initially calculated for this model.

As noted above, Comptonization models are hard-pressed to explain the origin of the energetic electrons. As a further difficulty, a viable model must also account for the QPOs in the SPL state. This is important since strong QPOs (see Figs. 4.13 and 4.14) are common in this state. SPL models and X-ray QPOs are discussed further in Section 4.4.

4.3.8 Intermediate states

The four states described above capture the behavior observed for most BHBs on many occasions. However, other forms of complex behavior are often seen, and these dispel the notion that every BHB observation can be classified via these X-ray states. In the following three subsections, we consider observations that challenge or combine elements of the four-state framework described above.

The hard-state energy spectra in Figs. 4.11 and 4.12 show little or no contribution from the accretion disk, while the PDS exhibit a "band-limited" power continuum (i.e., a flat power continuum at low frequencies that breaks to a steeper slope between 0.1 and 10 Hz). However, a band-limited power spectrum is sometimes seen in combination with a stronger contribution from the accretion disk. This condition of a BHB has been interpreted as an *intermediate* state that lies between the hard and TD states (e.g., Mendez & van der Klis 1997). We agree that the spectra in Fig. 4.11 do appear to show characteristics of both the hard and TD states; however, it lies within the boundaries we define for the hard state.

Other cases seem to display a different type of intermediate or hybrid emission state. For example, dozens of observations of XTE J1550–564 yielded energy spectra and QPOs that resemble the SPL state (Sobczak *et al*. 2000b), but the PDS showed band-limited continuum power that is reminiscent of the intermediate state described above (Homan *et al*. 2001). One example is shown in Fig. 4.15, along with a similar observation of GRS 1915+105. These observations can be described as SPL states with band-limited power continua. The significance of this PDS shape is yet to be fully understood. It could suggest an intermediate state linking the hard and SPL states, a detail further supported by the fact that the inner edges of the disks in the two systems appear to have cooler temperatures and larger radii than are observed for the TD state. However, such speculations may be ill-advised without

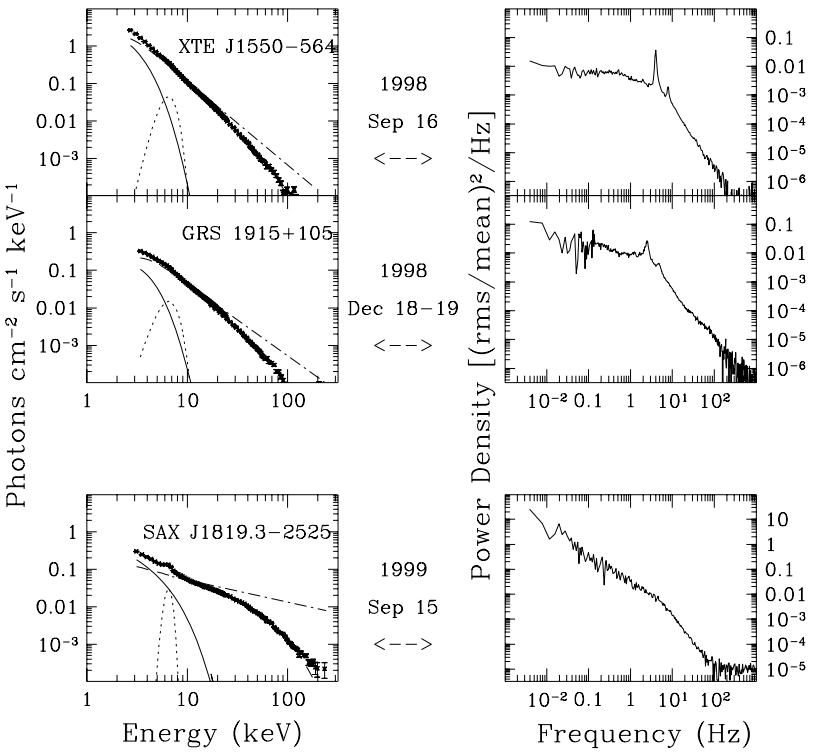

Fig. 4.15. Unusual spectra of three BHBs. The observations of XTE J1550–564 and GRS 1915+105 show spectral properties of the SPL state, but the PDS show a band-limited power continuum that is customarily seen as a characteristic of the hard state, rather than the SPL state. In the bottom panel, the flares and rapid fluctuations seen in SAX J1819.3–2525 (V4641 Sgr) do not coincide with any of the typical X-ray states of BHB systems.

considerations of sensitive radio measurements. We further note that the presence or absence of band-limited power observed in individual SPL-state observations of XTE J1550–564 is closely coupled to the amplitudes and phase lags of the associated QPOs (of types A, B, and C; Remillard *et al*. 2002a). Finally, while the energy spectra of XTE J1550–564 and GRS 1915+105 in Fig. 4.15 are distinctly steep, there is some ambiguity as to whether they are best modeled as a steep power law or as a flatter power law with an unusually low cutoff energy ($\sim$50 keV). In Table 4.4, we show the spectral parameters for the latter model, which is statistically preferred in the case of GRS 1915+105.

We conclude that it is inappropriate to refer to both the observations of XTE J1550–564 (Fig. 4.15) and the very different observations of GRO J1655–40 (Fig. 4.11) as representing a single BHB state, namely, the intermediate state. On the other hand, state transitions and hybrid emission properties are to be expected and *X-ray spectra and PDS should be interpreted as intermediate states when necessary, while specifying which states can be combined to yield the observed X-ray properties.* In summary, we describe the spectra of GRO J1655–40 (Fig. 4.11) as representing primarily a hard state or perhaps an intermediate state between hard and TD. On the other hand, the spectra and PDS of XTE J1550–564 and GRS 1915+105 considered here appear to show an intermediate state related to the SPL and hard states. Since

transitions between these latter two states are not generally seen, this hybrid combination merits further scrutiny.

4.3.9 X-ray states of Cygnus X-1 and GRS 1915+105

In this section we briefly summarize the efforts to integrate the behavior of two uncommon BHBs within the framework of the TD, hard/radio jet, and SPL states. We first return to the issue of Cyg X-1 and the nature of its transitions to a soft state of high intensity, which is unlike the canonical TD (HS) state. As noted earlier (Sections 4.2.1.1 and 4.3.1), contrary to expectations the 1996 soft-state spectrum of Cyg X-1 revealed a power-law spectrum, rather than a TD spectrum (Zhang *et al*. 1997a; Frontera *et al*. 2001a; Fig. 4.14). Cyg X-1 has never been seen in the TD state, and the transition from a hard X-ray spectrum to a soft one must be seen as a transition from the hard state to the SPL state (Gierlinski *et al*. 1999; Zdziarski *et al*. 2001). However, this SPL-like state is unusual in two respects: the absence of QPOs and the relatively low temperature of the accretion disk (Table 4.4). Less surprising is the low luminosity of the SPL state (Zhang *et al*. 1997b), since this is also seen in other sources (e.g., XTE J1550–564; Remillard *et al*. 2002a). Whether the SPL state in Cyg X-1 requires a higher mass accretion rate than the hard state is a matter of controversy (Zhang *et al*. 1997b; Frontera *et al*. 2001a).

In the unique case of GRS 1915+105, the wildly varying X-ray lightcurves indicate an imposing number of instability modes (Belloni *et al*. 2000). Nevertheless, within this complexity it is often possible to identify the canonical states of a BHB (Muno *et al*. 1999; Belloni *et al*. 2000). About half of the observations of GRS 1915+105 show fairly steady X-ray flux (rms $< 15\%$ in 1 s bins at 2–30 keV), and most of these intervals yield spectra and PDS that resemble either the TD or hard states (Muno *et al*. 1999; Fender 2001; Klein-Wolt *et al*. 2002). There are, however, some noteworthy anomalies encountered while interpreting the behavior of GRS 1915+105 in terms of the canonical X-ray states. First, the condition of steady radio and X-ray emission extends to $L_X > 10^{38}$ erg s^{-1}, which is a factor ~ 100 higher than is observed for other BHBs in the hard state. Second, the X-ray photon index ($\Gamma \sim 2.2$) is steeper than usual, although it remains flatter than the index seen in in the SPL state ($\Gamma \geq 2.4$) or the hard tail of the TD state ($\Gamma \approx 3$; see Table 4.4). In short, the spectral index for GRS 1915+105 in the hard state appears shifted to a somewhat higher value compared to other BHBs.

Overall, the spectral and temporal properties of Cyg X-1 and GRS 1915+105 are best integrated into the standard description of BH X-ray states if we relax the assumptions regarding the relative or absolute luminosity ranges that are appropriate for the various states. As we will see in Section 4.5.1, the spectral evolution of XTE J1550–564 motivates a similar conclusion, since the luminosity in the SPL state can lie well below that of the TD state. Undoubtedly, there is an overall correlation between spectral states and luminosity intervals in accreting BHB systems. However, *the canonical X-ray states are most usefully defined in terms of the properties of the energy spectrum and PDS, rather than in terms of luminosity*.

4.3.10 Anomalous behavior of SAX J1819.3–2525

Finally, we consider whether BHBs exhibit characteristics that fall entirely outside the X-ray states considered thus far. The most challenging case may be the BHB SAX J1819.3–2525 (V4641 Sgr; Fig. 4.2). The PCA observations of 1999 September 15.9 show the source in a unique flaring state (Wijnands & van der Klis 2000). The spectral

hardness ratio remains remarkably constant throughout the brightest ∼500 s of this observation, despite the dramatic intensity fluctuations. The spectrum and PDS for this central time interval are shown in Fig. 4.15. The spectral analysis reveals a hot accretion disk and a broad Fe line, while the photon index is extraordinarily hard: $\Gamma = 0.60 \pm 0.03$ with a cutoff energy of 39 keV (Table 4.4). This source is also distinguished as a new prototype for a "fast X-ray nova" (Wijnands & van der Klis 2000) because it exhibited a 12 Crab flare that appeared and decayed in less than 1 day (Fig. 4.2). The multifrequency spectrum near X-ray maximum has been interpreted in terms of super-Eddington accretion with the binary immersed in an extended envelope (Revnivtsev *et al*. 2002).

4.4 Fast temporal variations: QPOs and broad power peaks

As shown in the preceding sections on X-ray states (Section 4.3.6–8), QPOs are prevalent in the SPL state, and they are sometimes seen in the hard state when thermal emission from the disk contributes some flux above 2 keV (e.g., GRO J1655 − 40 in Fig. 4.11). In this section we briefly consider the QPOs of BHBs and BHCs in greater detail. For references on PDS computation, defining QPOs, and QPO characteristics of NS systems, see Chapter 2. We supplement this work by discussing X-ray timing results for BHBs. Following van der Klis, we define QPOs as features (usually modeled as a Lorentzian function) in the PDS that have coherence parameter $Q = \nu/\Delta\nu > 2$, where $\Delta\nu$ is the FWHM of the QPO. Features with significantly lower Q values are regarded as "broad power peaks" and are discussed separately.

4.4.1 Low-frequency QPOs and radiation mechanisms

The X-ray PDS of many BH transients display low-frequency QPOs (LFQPOs) roughly in the range 0.1 to 30 Hz. The significance of these oscillations can be summarized as follows.

(1) LFQPOs are almost always seen during the SPL state, and they are often seen in the SPL-hard intermediate state. They can be exceedingly strong (see Figs. 4.13–4.15) with rms amplitudes (expressed as a fraction of the mean count rate) as high as $r > 0.15$ for sources such as GRS 1915+105 (Morgan *et al*. 1997) and XTE J1550–564 (Sobczak *et al*. 2000a). More generally, they are seen with $0.03 < r < 0.15$ whenever the steep power law contributes more than 20% of the flux at 2–20 keV (Sobczak *et al*. 2000a). LFQPOs have been observed at energies above 60 keV (Tomsick & Kaaret 2001).

(2) In several sources, the LFQPO frequency is correlated with the total disk flux (but not with temperature or inner disk radius; Sobczak *et al*. 2000a; Muno *et al*. 1999; Trudolyubov *et al*. 1999). This behavior, in combination with the role of the steep power law mentioned directly above, suggests that LFQPOs may provide a vital clue to the mechanism that couples the thermal and SPL components.

(3) LFQPOs can be quasi-stable features that persist for days or weeks. For example, in GRS 1915+105 QPOs at 2.0–4.5 Hz persisted for 6 months during late 1996 and early 1997 (Muno *et al*. 2001).

(4) In a general sense, it can be argued that oscillations as distinct and strong as these QPOs (often with $Q > 10$), represent global requirements for an organized emitting region. For example, in the context of models in which thermal radiation originates from MHD instabilities, one cannot accept the common picture of numerous and independent magnetic cells distributed throughout the inner disk.

The effort to tie LFQPOs to the geometry and flow of accreting gas is complicated by the fact that LFQPO frequencies are much lower than the Keplerian frequencies for orbits in the inner accretion disk. For example, for a BH mass of 10 $M_\odot$, an orbital frequency near 3 Hz coincides with a disk radius near $100R_g$, while the expected radius for maximum X-ray emission lies in the range 1–10 R_g (depending on the value of the BH spin parameter).

For the strongest QPOs in GRS 1915+105, the individual oscillations were tracked to determine the origin of frequency drifts and to measure the average "QPO-folded" oscillation profile (Morgan *et al*. 1997). The results show a random walk in QPO phase and a nearly sinusoidal waveform. The ramifications of these results for QPO models remain uncertain.

There are now a large number of proposed LFQPO mechanisms in the literature, and we mention only a few examples here. The models are driven by the need to account for both the QPO frequency and the fact that the oscillations are strongest at photon energies above 6 keV, i.e., where only the power-law component contributes substantially to the X-ray spectrum. The models include global disk oscillations (Titarchuk & Osherovich 2000), radial oscillations of accretion structures such as shock fronts (Chakrabarti & Manickam 2000), and oscillations in a transition layer between the disk and a hotter Comptonizing region (Nobili *et al*. 2000). Another alternative, known as the "accretion–ejection instability model," invokes spiral waves in a magnetized disk (Tagger & Pellat 1999) with a transfer of energy out to the radius where material corotates with the spiral wave. This model thereby combines magnetic instabilities with Keplerian motion to explain the observed QPO amplitudes and stability.

Further analyses have revealed phase lags associated with LFQPOs and their harmonics. The analysis technique uses Fourier cross-spectra to measure both the phase lags and the coherence parameter (versus frequency) between different X-ray energy bands, e.g., 2–6 vs. 13–30 keV. Unexpectedly, both positive and negative phase lags have been found (Wijnands *et al*. 1999; Cui *et al*. 2000b; Reig *et al*. 2000; Muno *et al*. 2001), and efforts have been made to classify LFQPOs by phase lag properties. The expansion of LFQPO subtypes may not be widely viewed as a welcome development. Nevertheless, it has been shown in the case of XTE J1550–564 that the properties of the phase lags clarify how LFQPO parameters correlate with both the accretion-disk and high-frequency QPO parameters (Remillard *et al*. 2002a).

4.4.2 Broad power peaks and comparisons of BH and NS systems

The study of broad features in the PDS has led recently to important developments. In many NS systems and in the hard state of BHBs, the PDS can be decomposed into a set of four or five broad power peaks (Nowak 2000; Belloni *et al*. 2002), generally with $0.5 < Q < 1.0$. The evolution of these features has been linked to major behavioral changes in Cyg X-1. For example, the disappearance of the third broad power peak occurred just at the time Cyg X-1 left the hard state and its steady radio jet was quenched (Pottschmidt *et al*. 2003).

Broad PDS features are also involved in renewed efforts to contrast accreting BHB and NS systems via their variability characteristics. It has been proposed that the observed high-frequency limit of the power continuum provides a means to distinguish accreting BH and NS systems (Sunyaev & Revnivtsev 2000), since only the latter exhibit intensity variations above 500 Hz.

Finally, some studies have used both QPOs and broad power peaks to examine the relationship between low- and high-frequency features and to make comparisons between different

NS subclasses and BHBs. There have been claims of a unified variability scheme that encompasses all X-ray binary types (Psaltis *et al*. 1999; Belloni *et al*. 2002). The bottom line of this scheme is that all of the oscillations must originate in the accretion disk. However, important aspects of this work remain controversial, particularly the handling of BH HFQPOs and their association with the lower kHz QPO observed for NSs (Remillard *et al*. 2002a).

4.4.3 High-frequency QPOs and general relativity

The topic of high-frequency QPOs (HFQPOs) in BHBs (40–450 Hz) continues to evolve in the RXTE era. These transient QPOs have been detected in seven sources (four BHBs and three BHCs). HFQPOs have rms amplitudes that are generally ∼1–3% of the mean count rate in a given energy band. Remarkably, three sources exhibit pairs of QPOs that have commensurate frequencies in a 3:2 ratio (Remillard *et al*. 2002b, 2003b; Table 4.2). As shown in Fig. 4.16, GRO J1655 − 40 and XTE J1550 − 564 each exhibit a single such pair of frequencies. GRS 1915+105, on the other hand, shows two pairs of HFQPOs; the complete set of four QPO pairs is shown in Fig. 4.16. In addition (see references in Tables 4.2 & 4.3), single-component HFQPOs have been observed in 4U1630–47 (184 Hz), XTE J1859+226 (190 Hz), XTE J1650–500 (250 Hz), and H 1743–322 (240 Hz). Their profiles are similar to the 300 Hz QPO for GRO J1655–40 shown in the top left panel of Fig. 4.16. HFQPOs occur in the SPL state, except for the 67 Hz QPO in GRS 1915+105 (see Fig. 4.16) which appears in the TD state, especially when $L_{\rm X} > 10^{38}$ erg s^{-1}.

The preponderance of evidence indicates that HFQPOs do not shift freely in frequency in response to luminosity changes, as do the kHz QPOs in NS systems (see Chapter 2). Instead, they appear to exhibit an "X-ray voiceprint". That is, the QPOs occur in harmonics of an unseen fundamental frequency which has a unique value for each BH. For the three cases that show 3:2 frequency pairs, the relationship between the HFQPO frequencies vs. BH mass scales as M_1^{-1}. This relationship is shown in Fig. 4.17, where we have plotted the frequency of the stronger feature (i.e., $2 \times \nu_0$), since the fundamental is generally not seen. These results offer strong encouragement for seeking interpretations of BH HFQPOs via GR theory, since each type of GR disk oscillation under strong gravity varies as M_1^{-1}, assuming the sampled BHs have similar values of the dimensionless spin parameter (a_*).

These commensurate frequencies can be seen as strong support for the idea that HFQPOs may represent some type of resonance phenomenon involving oscillations describable by GR, as originally proposed by Abramowicz and Kluzniak (2001). Resonances in some form may be applicable to both BH and NS systems (Abramowicz *et al*. 2003). We note that the 3:2 harmonic pattern cannot be attributed to a distorted sine wave with harmonic content because the individual detections (in a given energy band, on a given day) generally appear as a single peak in the PDS, and the presence of a pair of commensurate frequencies is recognized only when the ensemble of results is examined.

Coordinate frequencies and their differences (i.e., beat frequencies) in GR were proposed earlier to explain some of the X-ray QPOs from both NSs and BHs (Stella *et al*. 1999); however, this work did not treat the commensurate frequencies of interest here, which were discovered subsequently in three BHB systems. In the resonance hypothesis (Abramowicz & Kluzniak 2001), these harmonic frequencies are discussed in terms of accretion blobs following perturbed orbits in the inner accretion disk. Unlike Newtonian gravity, GR predicts independent oscillation frequencies for each spatial coordinate for orbits around a rotating compact object, as seen from the rest frame of a distant observer. Over the range of radii in

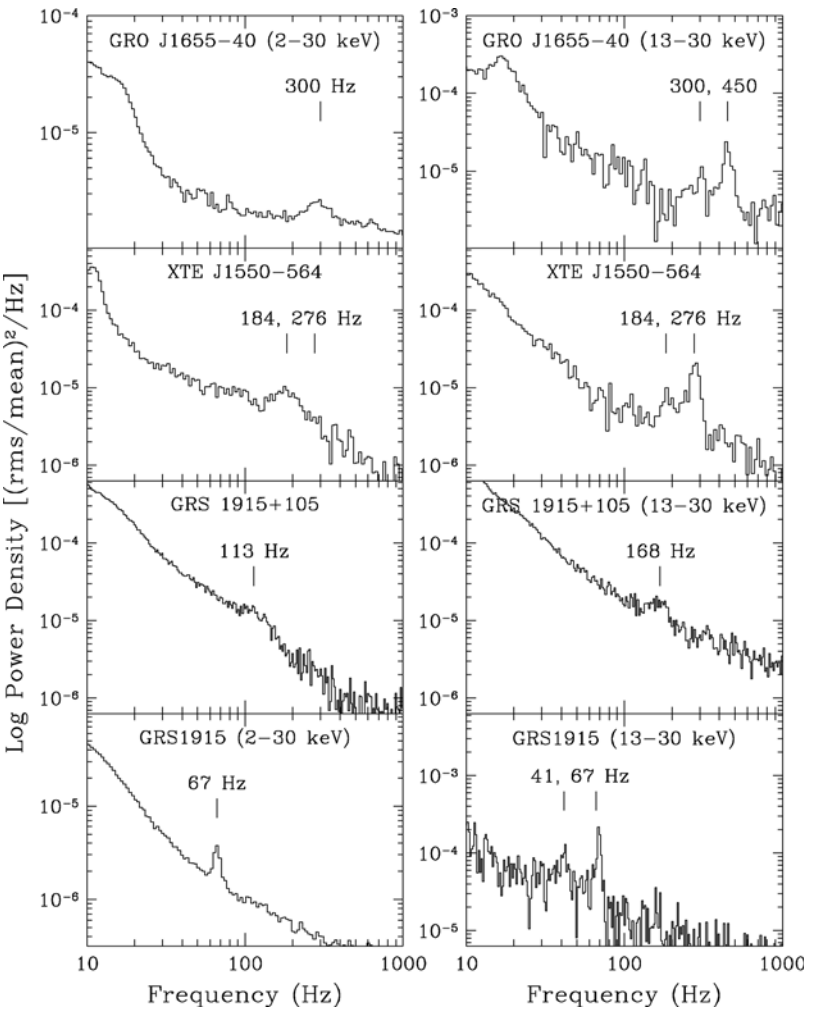

Fig. 4.16. Four pairs of HFQPOs observed in three black hole binary systems. The energy band is 6–30 keV unless otherwise indicated. These usually subtle oscillations are only visible during a fraction of the observations for each source.

the accretion disk where X-rays are expected to originate in the standard disk model, pairs of GR coordinate frequencies have varying, non-integral ratios. Therefore, the discovery of HFQPOs with commensurate frequencies can be seen to suggest enhanced emissivity at a particular radius where a pair of coordinate frequencies are in some type of resonance. Unlike the azimuthal and polar coordinate frequencies, the radial coordinate frequency reaches a maximum value and then falls to zero as the radius decreases toward $R_{\rm ISCO}$ (Kato 2001; Merloni *et al*. 2001). This ensures the possibility of commensurate coordinate frequencies somewhere in the inner disk. For example, there is a wide range in the dimensionless spin parameter, a_*, where one can find a particular radius that corresponds to a 2:1, 3:1, or 3:2 ratio in the orbital and radial coordinate frequencies. A resonance between the polar and radial coordinate frequencies is also possible. In the resonance scenario, linear perturbations may

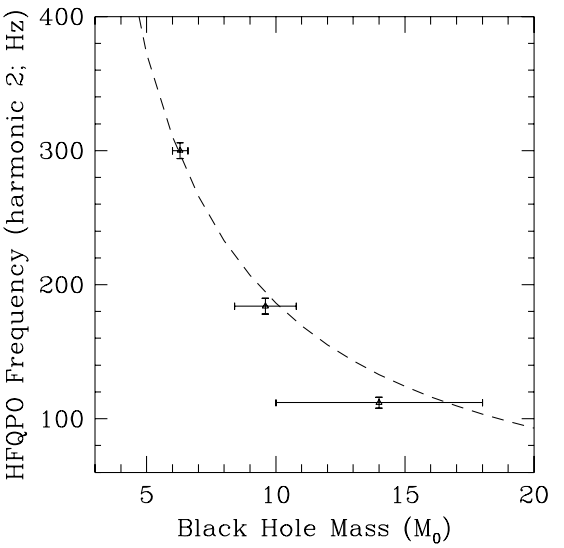

Fig. 4.17. Relationship between HFQPO frequency and BH mass for XTE J1550–564, GRO J1655–40, and GRS 1915+105. These three systems display a pair of HFQPOs with a 3:2 frequency ratio. The frequencies are plotted for the stronger QPO that represents $2 \times \nu_0$. The fundamental is generally not seen in the power spectra. The dashed line shows a relation, $\nu_0(\mathrm{Hz}) = 931(M/\mathrm{M}_\odot)^{-1}$, that fits these data.

grow at these radii, ultimately producing X-ray oscillations that represent some combination of the individual resonance frequencies, their sum, or their difference. However, there remain serious uncertainties as to whether such structures could overcome the severe damping forces and emit X-rays with sufficient amplitude and coherence to produce the observed HFQPOs (Markovic & Lamb 1998).

Models for "diskoseismic" oscillations adopt a more global view of the inner disk as a GR resonance cavity (Kato & Fukue 1980; Wagoner 1999). This paradigm has certain attractions for explaining HFQPOs, but integral harmonics are not predicted for the three types of diskoseismic modes derived for adiabatic perturbations in a thin accretion disk. Clearly, there is a need to investigate further the possibility of resonances within the paradigm of diskoseismology. Other models must be considered as well, e.g., the p-mode oscillations of an accretion torus surrounding a black hole (Rezzolla *et al*. 2003).

It has been argued by Strohmayer (2001a) that HFQPO frequencies are sufficiently high that they require substantial BH spin. For example, in the case of GRO 1655–40 the 450 Hz frequency exceeds the maximum orbital frequency (ν_ϕ) at the ISCO around a Schwarzschild BH (i.e., $a_* = 0$; Section 4.1.5) of mass $M_1 = 6.3 \pm 0.5\ \mathrm{M}_\odot$ (Greene *et al*. 2001). *If* the maximum Keplerian frequency is the highest frequency at which a QPO can be seen, then the results for GRO J1655–40 require a Kerr BH with prograde spin, for example, $a_* > 0.15$. However, the conclusion that spin is required may not be valid if the QPO represents the sum of two beating frequencies. On the other hand, even higher values of the spin parameter may be required if the QPO represents either resonant coordinate frequencies ($a_* > 0.3$; Remillard *et al*. 2002b) or diskoseismic oscillations ($a_* > 0.9$; Wagoner *et al*. 2001).

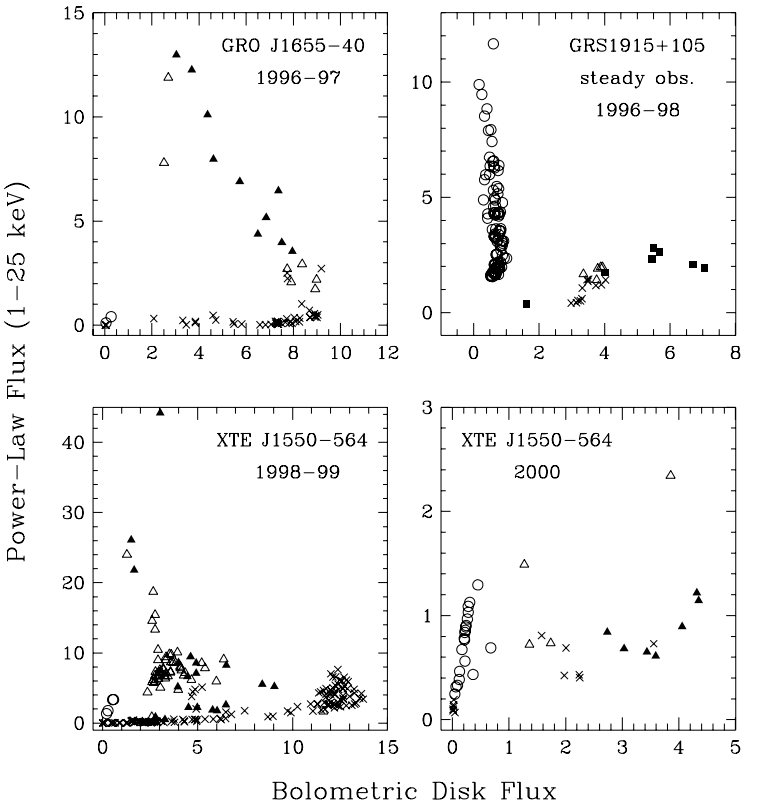

Fig. 4.18. Radiation energy division between the accretion disk and the power-law component. The symbol types denote the X-ray state as TD (×), hard (○), or SPL(Δ). Furthermore, in the SPL state, an open triangle is used when there is only an LFQPO, while a filled triangle denoted the additional presence of an HFQPO. Finally, the TD-like observations that show 67 Hz QPOs in GRS 1915+105 are shown with a filled square. All fluxes are in units of 10^{-8} erg cm^{-2} s^{-1} and corrected for absorption.

Accurate and sensitive measurements of X-ray HFQPO frequencies may lead to a determination of the GR mechanism that is responsible for these oscillations, and ultimately to secure measurements of the spin parameter, a_*, for a number of BHs. These spin measurements would be very valuable in assessing the role of BH rotation in the production of jets (Blandford & Znajek 1977). This is especially true since the three systems with paired frequencies have a history of relativistic mass ejections during some (but not all) of their outbursts.

4.5 Energetics and key variables determining BHB radiation

4.5.1 Division of spectral energy: disk and power-law components

A revealing view of the behavior of a BHB over the course of its entire outburst cycle can be obtained by plotting the flux in the power-law component vs. the flux from the accretion disk. Four such plots are shown in Fig. 4.18, where the various plotting symbols identify the emission states described in Section 4.3. The figure shows the flux diagrams for

three BHBs, while considering two of the outbursts of XTE J1550–564 (Muno *et al*. 1999; Remillard *et al*. 2001, 2002b). It has been shown that the emerging patterns in these flux diagrams are largely unaffected by the choice of integration limits, e.g., whether the energy measurements are computed in terms of bolometric flux or the integrated flux within the 2–25 keV PCA bandpass (Remillard *et al*. 2002a).

The TD points ($\times$ symbol; Fig. 4.18) for GRO J1655–40 and XTE J1550–564 (1998–9) appear well organized; they can be described as horizontal tracks in which accretion energy is freely converted to thermal radiation from the accretion disk. These tracks correspond to the standard accretion disk model (Shakura & Sunyaev 1973), and they may also convey moderate Comptonization effects expected from MHD turbulence (e.g., Hawley & Krolik 2001) as these tracks curve upward at high luminosity. The TD points at the highest flux levels correspond to Eddington luminosities of 0.2 for GRO J1655–40, 0.6 for XTE J1550–564 (1998–9), and 0.4 for GRS 1915+105, using the values for mass and distance given in Tables 4.1 and 4.2.

Observations in the hard state (i.e., a dominant power-law component with $1.4 < \Gamma < 2.2$) are plotted as circles in Fig. 4.18. These points form vertical tracks with only minor flux contributions from the disk. The hard-state points coincide with fairly steady radio emission for GRS1915+105 (Muno *et al*. 2001) and XTE J1550–564 in 2000 (Corbel *et al*. 2001), as expected for this state.

Observations in the SPL state (defined by a power-law index $\Gamma > 2.4$ and by QPOs) are plotted as triangles in Fig. 4.18; a solid symbol is used when there is an additional detection of an HFQPO above 100 Hz. The wide diversity in the relative contributions from the disk and power-law components within the SPL state are especially apparent for XTE J1550–564. It is these results, combined with the wide range in the luminosities of the TD and hard tracks shown in Fig. 4.18, that have caused us to abandon the luminosity requirements in defining the X-ray states of BHBs (Section 4.3). Finally, detections of the 67 Hz QPO in GRS 1915+105 are shown as filled squares. They appear to extend the TD branch out to $0.6\ L_{\rm Edd}$.

4.5.2 Key variables determining BHB radiation

Prior to the RXTE era, it was thought that the X-ray states primarily represent a simple progression in luminosity, and that the emission properties depend only on the accretion rate and the BH mass (e.g., Tanaka & Lewin 1995). The behavioral complexity of sources such as XTE J1550–564 (Fig. 4.18) have challenged this viewpoint (Homan *et al*. 2001; Remillard *et al*. 2002b) because it now appears that any of the three active states of accretion may occur at a given luminosity.

Finally, what other parameters must be considered in the theory of BH accretion? It is clear that BH spin and the angle between the spin and disk axes must also be considered in a complete theory of BH accretion, but these would not help to explain the types of rapid state transitions seen in many systems. As noted in several previous sections, MHD instabilities are widely invoked to explain non-thermal radiation, and magnetic fields are additionally expected to play a leading role in the formation and collimation of jets. It then seems relevant to question whether a parameter of magnetism, such as the ratio of magnetic to gas pressure, should be considered a key variable in accretion physics. The global magnetic field geometry may also play an essential role in the formation of some X-ray states. The

continued development of 3-D MHD simulations is expected to be very fruitful in gaining a deeper understanding of the radiation emitted by black hole binaries.

4.6 Concluding remarks

As reviewed in Section 4.4.3, high-frequency QPOs at 40–450 Hz have been observed with RXTE for four BHBs and three BHCs. Furthermore, three of these sources show harmonic (3:2) pairs of frequencies that scale as $M_{\rm BH}^{-1}$. The models for these QPOs (e.g., orbital resonance and diskoseismic oscillations) invoke strong-field GR effects in the inner accretion disk, and they depend on both the mass and spin of the BH. On the other hand, studies of broadened Fe Kα emission lines (Section 4.2.3), which can also reveal the conditions in the very inner accretion disk, may prove as revealing as timing studies. The line photons that reach a distant observer are gravitationally redshifted and Doppler and transverse-Doppler shifted. Encoded in the line profile are the mass and spin of the BH. The most provocative result has been obtained for the BHC XTE J1650–500 (Section 4.2.3), where the line profile suggests the presence of an extreme Kerr BH.

The behavior of the massive compact objects reviewed herein supports the view that they are bona fide BHs, which are described by GR and were formed by the complete gravitational collapse of matter. Our challenge is to prove that this conclusion is correct by making clean quantitative measurements of relativistic effects in the strong gravitational fields near these objects. At present, no one can say which future mission can best help us meet this challenge: LISA, MAXIM, Constellation-X, or an X-ray Timing Observatory (XTO). Perhaps all of the approaches will be required. In any case, an XTO with effective area and telemetry ten times that of RXTE and with improved energy resolution, would be a powerful probe of physics near the event horizon. Consider that RXTE, with just 1.6 times the effective area of Ginga, broke through to discover kHz QPOs in NSs, a discovery that led quickly to hard constraints on dense matter.

Recent optical studies have promoted two of the black hole candidates listed in Table 4.3 to the status of black hole binaries: (1) GS 1354–64 (Casares *et al.* 2004), and (2) XTE J1650–500 (Orosz *et al.* 2004). Thus the number of confirmed black hole binaries is now 20 (see Tables 4.1 & 4.2).

Acknowledgements

We thank Jon Miller, Mike Muno, David Smith, Jean Swank, John Tomsick, and Rudy Wijnands for their help in assembling the catalogue of candidate BHBs presented in Table 4.3, and Keith Arnaud, George Field, Mike Garcia, Aya Kubota, Kazuo Makishima, and Mike Revnivtsev for valuable comments. We are indebted to Andy Fabian, Jon Miller, Ramesh Narayan, Jerry Orosz and Andrej Zdziarski for a careful reading of portions of the manuscript and their valuable comments. We are especially grateful to Jeroen Homan and John Tomsick for their detailed comments on a near-final draft of the manuscript. We thank Ann Esin for supplying Fig. 4.1, Jon Miller for supplying Fig. 4.6, John Tomsick and Emrah Kalemci for the use of unpublished data on 4U1543–47, John Huchra for advice on the distance to the LMC, and Suresh Kumar for his assistance in typesetting the manuscript. This work was supported in part by NASA under Grants NAG5-10813 and by the NASA contract to MIT for support of RXTE.

References

Abramowicz, M. A. (1998) in *Theory of Black Hole Accretion Discs*, eds. M. A. Abramowicz, G. Bjornsson and J. E. Pringle (Cambridge, Cambridge University Press), 50–60

Åbramowicz, M. A. and Kluzniak, W. (2001), *A&A* **374**, L19–L20

Abramowicz, M. A., Karas, V., Kluzniak, W., *et al*. (2003), *PASJ* **55**, 467–471

Agol, E. and Krolik, J. H. (2000), *ApJ* **528**, 161–170

Agol, E., Kamionkowski, M., Koopmans, L.V. E. and Blandford, R. D. (2002), *ApJ* **576**, L131–L135

Arnaud, K. and Dorman, B. (2002), XSPEC (An X-ray Spectral Fitting Package), version 11.2x (NASA/GSFC/HEASARC, Greenbelt)

Augusteijn, T., Kuulkers, E. and van Kerkwijk, M. H. (2001), *ApJ* **375**, 447–454

Baganoff, F. K., Bautz, M. W., Brandt, W. N., *et al*. (2001), *Nature* **413**, 45–48

Bahcall, J. N. (1986), *ARA&A* **24**, 577–611

Ball, L., Kesteven, M. J., Campbell-Wilson, D., *et al*. (1995), *MNRAS* **273**, 722–730

Balucinska-Church, M. and Church M. J. (2000), *MNRAS* **312**, L55–L59

Barr, P., White, N. E. and Page, C.G. (1985), *MNRAS* **216**, 65P–70P

Barret, D., Roques, J. P., Mandrou, P., *et al*. (1992), *ApJ* **392**, L19–L22

Barret, D., Grindlay, J. E., Bloser, P. F., *et al*. (1996a), *IAU Circ*. 6519

Barret, D., McClintock, J. E. and Grindlay, J. E. (1996b), *ApJ* **473**, 963–973

Barret, D., Olive, J. F. and Boirin, L. (2000), *ApJ* **533**, 329–351

Belloni, T., van der Klis, M., Lewin, W. H. G., *et al*. (1997), *A&A* **322**, 857–867

Belloni, T., Mendez, M., van der Klis, M., *et al*. (1999), *ApJ* **519**, L159–L163

Belloni, T., Klein-Wolt, M., Mendez, M., *et al*. (2000), *A&A* **355**, 271–290

Belloni, T., Psaltis, D. and van der Klis, M. (2002), *ApJ*, **572**, 392–406

Blandford, R. D. (2002), in *Lighthouses of the Universe*, eds. M. Gilfanov, R. Sunyaev, *et al*. (Berlin, Springer) (astro-ph 0202265)

Blandford, R. D. and Begelman, M. C. (1999), *MNRAS* **303**, L1–L5

Blandford, R. D. and Znajek, R. L. (1977), *MNRAS* **179**, 433–456

Bolton, C. T. (1972), *Nature* **240**, 124–126

Borozdin, K. N., Aleksandrovich, N. L., Aref'ev, V. A., *et al*. (1995), *AstL* **21**, 212–216

Borozdin, K. N., Revnivtsev, M. G., Trudolyubov, S. P., *et al*. (1998), *AstL* **24**, 435–444

Boyd, P. T., Smale, A. P., Homan, J., *et al*. (2000), *ApJ* **542**, L127–L130

Bradt, H., Levine, A. M., Remillard, R. A. and Smith, D. A. (2001), *MmSAI* **73**, 256–271

Bradt, H. V. D. and McClintock, J. E. (1983), *ARA&A* **21**, 13–66

Branduardi, G., Ives, J. C., Sanford, P. W., *et al*. (1976), *MNRAS* **175**, 47P–56P

Brocksopp, C., Fender, R. P., Larionov, V., *et al*. (1999), *MNRAS* **309**, 1063–1073

Brocksopp, C., Jonker, P. G., Fender, R. P., *et al*. (2001), *MNRAS* **323**, 517–528

Brocksopp, C., Fender, R. P., McCollough, M., *et al*. (2002), *MNRAS* **331**, 765–775

Bronfman, L., Cohen, R. S., Alvarez, H., *et al*. (1988), *ApJ* **324**, 248–266

Brown, G. E. and Bethe, H. A. (1994), *ApJ* **423**, 659–664

Brown, G. E., Lee, C.-H, Wijers, R. A. M. J. and Bethe, H. A. (2000a), *Phys. Rep.* **333–334**, 471–504

Brown, G. E., Lee, C.-H., Wijers, R. A. M., *et al*. (2000b), *NewA* **5**, 191–210

Campana, S., Stella, L., Belloni, T., *et al*. (2002), *A&A* **384**, 163–170

Cannizzo, J. K. (1993), *ApJ* **419**, 318–336

Casares, J. and Charles, P. A. (1994), *MNRAS* **271**, L5–L9

Casares, J., Charles, P. A., Naylor, T. and Pavlenko, E. P. (1993), *MNRAS* **265**, 834–852

Casares, J., Charles, P. A. and Marsh, T. R. (1995), *MNRAS* **277**, L45–L50

Casares *et al*. 2004, *ApJ* **613**, L133–L136

Chakrabarti, S. K. and Manickam, S. G. (2000), *ApJ* **531**, L41–L44

Chaty, S., Mignani, R. P. and Israel, G. L. (2002), *MNRAS* **337**, L23–L26

Chen, W., Shrader, C. R. and Livio, M. (1997), *ApJ* **491**, 312–338

Churazov, E., Gilfanov, M., Sunyaev, R., *et al*. (1993), *ApJ* **407**, 752–757

Churazov, E., Gilfanov, M. and Revnivtsev, M. (2001), *MNRAS* **321**, 759

Coe, M. J., Engel, A. R. and Quenby, J. J. (1976), *Nature* **259**, 544–545

Cooke, B. A., Levine, A. M., Lang, F. L., *et al*. (1984), *ApJ* **285**, 258–263

Corbel, S., Fender, R. P., Tzioumis, A. K., *et al*. (2000), *A&A* **359**, 251–268

Corbel, S., Kaaret, P., Jain, R. K., *et al*. (2001), *ApJ* **554**, 43–48
Corbel, S., Fender, R. P., Tzioumis, A. K., *et al*. (2002), *Science* **298**, 196–199
Corbel, S., Nowak, M. A., Fender, R. P., *et al*. (2003), *A&A*, **400**, 1007–1012
Cowley, A. P., Crampton, D., Hutchings, J. B., *et al*. (1983), *ApJ* **272**, 118–122
Cowley, A. P., Crampton, D. and Hutchings, J. B. (1987), *AJ* **92**, 195–199
Cowley, A. P., Schmidtke, P. C., Ebisawa, K., *et al*. (1991), *ApJ* **381**, 526–533
Cowley, A. P., Schmidtke, P. C., Anderson, A. L. and McGrath, T.K. (1995), *PASP* **107**, 145–147
Cui, W., Heindl, W. A., Swank, J. H., *et al*. (1997a), *ApJ* **487**, L73–L76
Cui, W., Zhang, S. N., Focke, W. and Swank, J. H. (1997b), *ApJ* **484**, 383–393
Cui, W., Shrader, C. R., Haswell, C. A. and Hynes, R. I. (2000a), *ApJ* **535**, L123–L127
Cui, W., Zhang, S. N. and Chen, W. (2000b), *ApJ* **531**, L45–L48
Cui, W., Schulz, N. S., Baganoff, F. K., *et al*. (2001), *ApJ* **548**, 394–400
Dal Fiume, D., Frontera, F., Orlandini, M., *et al*. (1999), *IAU Circ*. 7291
Davies, R. D., Walsh, D. and Browne, I. W. A., *et al*. (1976), *Nature* **261**, 476–478
Dhawan, V., Mirabel, I. F. and Rodriguez, L. F. (2000), *ApJ* **543**, 373–385
Dieters, S.W., Belloni, T., Kuulkers, E., *et al*. (2000), *ApJ* **538**, 307–314
Dijk, R. van , Bennett, K., Collmar, W., *et al*. (1995), *A&A* 296, L33–L36
di Matteo, T., Celotti, A. and Fabian, A. C. (1999), *MNRAS* **304**, 809–820
Di Salvo, T., Done, C., Zycki, P. T., *et al*. (2001), *ApJ* **547**, 1024–1033
Done, C. and Nayakshin, S. (2001), *MNRAS* **328**, 616–622
Done, C. and Zycki, P. T. (1999), *MNRAS* **305**, 457–468
Done, C., Mulchaey, J. S., Mushotzky, R. F. and Arnaud, K. A. (1992), *ApJ* **395**, 275–288
Dove, J. B., Wilms, J. and Begelman, M. C. (1997a), *ApJ* **487** 747–758
Dove, J. B., Wilms, J., Maisack, M. and Begelman, M. C. (1997b), *ApJ* **487**, 759–768
Dubus, G., Hameury, J.-M and Lasota, J.-P. (2001), *A&A* **373**, 251–271
Ebisawa, K., Mitsuda, K. and Inoue, H. (1989), *PASJ* **41**, 519–530
Ebisawa, K., Mitsuda, K. and Tomoyuki, H. (1991), *ApJ* **367**, 213–220
Ebisawa, K., Makino, F., Mitsuda, K., *et al*. (1993), *ApJ* **403**, 684–689
Ebisawa, K., Ogawa, M., Aoki, T., *et al*. (1994), *PASJ* **46**, 375–394
Elvis, M., Page, C. G., Pounds, K. A., *et al*. (1975), *Nature* **257**, 656–657
Esin, A. A., McClintock, J. E. and Narayan, R. (1997), *ApJ* **489**, 865–889
Esin, A. A., Narayan, R., Cui, W., *et al*. (1998), *ApJ* **505**, 854–868
Esin, A. A., McClintock, J. E., Drake, J. J., *et al*. (2001), *ApJ* **555**, 483–488
Fabbiano, G., Zezas, A. and Murray, S. S. (2001), *ApJ* **554**, 1035–1043
Fabian, A. C., Rees, M. J., Stella, L. and White, N. E. (1989), *MNRAS* **238**, 729–736
Fabian, A. C., Iwasawa, K., Reynolds, C. S. and Young, A. J. (2000), *PASP* **112**, 1145–1161
Falcke, H. and Biermann, P. L. (1995), *A&A* **293**, 665–682
Fender, R. P. (2001), *MNRAS*, **322**, 31–42
Fender, R., Corbel, S., Tzioumis, T., *et al*. (1999a), *ApJ* **519**, L165–L168
Fender, R. P., Garrington, S. T., McKay, D. J., *et al*. (1999b), *MNRAS* **304**, 865–876
Fender, R. P., Hjellming, R. M., Tilanus, R. P. J., *et al*. (2001), *MNRAS* **322**, L23–L27
Feng, Y. X., Zhang, S. N., Sun, X., *et al*. (2001), *ApJ* **553**, 394–398
Field, R. D. and Rogers, R. D. (1993), *ApJ* **403**, 94–109
Filippenko, A. V. and Chornock, R. (2001), *IAU Circ*. 7644
Filippenko, A. V., Matheson, T. and Ho, L. C. (1995a), *ApJ* **455**, 614–622
Filippenko, A. V., Matheson, T. and Barth, A. J. (1995b), *ApJ* **455**, L139–L142
Filippenko, A. V., Matheson, T., Leonard, D. C., *et al*. (1997), *PASP* **109**, 461–467
Filippenko, A. V., Leonard, D. C., Matheson, T., *et al*. (1999), *PASP* **111**, 969–979
Freedman, W. L., Madore, B. F., Gibson, B. K., *et al*. (2001), *ApJ* **553**, 47–72
Frontera, F., Palazzi, E., Zdziarski, A. A., *et al*. (2001a), *ApJ* **546**, 1027–1037
Frontera, F., Zdziarski, A. A., Amati, L., *et al*. (2001b), *ApJ* **561**, 1006–1015
Frontera, F., Amati, L., Zdziarski, A. A., *et al*. (2003), *ApJ* **592**, 1110–1118
Fryer, C. and Kalogera V. (2001), *ApJ* **554**, 548–560
Garcia, M. R., McClintock, J. E., Narayan, R., *et al*. (2001), *ApJ* **553**, L47–L50
Gelino, D. M., Harrison, T. E. and McNamara, B. J. (2001a), *AJ* **122**, 971–978
Gelino, D. M., Harrison, T. E. and Orosz, J. A. (2001b), *AJ* **122**, 2668–2678
George, I. M. and Fabian, A. C. (1991), *MNRAS* **249**, 352–367

Gierlinski, M., Zdziarski, A. A., Poutanen, J., *et al*. (1999), *MNRAS* **309**, 496–512
Gierlinski, M., Maciolek-Niedzwiecki, A. and Ebisawa, K. (2001), *MNRAS* **325**, 1253–1265
Gies, D. R. and Bolton, C. T. (1982), *ApJ* **260**, 240–248
Goldoni, P., Vargas, M., Goldwurm, A., *et al*. (1999), *ApJ* **511**, 847–851
Greene, J., Bailyn, C. D. and Orosz, J. A. (2001), *ApJ* **554**, 1290–1297
Greiner, J., Dennerl, K. and Predehl, P. (1996), *A&A* **314**, L21–L24
Greiner, J., Cuby, J. G. and McCaughrean, M. J (2001a), *Nature* **414**, 522–525
Greiner, J., Cuby, J. G., McCaughrean, M. J., *et al*. (2001b), *A&A* **373**, L37–L40
Groot, P., Tingay, S., Udalski, A. and Miller, J. (2001), *IAU Circ*. 7708
Grove, J. E., Johnson, W. N., Kroeger, R. A., *et al*. (1998), *ApJ* **500**, 899–908
Gursky, H., Bradt, H., Doxsey, R., *et al*. (1978), *ApJ* **223**, 973–978
Haardt, F. and Maraschi, L. (1991), *ApJ* **380**, L51–L54
Hameury, J.-M., Lasota, J.-P., McClintock, J. E. and Narayan, R. (1997), *ApJ* **489**, 234–243
Hameury, J.-M., Barret, D., Lasota, J.-P., *et al*. (2003), *A&A* **399**, 631–637
Han, X. and Hjellming, R. M. (1992), *ApJ* **400**, 304–314
Hannikainen, D. C., Hunstead, R. W., Campbell-Wilson, D., *et al*. (2000), *ApJ* **540**, 521–534
Hannikainen, D., Campbell-Wilson, D., Hunstead, R., *et al*. (2001), *ApSSS* **276**, 45–48
Harlaftis, E. T., Horne, K. and Filippenko, A. V. (1996), *PASP* **108**, 762–771
Hawley, J. F. and Krolik, J. H. (2001), *ApJ* **548** 348–367
Heuvel, E. P. J. van den (1992), in *ESA, Environment Observation and Climate Modelling Through International Space Projects* (SEE N93–23878 08–88)
Hjellming, R. M. and Rupen, M. P. (1995), *Nature* **375**, 464–468
Hjellming, R. M., Calovini, T. A. and Han, X. H. (1988), *ApJ* **335**, L75–L78
Hjellming, R. M., Rupen, M. P. and Mioduszewski, A. J. (1998a), *IAU Circ*. 6924
(1998b), *IAU Circ*. 6934
Hjellming, R. M., Rupen, M. P., Mioduszewski, A. J., *et al*. (1999), *ApJ* **514**, 383–387
Hjellming, R. M., Rupen, M. P., Hunstead, R. W., *et al*. (2000), *ApJ* **544**, 977–992
Homan, J., Wijnands, R., van der Klis, M., *et al*. (2001), *ApJS* **132**, 377–402
Homan, J., Klein-Wolt, M., Rossi, S., *et al*. (2003a), *ApJ* **586**, 1262–1267
Homan, J., Miller J. M., Wijnands, R., *et al*. (2003b), *ATEL* 162
Hooft, F. van der, Kouveliotou, C., van Paradijs, J., *et al*. (1996), *ApJ* **458**, L75–L78
(1999), *ApJ* **513**, 477–490
Humphrey, P. J., Fabbiano, G., Elvis, M., *et al*. (2003), *MNRAS* **344**, 134–148
Hutchings, J. B., Crampton, D., Cowley, A. P., *et al*. (1987), *AJ* **94**, 340–344
Hynes, R. I., Steeghs, D., Casares, J., *et al*. (2003), *ApJ* **583**, L95–L98
Hynes, R. I., Roche, P., Charles, P.A and Coe, M. J. (1999), *MNRAS* **305**, L49–L53
Igumenshchev, I. V. and Abramowicz, M. A. (1999), *MNRAS* **303**, 309–320
in't Zand, J. J. M., Markwardt, C. B., Bazzano, A., *et al*. (2002a), *A&A* **390**, 597–609
in't Zand, J. J. M., Miller, J. M., Oosterbroeck, T. and Parmar, A. N. (2002b), *A&A* **394**, 553–560
Israelian, G., Rebolo, R. and Basri, G. (1999), *Nature* **401**, 142–144
Jones, C., Forman, W., Tananbaum, H. and Turner, M. J. L. (1976), *ApJ* **210**, L9–L11
Kalemci, E., Tomsick, J. A., Rothschild, R. E., *et al*. (2002) *ApJ* **586**, 419–426
Kalogera, V. and Baym, G. (1996), *ApJ* **470**, L61–L64
Kaluzienski, L. J., Holt, S. S., Boldt, E. A., *et al*. (1975), *ApJ* **201**, L121–L124
Kato, S. (2001), *PASJ* **53**, 1–24
Kato, S. and Fukue, J. (1980), *PASJ* **32**, 377–388
Kato, S., Fukue, J. and Mineshige, S. (1998), *Black-Hole Accretion Disks* (Japan, Kyoto University Press)
Kawaguchi, T., Shimura, T. and Mineshige, S. (2000), *NewAR* **44**, 443–445
Kennea, J. A. and Skinner, G. K. (1996), *PASJ* **48**, L117–L117
King, A. R., Davies, M. B., Ward, M. J., *et al*. (2001), *ApJ* **552**, L109–L112
Kitamoto, S., Tsunemi, H., Pedersen, H., *et al*. (1990), *ApJ* **361**, 590–595
Klein-Wolt, M., Fender, R. P., Pooley, G. G., *et al*. (2002), *MNRAS* **331**, 745–764
Klis M. van der (1994), *ApJS* **92**, 511–519
(1995), in *X-ray Binaries*, eds. W. H. G. Lewin, J. van Paradijs and E. P. J. van den Heuvel (Cambridge, Cambridge University Press), 252–307
Kong, A. K. H., Charles, P. A., Kuulkers, E. and Kitamoto, S. (2002), *MNRAS* **329**, 588–596
Kong, A. K. H., McClintock, J. E., Garcia, M. R., *et al*. (2002), *ApJ* **570**, 277–286

Kotani, T., Kawai, N., Nagase, F., *et al*. (2000), *ApJ* **543**, L133–L136
Kubota, A. and Makishima, K. 2003, *ApJ*, **601**, 428–438
Kubota, A., Makishima, K. and Ebisawa, K. (2001), *ApJ* **560**, L147–L150
Kuulkers, E., Wijnands, R., Belloni, T., *et al*. (1998), *ApJ* **494**, 753–758
Kuulkers, E., Fender, R. P., Spencer, R. E., *et al*. (1999), *MNRAS* **306**, 919–925
Laor, A. (1991), *ApJ* **376**, 90–94
Lasota, J.-P. (2001), *NewAR* **45**, 449–508
Levine, A. M., Bradt, H., Cui, W., *et al*. (1996), *ApJ* **469**, 33–36
Ling, J. C., Mahoney, W. A., Wheaton, W. A. and Jacobson, A. S. (1987), *ApJ* **321**, L117–L122
Ling, J. C., Wheaton, W. A., Wallyn, P., *et al*. (2000), *ApJS* **127**, 79–124
Liu, B. F., Mineshige, S. and Shibata, K. (2002), *ApJ* **572**, L173–L176
Liu, Q. Z., van Paradijs, J. and van den Heuvel, E. P. J. (2000), *A&As* **147**, 25–49
Liu, Q.Z., van Paradijs, J. and van den Heuvel, E. P. J. (2001), *A&A* **368**, 1021–1054
Loewenstein, M., Mushotzky, R. F., Angelini, L., *et al*. (2001), *ApJ* **555**, L21–L24
Lowes, P., in 't Zand, J. J. M., Heise, J., *et al*. (2002), *IAU Circ*. 7843
Lynden-Bell, D. and Pringle, J. E. (1974), *MNRAS* **168**, 603–637
Makishima, K., Maejima, Y., Mitsuday, K., *et al*. (1986), *ApJ* **308**, 635–643
Makishima, K., Kubota, A, Mizuno, T., *et al*. (2000), *ApJ* **535**, 632–643
Malzac, J., Belloni, T., Spruit, H. C. and Kanbach, G. (2003), *A&A* **407**, 335–345
Mandelbrot, B. B. (1999), *Multifractals and 1/f Noise: Wild Self-Affinity in Physics* (Heidelberg, Springer-Verlag)
Margon, B., Thorstensen, J. R. and Bowyer, S. (1978), *ApJ* **221**, 907–911
Markert, T. H., Canizares, C. R., Clark, G. W., *et al*. (1973), *ApJ* **184**, L67–L70
Markoff, S., Falcke, H. and Fender, R. (2001), *A&A* **372**, L25–L28
Markovic, D. and Lamb, F. K. (1998), *ApJ* **507**, 316–326
Markwardt, C. (2001), *ApSS* **276**, 209–212
Markwardt, C. B. and Swank, J. H. (2003), *IAU Circ*. 8056
Marsh, T. R., Robinson, E. L. and Wood, J. H. (1994), *MNRAS* **266**, 137–154
Marti, J., Mirabel, I. F., Duc, P.-A. and Rodriguez, L. F. (1997), *A&A* **323**, 158–162
Marti, J., Mirabel, I. F., Chaty, S. and Rodriguez, L. F. (2000), *A&A* **363**, 184–187
Marti, J., Mirabel, I. F., Rodriguez, L. F. and Smith, I. A. (2002), *A&A* **386**, 571–575
Martocchia, A., Matt, G., Karas, G., *et al*. (2002), *A&A* **387**, 215–221
Matt, G., Perola, G.C. and Piro, L. (1991), *A&A* **247**, 25–34
Mendez, M. and van der Klis, M. (1997), *ApJ* **479**, 926–932
McClintock, J. E. and Remillard, R. A. (1986), *ApJ* **308**, 110–122
(2000), *ApJ* **531**, 956–962
McClintock, J. E., Horne, K. and Remillard, R. A. (1995), *ApJ* **442**, 358–365
McClintock, J. E., Garcia, M. R., Caldwell, N., *et al*. (2001a), *ApJ* **551**, L147–L150
McClintock, J. E., Haswell, C.A., Garcia, M. R., *et al*. (2001b), *ApJ* **555**, 477–482
McClintock, J. E., Narayan, R., Garcia, M. R., *et al*. (2003), *ApJ* **539**, 435–451
McConnell, M. L., Zdziarski, A. A., Bennett, K., *et al*. (2002), *ApJ* **572**, 984–995
McKinney, J. C. and Gammie, C. F. (2002), *ApJ* **573**, 728–737
Mendez, M. and van der Klis, M. (1997), *ApJ* **479**, 926–932
Menou, K., Esin, A. A., Narayan, R., *et al*. (1999), *ApJ* **520**, 276–291
Merloni, A. and Fabian, A. C. (2001a), *MNRAS* **321**, 549–552
(2001b), *MNRAS* **328**, 958–968
(2002), *MNRAS* **332**, 165–175
Merloni, A., Fabian, A. C. and Ross, R. R. (2000), *MNRAS* **313**, 193–197
Merloni, A., Vietri, M., Stella, L. and Bini, D. (2001), *MNRAS* **304**, 155–159
Meyer, F., Liu, B. F. and Meyer–Hofmeister, E. (2000), *A&A* **361**, 175–188
Miller, J. M., Fox, D. W., Di Matteo, T., *et al*. (2001), *ApJ* **546**, 1055–1067
Miller, J. M., Fabian, A. C., in't Zand, J. J. M., *et al*. (2002a), *ApJ* **577**, L15–L18
Miller, J. M., Fabian, A. C., Wijnands, R., *et al*. (2002b), *ApJ* **570**, L69–L73
(2002c), *ApJ* **578**, 348–356
Miller, J. M., Wijnands, R., Rodriguez–Pascual, P. M., *et al*. (2002d), *ApJ* **566**, 358–364
Miller, J. M., Fabbiano, G., Miller, M. C., and Fabian, A. C. (2003a), *ApJ* **585**, L37–L40
Miller, J. M., Zezas, A., Fabbiano, G. and Schweizer, F. (2003b), *ApJ* **609**, 728–734 (astro-ph/0302535)

Mirabel, I. F. and Rodriguez, L. F. (1994), *Nature* **371**, 46–48
(1999), *ARA&A* **37**, 409–443
(2003), *Science* **300**, 1119–1120
Mirabel, I. F., Rodriguez, L. F. and Cordier, B. (1993), *IAU Circ*. 5876
Mitsuda, K., Inoue, H., Koyama, K., *et al*. (1984), *PASJ* **36**, 741–759
Miyamoto, S. and Kitamoto, S. (1991), *ApJ* **374**, 741–743
Miyamoto, S., Iga, S., Kitamoto, S. and Kamado, Y. (1993), *ApJ* **403**, L39–L42
Morgan, E. H., Remillard, R. A. and Greiner, J. (1997), *ApJ* **482**, 993–1010
Motch, C., Guillout, P., Haberl, F., *et al*. (1998), *A&AS* **132**, 341–359
Muno, M. P., Morgan, E. H. and Remillard, R. A. (1999), *ApJ* **527**, 321–340
Muno, M. P., Morgan, E. H., Remillard, R. A., *et al*. (2001), *ApJ*, **556**, 515–532
Murdin, P., Griffiths, R. E., Pounds, K. A., *et al*. (1977), *MNRAS* **178**, 27P–32P
Narayan, R. (1996), *ApJ* **462**, 136–141
Narayan, R. (2002), in *Lighthouses of the Universe*, eds. M. Gilfanov, R. Sunyaev, *et al*. (Berlin, Springer)
Narayan, R. and Insu, Y. (1994), *ApJ* **428**, L13–L16
(1995), *ApJ* **444**, 231–243
Narayan, R., McClintock, J. E. and Yi, I. (1996), *ApJ* **457**, 821–833
Narayan, R., Garcia, M. R. and McClintock, J. E. (1997), *ApJ* **478**, L79–L82
Narayan, R., Igumenshchev, I. V. and Abramowicz, M. A. (2000), *ApJ* **539**, 798–808
Narayan, R., Garcia, M. R. and McClintock, J. E. (2002), in *Proc. Ninth Marcel Grossmann Meeting*, eds. V.G. Gurzadyan *et al*. (Singapore, World Scientific), 405–425
Nelemans, G. and van den Heuvel, E. P. J. (2001), *A&A* **376**, 950–954
Nobili, L., Turolla, R., Zampieri, L. and Belloni, T. (2000), *ApJ* **538**, L137–L140
Novikov, I. D. and Thorne, K. S. (1973), in *Black Holes*, eds. C. DeWitt and B. DeWitt (New York, Gordon & Breach)
Nowak, M. A. (2000), *MNRAS* **318**, 361–367
Nowak, M. A. and Wilms, J. (1999), *ApJ* **522**, 476–486
Nowak, M. A., Wilms, J., Heindl, W. A., *et al*. (2001), *MNRAS* **320**, 316–326
Nowak, M. A., Wilms, J. and Dove, J. B. (2002), *MNRAS* **332**, 856–878
Ogley, R. N., Ash, T. D. C. and Fender, R. P. (1997), *IAU Circ*. 6726
Orosz, J. A. and Bailyn, C. D. (1997), *ApJ* **477**, 876–896
Orosz, J. A., Bailyn, C. D., McClintock, J. E. and Remillard, R. A. (1996), *ApJ* **468**, 380–390
Orosz, J. A., Jain, R. K., Bailyn, C. D., *et al*. (1998), *ApJ* **499**, 375–384
Orosz, J. A., Kuulkers, E., van der Klis, M., *et al*. (2001), *ApJ* **555**, 489–503
Orosz, J. A., Groot, P. J., van der Klis, M., *et al*. (2002a), *ApJ* **568**, 845–861
Orosz, J. A., Polisensky, E. J., Bailyn, C. D., *et al*. (2002b), *BAAS* 201, 1511
Orosz *et al*. (2004), *ApJ* **616**, 376–382
Osaki, Y. (1974), *PASJ* **26**, 429–436
Owen, F. N., Balonek, T. J., Dickey, J., *et al*. (1976), *ApJ* **203**, L15–L16
Pan, H. C., Skinner, G. K., Sunyaev, R. A. and Borozdin, K. N. (1995), *MNRAS* **274**, L15–L18
Paradijs, J. van (1995), in *X-ray Binaries*, eds. W. H. G. Lewin, J. van Paradijs and E. P. J. van den Heuvel (Cambridge, Cambridge University Press), 536–577
Paradijs, J. van and McClintock, J. E. (1995), in *X-ray Binaries*, eds. W. H. G. Lewin, J. van Paradijs and E. P. J. van den Heuvel (Cambridge, Cambridge University Press), 58–125
Parmar, A. N., Angelini, L., Roche, P. and White, N. E. (1993), *A&A* **279**, 179–187
Pottschmidt, K., Wilms, J., Nowak, M. A., *et al*. (2003), *A&A* **407**, 1039–1058
Poutanen, J. and Fabian, A. C. (1999), *MNRAS* **306**, L31–L37
Pringle, J. E. (1981), *AR&A* **19**, 137–162
Pringle, J. E. and Rees, M. J. (1972), *A&A* **21**, 1–9
Psaltis, D., Belloni, T. and van der Klis, M. (1999), *ApJ* **520**, 262–270
Quataert, E. and Gruzinov, A. (2000), *ApJ* **539**, 809–814
Quataert, E. and Narayan, R. (1999), *ApJ* **520**, 298–315
Reig, P., Belloni, T., van der Klis, M., *et al*. (2000), *ApJ* **541**, 883–888
Remillard, R. A. and Morgan, E. H., (1999), *Bull. AAS* **31**, 1421
Remillard, R. A., Orosz, J. A., McClintock, J. E. and Bailyn, C. D. (1996), *ApJ* **459**, 226–235
Remillard, R., Levine, A., Swank, J. and Strohmayer, T. (1997), *IAU Circ*. 6710
Remillard, R. A., Morgan, E. H., McClintock, J. E. *et al*. (1999), *ApJ* **522**, 397–412

Remillard, R. A., Morgan, E. H. and Muno, M. (2001), in *Proc. Ninth Marcel Grossmann Meeting*, eds. V. G. Gurzadyan, *et al*. (Singapore, World Scientific), 2220–2223
Remillard, R. A., Muno, M. P., McClintock, J. E. and Orosz, J. A. (2002a), *ApJ* **580**, 1030–1042
Remillard, R. A., Sobczak, G. J., Muno, M. P. and McClintock, J. E. (2002b), *ApJ* **564**, 962–973
Remillard, R. A., Levine, A. M., Morgan, E. H., *et al*. (2003a), *IAU Circ*. 8050
Remillard, R. A., Muno, M. P., McClintock, J. E. and Orosz, J. A. (2003b), *BAAS* **35**, 648
Revnivtsev, M., Gilfanov, M. and Churazov, E. (1998a), *A&A* **339**, 483–488
Revnivtsev, M., Gilfanov, M., Churazov, E., *et al*. (1998b), *A&A* **331**, 557–563
Revnivtsev, M., Borozdin, K. N., Priedhorsky, W. C. and Vikhlinin, A. (2000a), *ApJ* **530**, 955–965
Revnivtsev, M., Sunyaev, R. and Borozdin, K. (2000b), *A&A* **361** L37–L39
Revnivtsev, M., Trudolyubov, S. P. and Borozdin, K. N. (2000c), *MNRAS* **312**, 151–158
Revnivtsev, M., Gilfanov, M. and Churazov, E. (2001), *A&A* **380**, 520–525
Revnivtsev, M., Gilfanov, M., Churazov, E. and Sunyaev, R. (2002), *A&A* **391**, 1013–1022
Revnivtsev, M., Chernvakova, M., Capitanio, F., *et al*. (2003), *ATEL* 132
Reynolds, C. S. and Nowak, M. A. (2003), *Phys. Rep.* **377**, 389–466
Reynolds, A. P., Quaintrell, H., Still, M. D., *et al*. (1997), *MNRAS* **288**, 43–52
Rezzolla, L., Yoshida, S., Maccarone, T. J. and Zanotti, O. (2003), *MNRAS* **344**, L37–L41
Rhoades, C. E. and Ruffini, R. (1974), *Phys. Rev. Lett*. **32**, 324
Rodriguez, L. F., Mirabel, I. F. and Marti, J. (1992), *ApJ* **401**, L15–L18
Romani, R. W. (1998), *A&A* **333**, 583–590
Rothschild, R. E., Blanco, P. R., Gruber, D. E., *et al*. (1998), *ApJ* **496**, 538–549
Rothstein, D. M., Eikenberry, S. S., Chatterjee, S., *et al*. (2002), *ApJ* **580**, L61–L63
Rozanska, A. and Czerny, B. (2000), *A&A* **360**, 1170–1186
Rupen, M. P., Hjellming, R. M. and Mioduszewski, A. J. (1998), *IAU Circ*. 6938
Rupen, M. P., Dhawan, V. and Mioduszewski, A. J. (2002), *IAU Circ*. 7874
Rupen, M. P., Brocksopp, C., Mioduszewski, A. J., *et al*. (2003), *IAU Circ*. 8054
Rutledge, R. E., Lewin, W. H. G., van der Klis, M., *et al*. (1999), *ApJS* **124**, 265–283
Sanchez-Fernandez, C., Zurita, C., Casares, J., *et al*. (2002), *IAU Circ*. 7989
Seon, K., Min, K., Kenji, Y., *et al*. (1995), *ApJ* **454**, 463–471
Shahbaz, T., Ringwald, F. A., Bunn, J. C., *et al*. (1994), *MNRAS* **271**, L10–L14
Shahbaz, T., Naylor, T. and Charles, P. A. (1997), *MNRAS* **285**, 607–612
Shahbaz, T., van der Hooft, F., Casares, J., *et al*. (1999), *MNRAS* **306**, 89–94
Shakura, N. I. and Sunyaev, R. A. (1973), *A&A* **24**, 337–366
Shapiro, S. L. and Teukolsky, S. A. (1983), *Black Holes, White Dwarfs and Neutron Stars: The Physics of Compact Objects* (New York, Wiley)
Shimura, T. and Takahara, F. (1995), *ApJ* **445**, 780–788
Shrader, C. R., Wagner, R. M., Hjellming, R. M., *et al*. (1994), *ApJ* **434**, 698–706
Skinner, G. K., Foster, A. J., Willmore, A. P. and Eyles, C. J. (1990), *MNRAS* **243**, 72–77
Smak, J. (1971), *Acta Astron*. **21**, 15–21
Smith, D. M., Heindl, W. A., Swank, J., *et al*. (1997), *ApJ* **489**, L51–L54
Smith, D. M., Heindl, W. A., Markwardt, C. B. and Swank, J. H. (2001), *ApJ* **554**, L41–L44
Smith, D. M., Heindl, W. A. and Swank, J. (2002), *ApJ* **578**, L129–L132
Sobczak, G. J., McClintock, J. E., Remillard, R. A., *et al*. (1999), *ApJ* **520**, 776–787
(2000a), *ApJ* **531**, 537–545
(2000b), *ApJ* **544**, 993–1015
Steeghs, D., Miller, J. M., Kaplan, D. and Rupen, M. (2003), *ATEL* 146
Stella, L., Vietri, M. and Morsink, S.M. (1999), *ApJ* **524**, L63–L66
Stirling, A. M., Spencer, R. E., de la Force, C. J., *et al*. (2001), *MNRAS* **327**, 1273–1278
Stone, J. M., Pringle, J. E. and Begelman, M. C. (1999), *MNRAS* **310**, 1002–1016
Strohmayer, T. E. (2001a), *ApJ* **552**, L49–L53
(2001b), *ApJ* **554**, L169–L172
Sunyaev, R. and Revnivtsev, M. (2000), *A&A* **358**, 617–623
Sunyaev, R. A., Lapshov, I.Yu., Grebenev, S. A., *et al*. (1988), *SvAL* **14**, 327–333
Sunyaev, R., Gilfanov, M., Churazov, E., *et al*. (1991a), *SvAL* **17**, 50–54
Sunyaev, R. A., Kaniovskii, A. S., Efremov, V. V., *et al*. (1991b), *SvAL* **17**, 123–130
Sunyaev, R., Churazov, E., Gilfanov, M., *et al*. (1992), *ApJ* **389**, L75–L78
Sutaria, F. K., Kolb, U., Charles, P., *et al*. (2002), *A&A* **391**, 993–997

Swank, J. (1998), in *The Active X-ray Sky: Results from BeppoSAX and Rossi–XTE*, eds. L. Scarsi, *et al*., *Nucl. Phys. B Proc. Suppl.* (astro–ph/9802188)
Tagger, M. and Pellat, R. (1999), *A&A* **349**, 1003–1016
Takahashi, K., Inoue, H. and Dotani, T. (2001), *PASJ* **53**, 1171–1177
Tanaka, Y. and Lewin, W. H. G. (1995), in *X-ray Binaries*, eds. W. H. G. Lewin, J. van Paradijs and E. P. J. van den Heuvel (Cambridge, Cambridge University Press), 126–174, TL95
Tanaka, Y. and Shibazaki, N. (1996), *ARA&A* **34**, 607–644, TS96
Tanaka, Y., Nandra, K. and Fabian, A. C. (1995), *Nature* **375**, 659–661
Tananbaum, H., Gursky, H., Kellogg, E., *et al*. (1972), *ApJ* **177**, L5–L10
Timmes, F. X., Woosley, S. E. and Weaver, T. A. (1996), *ApJ* 457, 834–843
Titarchuk, L. and Osherovich, V. (2000), *ApJ* **542**, L111–L114
Titarchuk, L. and Shrader, C. (2002), *ApJ* **567**, 1057–1066
Tomsick, J. A. and Kaaret, P. (2000), *ApJ* **537**, 448–460
Tomsick J. A. and Kaaret, P. (2001), *ApJ* **548**, 401–409
Tomsick, J. A., Kaaret, P., Kroeger, R. A. and Remillard, R. A. (1999), *ApJ* **512**, 892–900
Trudolyubov, S., Churazov, E., Gilfanov, M., *et al*. (1999), *A&A* **342**, 496–501
Turner, M. J. L., Thomas, H. D., Patchett, B. E., *et al*. (1989), *PASJ* **41**, 345–372
Turner, N. J., Stone, J. M. and Sano, T. (2002), *ApJ* **566**, 148–163
Turolla, R., Zane, S. and Titarchuk, L. (2002), *ApJ* **576**, 349–356
Ueda, Y., Dotani, T., Uno, S., *et al*. (1997), *IAU Circ*. 6627
Vargas, M., Goldwurm, A., Paul, J., *et al*. (1996), *A&A* **313**, 828–832
Vargas, M., Goldwurm, A., Laurent, P., *et al*. (1997), *ApJ* **476**, L23–L26
Vasiliev, L., Trudolyubov, S. and Revnivtsev, M. (2000), *A&A* **362**, L53–L56
Vikhlinin, A., Finoguenov, A., Sitdikov, A., *et al*. (1992), *IAU Circ*. 5608
Vikhlinin, A., Churazov, E., Gilfanov, M., *et al*. (1994), *ApJ* **424**, 395–400
Wagner, R. M., Starrfield, S. G., Hjellming, R. M., *et al*. (1994), *ApJ* **429**, L25–L28
Wagner, R. M., Foltz, C. B., Shahbaz, T., *et al*. (2001), *ApJ* **556**, 42–46
Wagoner, R. V. (1999), *Phys. Rep.* **311**, 259–269
Wagoner, R. V., Silbergleit, A. S. and Ortega-Rodriguez, M. (2001), *ApJ* **559**, L25–L28
Wardzinski, G., Zdziarski, A. A., Gierlinski, M., *et al*. (2002), *MNRAS* **337**, 829–839
Weaver, K. A., Gelbord, J. and Yaqoob, T. (2001), *ApJ* **550**, 261–279
Webster, B. L and Murdin, P. (1972), *Nature* **235**, 37–38
White, N. E. and Marshall, F. E. (1984), *ApJ* **281**, 354–359
White, N. E. and van Paradijs, J. (1996), *ApJ* **473**, L25–L29
White, N. E., Stella, L. and Parmar, A. N. (1988), *ApJ* **324**, 363–378
White, N. E., Nagase, F. and Parmar, A. N. (1995), in *X-ray Binaries*, eds. W. H. G. Lewin, J. van Paradijs and E. P. J. van den Heuvel (Cambridge, Cambridge University Press), 1–57
Wijnands, R. and Miller, J. M. (2002), *ApJ* **564**, 974–980
Wijnands, R. and van der Klis, M. (2000), *ApJ* **528**, L93–L96
Wijnands, R., Homan, J. and van der Klis, M. (1999), *ApJ* **526**, L33–L36
Wijnands, R., Mendez, M., Miller, J. M. and Homan, J. (2001), *MNRAS* **328**, 451–460
Wijnands, R., Miller, J. M. and van der Klis, M. (2002), *MNRAS* **331**, 60–70
Wilms, J., Nowak, M. A., Dove, J. B., *et al*. (1999), *ApJ* **522**, 460–475
Wilms, J., Nowak, M. A., Pottschmidt, K., *et al*. (2001a), *MNRAS* **320**, 327–340
Wilms, J., Reynolds, C. S., Begelman, M. C., *et al*. (2001b), *MNRAS* **328**, L27–L31
Wilson, A. M., Carpenter, G. F., Eyles, C. J., *et al*. (1977), *ApJ* **215**, L111–L115
Wilson, C. K. and Rothschild, R. E. (1983), *ApJ* **274**, 717–722
Wood, K. S., Ray, P. S., Bandyopadhyay, R. M., *et al*. (2000), *ApJ* **544**, L45–L48
Woods, P. M., Kouveliotou, C., Finger, M. H., *et al*. (2002), *IAU Circ*. 7856
Woosley, S. E., Heger, A. and Weaver, T. A. (2002), *RvMP* **74**, 1015–1071
Wu, K., Soria, R., Campbell–Wilson, D., *et al*. (2002), *ApJ* **565**, 1161–1168
Yaqoob, T., Ebisawa, K. and Mitsuda, K. (1993), *MNRAS* **264**, 411–420
Zdziarski, A. A. (2000), in *Highly Energetic Physical Processes*, Procs. IAU Symposium #195, eds. C.H. Martens, S. Tsuruta and M. A. Weber, ASP, 153–170, (astro-ph/0001078)
Zdziarski, A. A., Grove, J. E., Poutanen, J., *et al*. (2001), *ApJ* **554**, L45–L48
Zdziarski, A., Poutanen, J., Paciesas, W.S. and Wen, L. (2002), *ApJ* **578**, 357–373

Zdziarski, A. A., Lubinski, P., Gilfanov, M. and Revnivtsev, M. (2003), *MNRAS* **342**, 355–372
Zhang, S. N., Cui, W. and Chen, W. (1997a), *ApJ* **482**, L155–L158
Zhang, S. N., Cui, W., Harmon, B. A., *et al*. (1997b), *ApJ* **477**, L95–L98
Zurita, C., Sanchez-Fernandez, C., Casares, J., *et al*. (2002), *MNRAS* **334**, 999–1008
Zycki, P. T., Done, C. and Smith, D. A. (1999a), *MNRAS* **305**, 231–240
(1999b), MNRAS **309**, 561–575